SCUOLA INTERNAZIONALE
SUPERIORE di STUDI AVANZATI
International School
for Advanced Studies
via Beirut 2-4 • 34014 Trieste • ITALY
T +39 040 3787 11 • F +39 040 3787 528
w w w . s i s s a . i t

Calculating Thermodynamics Properties of Classical and Quantum Systems by a Metadynamics Monte Carlo Procedure.

Candidate: M.Sc. Yanier Crespo Hernández.

Supervisors: Prof. Alessandro Laio, Prof. Giuseppe Santoro and Prof. Erio Tosatti.

Thesis submitted for the degree of Doctor of Philosophy.

Trieste, Italy, October 2010.

Abstract

This thesis presents a new metadynamics-based quantum Monte Carlo approach to compute the phase diagram and equilibrium properties of condensed matter systems typically quantum solids whose Hamiltonian contain important and dominant quantum effects. Two main applications are presented the classical and the quantum Ising model. Using path integral Monte Carlo we study the re-entrant phase diagram of the molecular solid hydrogen deuterium (HD) under ultra-high pressure, as the first approach for a future application of the proposed metadynamics-based MC method to calculate the free energy of this quantum system.

Specifically, we show that in a MC metadynamics simulation of a classical Ising model the time average of the history-dependent potential converge to the free energy with the same law of an umbrella sampling performed *in optimal conditions*. The metadynamics-based MC method is illustrated also in the quantum Ising model proving that our approach is at least as good as the Wang Landau with an stochastic series expansion dynamics, the *state-of-the-art* on a lattice quantum problem, as well as being physically transparent and easily generalizable to off-lattice models. Finally we apply the metadynamics-based MC method introduced in this thesis to the HD system in the hexagonal closed-packed lattice finding the classical configuration of the molecules for which the interaction potential energy is minimum. With the help of this new structure the HD phase line is calculated obtaining its unusual re-entrant behavior with a respective minimum pressure of $p_m \approx 65$ close to the experimental value $p_m = 53$ GPa.

Acknowledgments

The happy end of this thesis had not been possible without the help of many people, that in different ways have contributed to its realization. Therefore I wish to thank my supervisors Prof. Alessandro Laio, Prof. Giuseppe Santoro and Prof. Erio Tosatti, for their guide, support, patience and the attention they give me every time I need to discuss something.

I would also like to thank, all my professors, that during the first year, helped me to learn all the basic knowledge I needed to do this and future works, specially to Sandro Sorella that helped me a lot with the discussions about quantum Monte Carlo. To my classmates and friends especially to Danielle, Gabrielle, Giovanni, Giussepe, Juan, Lorenzo, Marco, Monse, Pilar and Trang, for their disposition to teach me a lot of details, that were needed for doing all the assignments of this PhD thesis. I also want to thank my friend Rolando for his willingness to help me in any moment I needed and for the large number of discussions on several topics, even if they were not from his own field of research. Finally I thank my wife Dania, for all the support she gave me when calculations were not going so well, and for reminding me always with her behavior the things that are really important in life. Finally I want to thank the SISSA secretary staff for all their help with bureaucracy matters and the Condensed Matter selection committee for giving me the unequalled possibility to be in this PhD program.

Contents

Introduction

This thesis presents a new metadynamics-based quantum Monte Carlo (MC) approach to compute the phase diagram and equilibrium properties of condensed matter systems, typically quantum solids, whose Hamiltonian contain important and dominant quantum effects. Two main applications are presented the classical and the quantum Ising model. Using path integral MC (PIMC) we study the re-entrant phase diagram of the molecular solid hydrogen deuterium (HD) under ultra-high pressure, as the first approach for a future application of the proposed metadynamics-based MC method to calculate the free energy of this quantum system.

Calculating certain thermodynamical quantities, such as the free energy (F) or the entropy, by MC simulation is a notoriously difficult problem. The difficulty arises because standard MC [1] is devised so as to generate configurations $\mathbf{X}$ distributed according to their Boltzmann weight $W(\mathbf{X}) = e^{-\beta E(\mathbf{X})}$, where $E(\mathbf{X})$ is the energy of the configuration $\mathbf{X}$. This is efficient if we are interested in calculating quantities like the average energy $\langle E \rangle = Z^{-1} \sum_{\mathbf{X}} E(\mathbf{X}) W(\mathbf{X})$, where $Z = \sum_{\mathbf{X}} W(\mathbf{X})$ is the partition function, since the configurations generated by MC are just those that contribute significantly to the average. Calculating, however, the free energy, $F = -\beta^{-1} \ln[Z]$, requires a knowledge of the partition function Z which is not accurately given by the simulation.

In the last few years the use of history-dependent sampling techniques that

allows to calculate F has emerged as a novel paradigm in computational science. Prominent examples are the Wang-Landau (WL) [2] and the metadynamics [3] approaches, that have respectively become popular in the statistical physics [4] and in the computational chemistry community [5]. These methods, although different, are based on similar ideas. Wang-Landau is formulated in a MC framework and aims at calculating the density of states $g(E) = \sum_{\mathbf{X}} \delta(E - E(\mathbf{X}))$ where $\delta(\bullet)$ is the Dirac delta function, by iteratively flattening the energy histogram $\mathcal{B}(E)$. This is achieved by making the acceptance of the move depend on the reconstructed $1/g(E)$ up to that moment. Each time a certain move is proposed $g(E)$ is multiplied by a factor $f > 1$. Once $\mathcal{B}(E)$ is "flat", f is reduced and $\mathcal{B}(E)$ is reset to zero. This process is repeated until f becomes approximately one [2]. Metadynamics aims at calculating the free energy as a function of collective variables (CVs) $\mathbf{s}$ that are explicit functions of the system configurations $\mathbf{X}$. Like in WL, this is achieved by flattening the histogram as a function of these CVs: the normal molecular dynamics forces are combined with forces derived from a history-dependent potential $V_G(\mathbf{s})$ defined as a sum of Gaussians of height w centered along the trajectory in CVs space. After sufficient time the sum of the Gaussians, $V_G(\mathbf{s})$, approximately compensates the underlying free energy $\lim_{t\to\infty} V_G(\mathbf{s}, t) \sim -F(\mathbf{s})$ [6].

These two methods, WL and metadynamics, have in common the idea of using a history-dependent (non-Markovian) process to flatten the probability distribution as a function of the relevant variables: energy in WL, one or more CVs $\mathbf{s}$ in metadynamics. However here, we are mostly interested in quantum systems and the application of WL's idea to quantum systems is limited because it requires, in most cases, sampling a *multi-dimensional* density of states histogram [7]. The approach is therefore not very efficient. A much more convenient "*state-of-the-art*" route is based on the so-called stochastic series expansion (SSE) [8, 9], and involves using a WL approach to reconstruct the coefficients $g(n) = \mathrm{Tr}(-\hat{H})^n$ of a high-temperature expansion of the partition function $Z = \sum_n (\beta^n/n!) g(n)$ [10]. The SSE approach is par-

ticularly suited to treating quantum spin systems and other quantum lattice problems, but is in general not straightforward, for instance, for off-lattice quantum problems on the continuum. On the other hand, metadynamics is normally formulated in a molecular dynamics framework and, to the best of our knowledge, it has been applied so far just to classical problems. Application to quantum systems is therefore an appealing route to explore.

In order to recover the correct (*equilibrium*) thermodynamic properties the two algorithms adopt different strategies. In metadynamics, the history-dependent potential is assumed to be an estimator of F even if it is updated with Gaussians of finite w. This assumption is justified by the proof given in Ref.[6] that the history-dependent potential is an estimator of F whenever the dynamics along the variables biased by metadynamics is much slower than the dynamics along all the other degrees of freedom ("adiabatic separation"). Additional fictitious coordinates [11] or a suitable discretization procedure [3] can be employed to enforce, in generic many-body systems, this time-scale separation. However, in practical applications the adiabatic separation can be achieved only approximately. In WL, the equilibrium properties are recovered in a different manner. At the end of the simulation, the factor f converges to a number close to one, and the bias becomes approximately time-independent. Thus, the final analysis is performed on a histogram constructed in a quasi-equilibrium process. A similar strategy has also been successfully adopted in the metadynamics-based scheme introduced in Ref. [12].

In this thesis, we present a history-dependent method that integrates metadynamics in a MC procedure for the efficient calculation of the free-energy of classical and quantum systems. When embedded in a path integral formulation, it is of general applicability to a large variety of Hamiltonians [13]. Furthermore we numerically show that neither adiabatic separation nor an iterative reduction of w are necessary to obtain a reliable estimate of F in

metadynamics sampling.

The remainder of this thesis is organized as follows: In chapter one we describe stochastic techniques to calculate thermodynamics properties of classical systems. We start by introducing the standard classical MC method that allows to calculate the ratio of multidimensional integral and therefore is mainly used to compute the average of observable. Then we review the Wang-Landau scheme that calculates the density of states, providing an accurate knowledge of the partition function, the entropy and the free energy. In the last section of chapter one we study the convergence properties of this approach in a multidimensional system, with a Hamiltonian depending on several variables. This study is done by using the metadynamics-based MC procedure introduced in this thesis [13]. Specifically, we show that in a MC metadynamics simulation of a classical Ising model the time average of the history-dependent potential converge to $F(\mathbf{s})$ with the same law of an umbrella sampling performed *in optimal conditions* (*i.e.*, with a bias equal to minus the free energy) [14]. Remarkably, after a short transient, the error becomes approximately independent of the filling speed, showing that even in out-of-equilibrium sampling conditions metadynamics allows recovering an accurate estimate of $F(\mathbf{s})$. These results have been obtained by introducing a novel functional form of the history-dependent potential that avoids the onset of systematic errors near the boundaries of the free energy landscape [15].

In chapter two we describe some stochastic techniques to calculate the thermodynamics properties of *quantum* systems. We start by introducing the well known path integral Monte Carlo (PIMC) method. Next we present the stochastic series expansion (SSE) method and we describe how it is applied to a specific example, the quantum Ising model (QIM). We also show how to integrate the WL method with the SSE (WL-SSE) and with PIMC (WL-PIMC) for applications to quantum systems. In the last part we extend the metadynamics-based MC method, introduced in chapter one, to quantum

systems. We adopt the path-integral formulation of MC, that is applicable also to off-lattice quantum problems. We illustrate this approach by applying it again to the quantum Ising model where we reconstruct the free energy as a function of three CVs, the magnetization per spin, the potential energy per spin and the kinetic energy per spin. As we will show, a calculation performed at a single point in parameter space is sufficient to generate the free energy in a whole region around that point. The method is tested by comparing its efficiency against the *state-of-the-art* WL-SSE method [10] and a WL over a standard PIMC [7]: we prove that our approach is at least as good as the WL-SSE on a lattice quantum problem, but it is physically more transparent and, unlike WL-SSE, easily generalizable to off-lattice models.

As prototype of this off-lattice model, we study in chapter three the re-entrant phase line in solid HD near half a megabar pressure. The solid hydrogen compounds H_2, D_2 and HD are quantum molecular solids that exhibit complex phase diagrams in which the symmetry of the low-pressure quantum rotor states of the molecules gives way to a high-pressure anisotropic molecular crystal phase, generally called the "broken symmetry phase" (BSP) [16],[17],[18]. In hydrogen and deuterium the transition pressure of the BSP line increases with increasing temperature [17],[16] and is well understood (see Fig. 3.1 a)). In HD this line is re-entrant and the transition pressure first decreases and then increases with increasing temperature (see Fig. 3.1 b)) [18]; this behavior is still in need of quantitative and qualitative understanding. Existing theoretical studies of the re-entrant behavior of the BSP have been mainly done within the mean-field approximation [19],[20]. A recent attempt to study the re-entrant behavior in solid HD using standard PIMC was made in Ref. [21] where the authors consider asymmetric rotors with centers fixed on a face centered cubic (FCC) lattice and the electronic quadrupole-quadrupole interaction as the anisotropic interaction potential. The results were only of qualitative value.

In this chapter we address this problem using more accurate approach. We start describing the interaction potential of two isolated H_2 molecules, and how to use this pair potential in the molecular solid. We develop the theory of path integral (PI) representation of rotors, considering in particular the constant-pressure ensemble where temperature and pressure are controlled parameters, while the volume is calculated directly in the equilibrated simulation cell. The isotropic part of the interaction potential is tested by reproducing, within PIMC, the well known *ortho*-D_2 (see Appendix C) equation of state.

Finally we apply our metadynamics-based MC method to the HD system in the hexagonal closed-packed (HCP) lattice to find the classical configuration of the molecules for which the interaction potential energy is minimum, obtaining a new structure with the same characteristics of the result given earlier by Surh *et al.*, [22] but with different molecular orientations. Before applying our metadynamics-based MC method to the quantum solid HD we calculate the re-entrance phase line of the BSP to test both our PIMC algorithm and the interaction potential between the molecules. This calculation is done by using two order parameters, a lattice biased order parameter where the new structure is used as reference, and an order parameter related to the quadrupolar tensor of a single molecule. We obtain the unusual re-entrant behavior of the phase line at a pressure of ≈ 65 GPa for an HCP lattice, close to the experimental value. The stage is now ready for the application of the proposed metadynamics-based MC method to calculate the free energy of this quantum system: this future study will shed light on the physics of the quantum rotational melting at the physical root of the re-entrance in the phase diagram.

Chapter 1

Calculating Thermodynamics Properties: The Classical Case.

1.1 Introduction

In this chapter we describe some stochastic techniques to calculate thermodynamics properties of classical systems. We start by introducing the standard classical Monte Carlo (MC) method that allows to calculate the ratio of multidimensional integral and therefore is mainly used to compute the average of observables. Then we review the Wang-Landau (WL) scheme to calculate the density of states, providing an accurate knowledge of the partition function, the entropy and the free energy. Finally we focus on the metadynamics method, a powerful sampling technique that uses a non-equilibrium history-dependent process to reconstruct the free energy F surface as a function of the relevant collective variables (CVs) $\mathbf{s}$ [5] that are explicit functions of the system configurations $\mathbf{X}$. In the last section of this chapter we study the convergence properties of this approach in a multidimensional system, with a Hamiltonian depending on several variables. This study is done by using a method that integrates metadynamics in a MC procedure, to effectively calculate the free energy of a system as a function of physically relevant CVs [13].

Specifically, we show that in a MC metadynamics simulation of an Ising model the time average of the history-dependent potential converge to $F(\mathbf{s})$ with the same law of an umbrella sampling performed *in optimal conditions* (*i.e.*, with a bias exactly equal to the negative of the free energy) [14]. Remarkably, after a short transient, the error becomes approximately independent on the filling speed, showing that even in out-of-equilibrium sampling conditions metadynamics allows recovering an accurate estimate of $F(\mathbf{s})$. These results have been obtained by introducing a novel functional form of the history-dependent potential that avoids the onset of systematic errors near the boundaries of the free energy landscape [15]. Most of this results will be illustrated on a simple example, the classical Ising model.

1.2 The Classical Ising Model

The Ising model is the simplest model for ferromagnetism in statistical mechanics. The model consists of discrete variables σ, the spins, which can take only two values 1 or -1. We identify these two states as the two possible orientation of the physical spin, up or down $|\uparrow\rangle$, $|\downarrow\rangle$. The spins are arranged in a lattice, and each spin interacts only with its nearest neighbors. The total energy of the Ising model in the presence of a magnetic field h is:

$$E = -J \sum_{\langle ij \rangle} \sigma_i \sigma_j - h \sum_i \sigma_i \tag{1.1}$$

where $J > 0$, h is the strength of the parallel magnetic field, $i, j = 1 \dots N$ where N is the total number of spins. The sum $\langle ij \rangle$ is taken over pairs of nearest neighbor sites i, j. The thermodynamics properties of this system can be obtained through its partition function, defined as:

$$Z = \sum_{\{\mathbf{X}\}} e^{-\beta E(\mathbf{X})} \tag{1.2}$$

where $\mathbf{X} = \{\sigma_{i=1\cdots N}\}$ is a configuration of all N spins, $\beta = 1/k_B T$, k_B is the Boltzmann constant and T is the temperature. The average values of any

observable $O(\mathbf{X})$ that depend on the spin configuration can be calculated using the expression:

$$\langle O \rangle = \frac{1}{Z} \sum_{\{\mathbf{X}\}} O(\mathbf{X}) e^{-\beta E(\mathbf{X})}. \tag{1.3}$$

To calculate Z and $\langle O \rangle$ we need to estimate these multidimensional sums. The solution is generally obtained by using different Monte Carlo methods. Some of these techniques will be presented in the following sections.

1.3 Classical Monte Carlo (MC).

A Monte Carlo method is a computational algorithm that allows performing multidimensional integrations. A way of estimating averages like the one in Eq. (1.3) without introducing severe approximations is by an appropriate random sampling in configuration space. Suppose we are interested in the calculation of the ratio between two multidimensional integrals, like in the Eq. (1.3) for the average value of an observable. The average can be written as:

$$\langle O \rangle = \frac{\int d\mathbf{X} O(\mathbf{X}) W(\mathbf{X})}{\int d\mathbf{X} W(\mathbf{X})} = \int d\mathbf{X} O(\mathbf{X}) P(\mathbf{X}) \tag{1.4}$$

where $\mathbf{X}$ is a multidimensional vector, $W(\mathbf{X}) > 0$ is the distribution weight of the configuration $\mathbf{X}$ and

$$P(\mathbf{X}) = \frac{W(\mathbf{X})}{\int d\mathbf{X} W(\mathbf{X})} \tag{1.5}$$

can be interpreted as a probability density distribution of configurations $\mathbf{X}$. In practice this calculation is done by constructing a stochastic process of samples $\{\mathbf{X}_t, t = 0, 1 \dots\}$ distributed according to $P(\mathbf{X})$ and estimating Eq. (1.4) by:

$$\int d\mathbf{X} O(\mathbf{X}) P(\mathbf{X}) = \lim_{k \to \infty} \frac{1}{k+1} \sum_{t=0}^{k} O(\mathbf{X}_t) \tag{1.6}$$

Thus the problem is reduced to the generation of a stochastic process of samples $\{\mathbf{X}_t\}$ with a desired probability distribution. To show how this problem is solved we start by introducing Markov processes.

1.3.1 Markov chains and the Metropolis algorithm.

The majority of multidimensional integral calculations are done with various generalizations of the Metropolis algorithm [1], which produces a particular type of Markov chain in configuration space. A Markov process is defined as a stochastic process where the conditional probability of the system to be in the state $\mathbf{X}'$ at time $t+1$, given that at time t is in the state $\mathbf{X}$, depends only on $\mathbf{X}$. In others words it is a process that has no memory of the previous evolution of the system. The corresponding sequence of states $\{\mathbf{X}_{t=0,1,2...}\}$ is called a Markov chain.

To construct a Markov chain, the state of the system is changed according to a fixed transition probability $\pi(\mathbf{X} \to \mathbf{X}')$ of going from $\mathbf{X}$ to $\mathbf{X}'$, generating a random walk through state space $\{\mathbf{X}_{t=0,1,2...}\}$. The transition probability is usually set up so that it satisfies detailed balance [23]: that is, the transition rate from $\mathbf{X}$ to $\mathbf{X}'$ equals the reverse rate,

$$P(\mathbf{X})\pi(\mathbf{X} \to \mathbf{X}') = P(\mathbf{X}')\pi(\mathbf{X}' \to \mathbf{X}). \tag{1.7}$$

Assuming ergodicity, meaning that the system can move from any state to any other in a finite number of steps with a non zero probability, detailed balance is sufficient to guarantee that $P(\mathbf{X})$ is the stationary distribution for this Markov process and it is the solution of the equation [23][24]:

$$\sum_{\mathbf{X}} P(\mathbf{X})\pi(\mathbf{X} \to \mathbf{X}') = P(\mathbf{X}'). \tag{1.8}$$

In the Metropolis algorithm the detailed balance condition is imposed by splitting the transition probability into an "*a priori*" sampling distribution $P_S(\mathbf{X} \to \mathbf{X}')$ and an acceptance probability $P_A(\mathbf{X} \to \mathbf{X}')$ [1],

$$\pi(\mathbf{X}' \to \mathbf{X}) = P_S(\mathbf{X} \to \mathbf{X}')P_A(\mathbf{X} \to \mathbf{X}') \tag{1.9}$$

We generate trial moves according to $P_S(\mathbf{X} \to \mathbf{X}')$ and then we accept them with the probability:

$$P_A(\mathbf{X} \to \mathbf{X}') = \min\left[1, \frac{P_S(\mathbf{X}' \to \mathbf{X})P(\mathbf{X}')}{P_S(\mathbf{X} \to \mathbf{X}')P(\mathbf{X})}\right], \tag{1.10}$$

Substituting Eq. (1.10) and Eq. (1.9) into Eq. (1.7) it can be easily shown that detailed balance condition is satisfied. Note that if the new configuration $\mathbf{X}'$ generated with this scheme is accepted then the system goes to the new configuration, if it is rejected then the system remains in the same location for at least one more step. In this manner, accepted or rejected steps contribute equally to the average.

An important simplification introduced by the Metropolis algorithm is that to sample $P(\mathbf{X})$ it is sufficient to know the desired probability distribution $P(\mathbf{X})$ up to a normalization constant, because only the ratio $P(\mathbf{X}')/P(\mathbf{X})$ is required to calculate the acceptance probability $P_A(\mathbf{X} \to \mathbf{X}')$ in Eq. (1.10). This allows avoiding a useless, and often computationally prohibitive, normalization.

1.4 Free Energy Extrapolation.

The average value of an observable given by the Eq. (1.4) can be calculated using a different approach. Instead of estimating the ratio of the multidimensional integrals it is possible to calculate the free energy of the system as a function of some collective variable $F(s)$ (defined below), and use it to calculate the average. To illustrate how this approach works we start by rewriting the Eq. (1.4) as:

$$\langle s \rangle = \frac{\int d\mathbf{X} s(\mathbf{X}) W(\mathbf{X})}{\int d\mathbf{X} W(\mathbf{X})} = \frac{\int ds \int d\mathbf{X} s(\mathbf{X}) W(\mathbf{X}) \delta(s - s(\mathbf{X}))}{\int ds \int d\mathbf{X} W(\mathbf{X}) \delta(s - s(\mathbf{X}))} \tag{1.11}$$

where we have used the property of the Dirac delta function $\delta(\bullet)$

$$\int ds \delta(s - s(\mathbf{X})) = 1.$$

We now introduce the definition of the partition function as a function of a collective variable s as:

$$Z(s) \equiv \int d\mathbf{X} W(\mathbf{X}) \delta(s - s(\mathbf{X})) \tag{1.12}$$

with $Z = \int ds Z(s)$. Then the free energy as a function of the collective variable is defined as:

$$F(s) \equiv -\frac{1}{\beta} \ln \left[Z(s) \right] \equiv -\frac{1}{\beta} \ln \left[\int d\mathbf{X} W(\mathbf{X}) \delta(s - s(\mathbf{X})) \right] \tag{1.13}$$

Finally using Eq. (1.11) and Eq. (1.13) we obtain:

$$\langle s \rangle = \frac{\int ds \ s \ e^{-\beta F(s)}}{\int ds e^{-\beta F(s)}} \tag{1.14}$$

Suppose that we have a classical system (*e.g.*, the classical Ising model) whose statistics is described by the Boltzmann weight $W(\mathbf{X}) = e^{-\beta E(\mathbf{X})}$ (see section 1.2). Then if we select as collective variable the total energy, $s = E$, it is possible to show an important result of classical statistical mechanics. This result allows to calculate $F(E)$ at any temperature β' if the free energy as a function of the total energy $F(E)$ is known at a given temperature β. To demonstrate this we first substitute s by E in Eq. (1.13):

$$F(E)_\beta \equiv -\frac{1}{\beta} \ln \left[\int d\mathbf{X} e^{-\beta E(\mathbf{X})} \delta(E - E(\mathbf{X})) \right] \tag{1.15}$$

then using the properties of the Dirac delta $\delta(\bullet)$ we can extract the exponential factor $e^{-\beta E(\mathbf{X})}$ from the integral and write,

$$\beta F(E)_\beta = \beta E - \ln \left[\int d\mathbf{X} \delta(E - E(\mathbf{X})) \right]. \tag{1.16}$$

Note that the last term of Eq. (1.16) does not depend on temperature, so if we do the same for an arbitrary temperature β' we obtain

$$\beta' F(E)_{\beta'} = \beta' E - \ln \left[\int d\mathbf{X} \delta(E - E(\mathbf{X})) \right]. \tag{1.17}$$

Subtracting (1.17) from (1.16) gives:

$$F(E)_{\beta'} = \left(1 - \frac{\beta}{\beta'} \right) E + \frac{\beta'}{\beta} F(E)_\beta, \tag{1.18}$$

thus the free energy in terms of the total energy for the new temperature β' is obtained as a function of the already known free energy, the total energy

and the initial and final temperatures. An advantage of this result is that it allows the calculation of the average value of E for the new temperature by using Eq. (1.14). To obtain $F(E)_\beta$ we can use three methods: umbrella sampling, Wang and Landau and metadynamics that will be introduced in the following sections.

1.5 Getting Free Energy Using the Umbrella Sampling Technique

The average value of the collective variable s Eq. (1.14) can be written as follows:

$$\langle s \rangle = \int ds \; s \; P(s) \tag{1.19}$$

where we have introduced the probability distribution of s calculated as:

$$P(s) = \frac{e^{-\beta F(s)}}{\int ds e^{-\beta F(s)}} \tag{1.20}$$

Thus $P(s)$ is related to $F(s)$ through the equation

$$F(s) = -\beta^{-1} \ln[P(s)] \tag{1.21}$$

plus an irrelevant constant that will be neglected. Since $P(s)$ is an equilibrium quantity, it can be sampled during MC simulations. However, if the system is metastable the MC dynamics will be bound in a local minimum of $F(s)$ and will scape from it with a very low probability, giving an information of a small region of the $P(s)$ landscape and preventing us for obtaining a good estimate of $F(s)$.

The umbrella sampling method [14], introduces a biasing potential $V(s(\mathbf{X}))$ to the energy $E(\mathbf{X})$ of the system. The new energy becomes $E'(\mathbf{X}) = E(\mathbf{X}) + V(s(\mathbf{X}))$. Now the system is sampled through the new weight $W_\mathrm{b} = e^{-\beta E'(\mathbf{X})} = e^{-\beta E(\mathbf{X})} e^{-\beta V(s(\mathbf{X}))}$, where b means biasing. By properly choosing $V(s(\mathbf{X}))$, we can sample the values of s with low probability more

frequently. In the ideal case, if we were able to choose $V(s)$ to be $-F(s)$, all the values of s will be sampled with equal probability. But we have no knowledge of $F(s)$ since it is the very quantity we want compute.

In practice it is possible to use an iteration procedure for calculating $F(s)$. At the beginning of the simulation we set $V_0(s) = 0$ and we start the simulation, after the system has reached the equilibrium it is possible to have a first estimate of $F_1(s)$ using:

$$F_{t+1}(s) = F_t(s) - \beta^{-1} \ln[P(s)] \tag{1.22}$$

where $F_0(s) = 0$. Then we set $V_1(s) = -F_1(s)$ and we repeat the process until we have explore all region of interest.

1.6 The Wang and Landau Algorithm.

The standard MC technique [1] is generally used to create configurations $\mathbf{X}$ distributed according to their Boltzmann weight. This is efficient if we are interested in calculating quantities like the average energy $\langle E \rangle = \sum_{\mathbf{X}} E(\mathbf{X}) P(\mathbf{X})$, since the configurations generated by MC are just those that contribute significantly to the average. Calculating, however, the free-energy, $F = -\beta^{-1} \ln[Z]$, requires a knowledge of the partition function Z which is not accurately provided by the simulation.

In the Wang-Landau (WL) algorithm quantities like the free energy or the entropy can be directly calculated. The method is formulated in a Monte Carlo framework and aims at calculating the density of states $g(E)$, defined as:

$$g(E) = \sum_{\mathbf{X}} \delta(E - E(\mathbf{X})), \tag{1.23}$$

Given $g(E)$ the partition function or the free energy can be obtained for any

temperature using the following equations:

$$Z = \sum_E Z(E) = \sum_E g(E) e^{-\beta E} \tag{1.24}$$

and

$$F = -\frac{1}{\beta} \ln[Z] = -\frac{1}{\beta} \ln \left[\sum_E g(E) e^{-\beta E} \right] \tag{1.25}$$

where we have used the Eqs. (1.23), (1.2) and the properties of $\delta(\bullet)$ function. This is particularly useful if the system can undergo a first-order phase transition. Indeed, using the WL approach, the system can diffuse over free energy barriers in E between different local minima following pathways that would represent, in normal finite-temperature MC, "rare events".

The WL approach [2] estimates the density of states $g(E)$ generating a random walk in energy space. The algorithm is based on the observation that if configurations $\mathbf{X}$ with total energy $E(\mathbf{X})$ are sampled with the probability inversely proportional to $g(E)$, $P(\mathbf{X}) = 1/(g(E))$ the resulting energy histogram is "flat". The calculation of $g(E)$ is accomplished by modifying the estimate of $g(E)$ in a systematic way over the allowed range of energy, making it converge to the true value. $g(E)$ is iteratively updated at each step of the random walk and used to perform a further move in energy space.

At the beginning of the simulation, $g(E)$ is *a priori* unknown, so it is initialized with a guess, say, $g(E) = 1$ for all possible energies $E(\mathbf{X})$. Then the random walk through configuration space is carried out by randomly changing configurations. In general, if E and E' are energies before and after the move, the acceptance probability from energy level E to E' is:

$$P_A(E \to E') = \min \left[1, \frac{g(E)}{g(E')} \right] \tag{1.26}$$

Whether the move is accepted or not, each time an energy level E is visited, $g(E)$ is modified using $g(E) \to g(E) f_0$ where $f_0 > 1$. In practice it is used the formula $\ln[g(E)] = \ln[g(E)] + \ln[f_0]$ to fit all possible values of $g(E)$ into

double precision numbers. By doing so we decrease the probability of the state E and it becomes less likely to visit states with the same energy again.

During the simulation one also accumulates an energy histogram $\mathcal{B}(E)$ counting how many times the state E is visited. When the histogram is "flat" in the energy range of the random walk, $g(E)$ has converged to the true value with an accuracy proportional to $\ln[f_0]$. The modification factor f_0 is then reduced using any function that monotonically decreases to 1 such as $f_1 = \sqrt{f_0}$, the histogram is reset to $\mathcal{B}(E) = 0$ and the simulation is continued. This process is repeated until f is approximately one, for example less than $\exp(10^{-8})$.

1.7 The Metadynamics Method.

If one has to work with large systems and it is important to control not only the energy, but also other variables that describes the state, the free energy can be computed using metadynamics [3]. This approach is normally formulated in a molecular dynamics framework, and aims at calculating F as a function of CVs $\mathbf{s}$ that are explicit functions of the system coordinates. Like in Wang-Landau, this is achieved by flattening the histogram as a function of these CVs: the normal molecular dynamics forces are combined with forces derived from a history-dependent potential $V_G(\mathbf{s}, t)$ defined as a sum of Gaussians of height w centered along the trajectory in CVs space (see Eq. (1.30)).

To be more explicit, let us consider a system described by a set of coordinates $\mathbf{X}$ and an energy $E(\mathbf{X})$, whose equilibrium distribution is proportional to $e^{-\beta E(\mathbf{X})}$. We are interested in exploring the properties of the system as a function of a finite number of CVs $\mathbf{s} = \{s_i\}$, $i = 1, \cdots, a$ where a is a small number. The equilibrium behavior of these variables is completely defined

by the probability distribution:

$$P(\mathbf{s}) = \frac{e^{-\beta F(\mathbf{s})}}{\int d\mathbf{s} e^{-\beta F(\mathbf{s})}} \tag{1.27}$$

where the free energy $F(\mathbf{s})$ is given by:

$$F(\mathbf{s}) = -\frac{1}{\beta} \ln \left[\int d\mathbf{X} e^{-\beta E(\mathbf{X})} \delta(\mathbf{s} - \mathbf{s}(\mathbf{X})) \right] \tag{1.28}$$

(see section 1.4). Consider now a trajectory whose equilibrium distribution is given by Eq. (1.27). If this trajectory could be computed for a very long time, $P(\mathbf{s})$ could be obtained by taking the histogram of the collective variable $\mathbf{s}$ along this trajectory, *i.e.*, at time t

$$P(\mathbf{s}) = \frac{1}{t} \int_0^t dt' \delta(\mathbf{s}(\mathbf{X}(t')) - \mathbf{s}) \tag{1.29}$$

If the system displays metastability, the motion of $\mathbf{s}$ will be bound in some local minimum of the free energy and it will escape from this minimum with a low probability on a time scale determined for $E(\mathbf{X})$ alone.

In metadynamics the exploration of the free energy is done by adding to the energy $E(\mathbf{X})$ a history-dependent potential $V_G(\mathbf{s}, t)$ constructed as a sum of Gaussian of height w and width Δs centered in all the points explored by the dynamics in the CVs space up to time t

$$V_G(\mathbf{s}, t) = w \sum_{t' \leq t} \exp \left[-\frac{|\mathbf{s} - \mathbf{s}(t')|^2}{2\Delta \mathbf{s}^2} \right] \tag{1.30}$$

The parameters w, $\Delta \mathbf{s}$ determine the accuracy and the efficiency of the free energy reconstruction [5]. The local increment on the potential produced by adding these Gaussians discourages the dynamics from revisiting the same point in configuration space and encourages an efficient exploration of the free energy surface. In this manner the collective variables will perform a "metadynamics" in their space, visiting configurations different from the ones they would have explored under the dynamics produced by the energy $E(\mathbf{X})$ alone. As the point that explores the CVs diffuses, the Gaussian

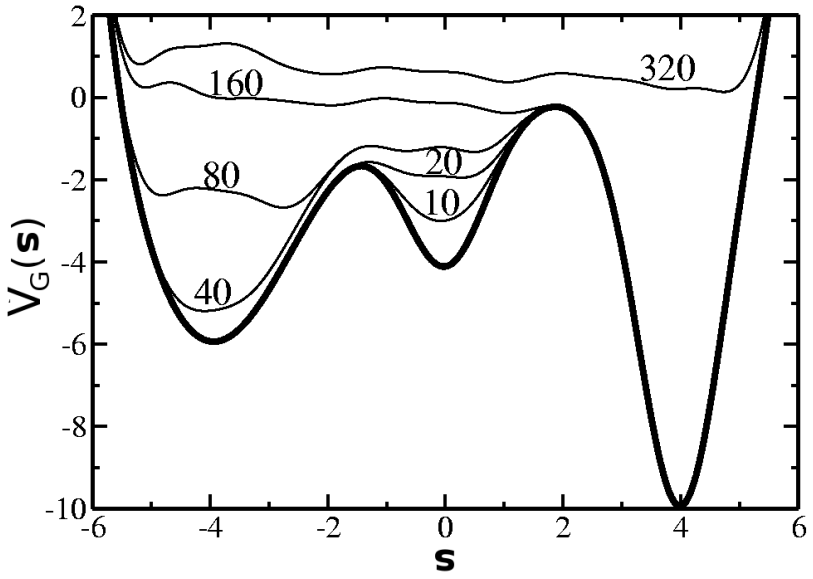

Figure 1.1: Time evolution of the accumulating Gaussian terms of Eq. (1.30). The dynamic evolution (thin lines) is labeled by the number of dynamical iterations. The starting free energy (thick line) has three minima and the dynamics is initialized in the second minimum, at $s = 0$.

potential accumulates and fills the free energy basin, allowing the system to migrate from well to well. After sufficient time the sum of the Gaussians, V_G, approximately compensates the underlying free energy [6].

$$\lim_{t\to\infty} V_G(\mathbf{s}, t) \sim -F(\mathbf{s}) \tag{1.31}$$

Eq. (1.31) is the basic assumption of metadynamics. It states that an equilibrium quantity, namely the free energy, can be estimated by a non-equilibrium dynamics, in which the underlying potential is changed every time a new Gaussian is added. This relation does not derive from any standard identity for the free energy. In Ref. [3] Eq. (1.31) was postulated in a heuristic manner, observing the behavior of the dynamics on free energy surfaces of known functional form. Nevertheless a non trivial mathematical proof of Eq. (1.31)

was given by Bussi *et al.*, [6].

An example of how the method works is given in Fig.3.9 where we consider a free energy with three local minima. For this system if the dynamics starts from the central local minimum, the corresponding well is filled by the Gaussians in $\sim$ 20 steps. After that the dynamics escapes from this well, repeating the process until the full $F(s)$ landscape is explored.

1.8 A Metadynamics-Based Monte Carlo Method.

In this section we introduce a new method, that integrates metadynamics in a MC procedure, to effectively calculate the free energy of a system as a function of physically relevant CVs [13]. The algorithm is implemented as follows. A history-dependent potential V_G is included in the Boltzmann factor of the Metropolis algorithm. At the beginning of the simulation V_G is set to zero. Then a random move $\mathbf{x} \rightarrow \mathbf{X}'$ is proposed. The acceptance probability of the move is:

$$\begin{aligned} P_A(\mathbf{X} \rightarrow \mathbf{X}', t) \quad \equiv \quad & \min\{1, \exp\left(-\beta\left[E(\mathbf{x}') + V_G(\mathbf{s}(\mathbf{X}'), t) - \right.\right. \\ & \left.\left. E(\mathbf{X}) - V_G(\mathbf{s}(\mathbf{X}), t)\right)\right]\} \end{aligned} \tag{1.32}$$

At each step the history-dependent potential is updated as [13]:

$$V_G(\mathbf{s}, t+1) = V_G(\mathbf{s}, t) + w \exp\left[-\frac{|\mathbf{s} - \mathbf{s}(\mathbf{X})|^2}{2\Delta s^2}\right] \tag{1.33}$$

After a sufficient time, hereafter call the "filling time" t_F, V_G relaxes to its "equilibrium" shape approximately compensating the underlying free energy. After t_F the system diffuses freely in $\mathbf{s}$ [5]. In this scheme, like in WL sampling, the history-dependent potential iteratively reduces the probability of the system to remain in the same state. An advantage with respect to the WL method is that here the Boltzmann factor keeps the system in regions of relevance at the temperature of interest.

1.8.1 Novel functional form of the history-dependent potential.

To achieve stationary fluctuations of the history-dependent potential around the correct F it is necessary to solve a technical problem. In metadynamics in order to reduce the computational cost it is customary to use finite width Gaussians, that "fill" the free energy surface quickly. On the other hand, finite-width Gaussians can induce systematics errors at the boundaries ($\partial\Omega$) of the CVs space [5]. These errors are due to the fact that a sum of Gaussians cannot accurately reproduce discontinuities on the free energy profile. The presence of discontinuities is common for several types of CVs that are intrinsically limited, *e.g.*, the magnetization per spin in the Ising model, etc [5]. At the beginning of the simulation these errors are small and usually overlooked, but at long times they can become important, preventing the system from reaching a stationary state. In ref [6] it was shown that if the component of the free energy gradient in the direction normal to $\partial\Omega$ vanishes at the boundaries ($\nabla_n F(\partial\Omega) = 0$), the systematic errors can be eliminated by choosing a functional form for the history-dependent potential that satisfies the same condition ($\nabla_n V_G(\partial\Omega) = 0$). In this thesis we introduce a more general functional form of V_G that eliminates systematic errors even if $\nabla_n F(\partial\Omega) \neq 0$, like in the case of the Ising model.

Systematic errors in the free energy reconstruction close to $\partial\Omega$ are eliminated in the following manner. To simplify the notation, we here assume the CV space is one-dimensional and defined by the equation $s \geq 0$, with the boundary at $s = 0$. The procedure can be straightforwardly generalized to multi-dimensional CVs space, etc. If the system is in s, one extra Gaussian is added in $-s$ with the scope of iteratively imposing that, in a suitably chosen interval around $s = 0$,

$$V_G(-s, t) \approx 2V_G(0, t) - V_G(s, t) \tag{1.34}$$

This property ensures that, at stationary conditions, the history-dependent

potential is approximately linear close to the boundary in order to compensate for the $\nabla_n F(\partial\Omega) \neq 0$ case, but it does not impose the value of its derivative, that is iteratively determined by the thermodynamic bias. In practice, the extra Gaussian is added according to the following rules:

- An interval centered in 0 is chosen, whose width χ is of the order of Δs.
- If $s < \chi$ another Gaussian centered in $-s$ and with the same width and height is added.
- If $s > \chi$ another Gaussian centered in $-s$ and with the same width is added. In this case, the height of the extra Gaussians depends on V_G and is given by:

$$w = \left[2V_G(0,t) - V_G(s,t) - V_G(-s,t)\right] y(s), \tag{1.35}$$

where $y(s) = 1/\left[1 + (s/(4\chi))^n\right]$ with $n = 10$

The second factor in Eq. (1.35) is approximately one for $\mid s \mid < 4\chi$ and goes to zero for $\mid s \mid > 4\chi$. This ensures that V_G goes smoothly to zero in the unphysical region.

1.9 Convergence of Metadynamics in a Multidimensional System.

The proposed boundary correction scheme was tested by performing a metadynamics simulation on a one-dimensional overdamped Langevin model, with a reflective wall at $s = 0$ and a linear free energy $F(s) = \frac{1}{\beta}\frac{b}{\Delta s}s$ (see Fig.1.2). b is a dimensionless parameter that defines the slope of the free energy, $\beta = 1$ and $\Delta s = 0.05$. In Fig.1.2, it is shown that, for $b = -1$ and $\chi = 2\Delta s$, the algorithm ("New algorithm" in Figure) is capable of producing a V_G that

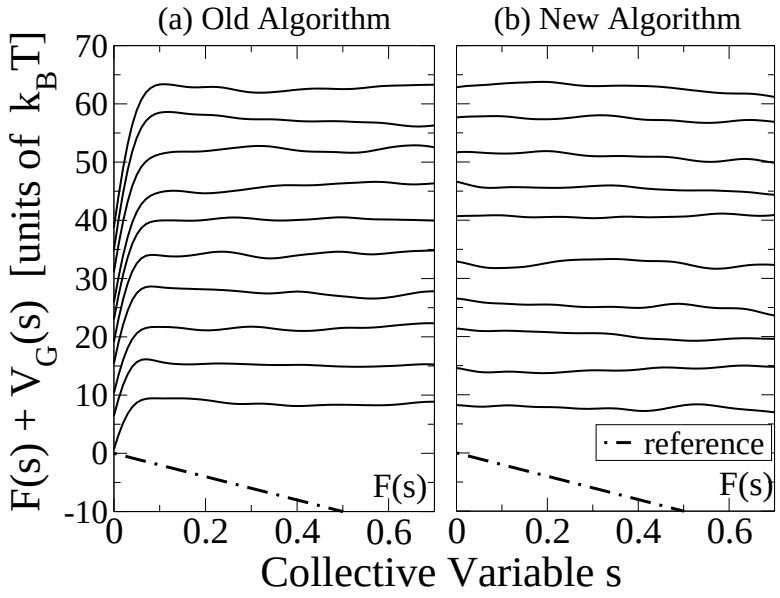

Figure 1.2: Sum of the reference free energy (dot dashed line) and the history-dependent potential ($F(s) + V_G(s)$) as a function of s for a one-dimensional over-damped Langevin model, with reflective wall at $s = 0$ and linear free energy $F(s) = \frac{1}{\beta}\frac{b}{\Delta s}s$ (dot dashed line). The following parameters were used: $\Delta s = 0.05$, $w = 0.3$, $\beta = 1.0$, $b = -1.0$ and diffusion coefficient $D = 2.0$. The results are shown for different simulations times (solid lines) (a) normal metadynamics ("Old algorithm") (b) metadynamics including the proposed boundary correction with $\chi = 2\Delta s$ ("New algorithm").

compensates $F(s)$ almost exactly ($F(s) + V_G(s) \simeq$ constant). Instead, if the extra Gaussians are not added ("Old algorithm"), large systematic errors are developed close to the boundary, and the system cannot reach a stationary state. It was verified that for values of $\chi \in [1.5\Delta s, 3\Delta s]$, $n \in [4, 20]$ and $b \in [-10, 10]$ the error does not change significantly.

Next, the algorithm described above was applied to a 16×16 two-dimensional classical Ising model. As a collective variable we used the magnetization per spin $M = N^{-1}\sum_i \sigma_i$. Clearly, the evolution of this system takes place in the

16^2 dimensional space of its spins variables, and it cannot be expressed as a one-dimensional Markov process in m alone. This means that m is not adiabatically separated from the other degree of freedom as it would be required to apply the results of ref [6]. The height and the width of the Gaussians where $w = 1.0 \times 10^{-4}$ and $\Delta s = 1.4 \times 10^{-2}$ respectively. For this system, the "exact" free energy $F(M)$ was calculated in a long umbrella sampling simulation [14].

In Fig. 1.3 (a), (b) we plot $F(M)+V_G(M)$ at different times for the "Old" and the "New" algorithm. Like in the test model of Fig. 1.2-(a), the old algorithm generates systematic errors in the calculation of F close to the boundaries. Moreover, these errors increase as a function of MC time, and the simulation cannot reach a stationary state. In Fig. 1.3-(b) we plot $F(M) + V_G(M)$ for the new algorithm using $\chi = 2\Delta s$, at the same MC times of panel (a). The boundary corrections introduced in this work reduce the systematics errors and allow the simulation to reach a stationary state where the history-dependent profiles are approximately parallel to each other. In Fig. 1.3-(c) we show that the $V_G(M,t)$ at different MC times (color lines) oscillate around the exact free-energy profile $F(M)$ (black line). Thus the algorithm is able to reach a stationary condition in which the history-dependent potential is, at each time t, a reliable estimator of the equilibrium free energy.

Following Ref. [5] we considered the arithmetic average of all the profiles between the "filling time" t_F and the time $t > t_F$:

$$\overline{V_G}(s,t) = \frac{1}{t - t_F} \int_{t_F}^{t} dt' V_G(s,t') \tag{1.36}$$

If $V_G(s,t)$ after t_F is an unbiased estimator of $-F$, then $\lim_{t\to\infty} \overline{V_G}(s,t) = -F(s)$, modulus an irrelevant constant that will be neglected in the following to simplify the notation. At finite simulation time, $\overline{V_G}(s,t) + F(s)$ will show deviations from zero that become smaller for large t. To study how the error depends on time, we first considered the case of a one dimensional

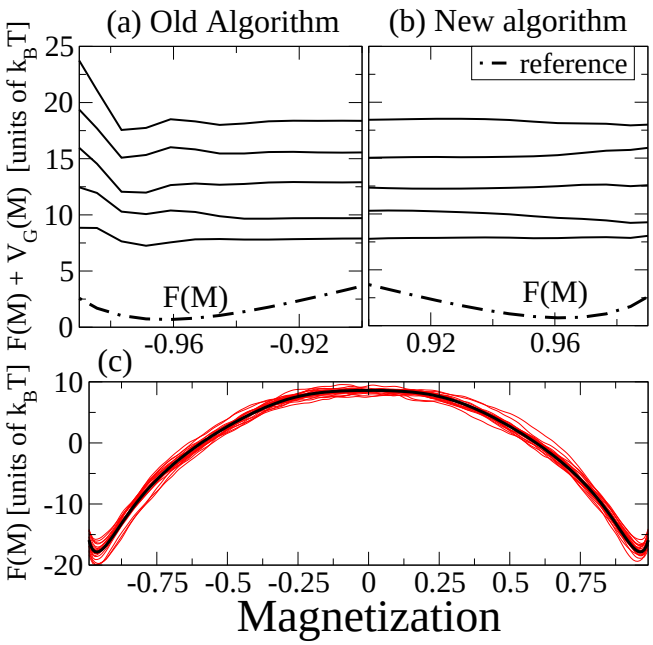

Figure 1.3: Sum of the reference free energy (dot dashed line) and the reconstructed history-dependent potential ($F(M) + V_G(M)$) as a function of the magnetization per spin for $\beta = 1./1.86$, $\Delta s = 1.4 \cdot 10^{-2}$, $w = 1.0 \cdot 10^{-4}$. The results are shown for different simulations times (solid lines) (a) normal metadynamics ("Old algorithm") (b) metadynamics including the proposed boundary correction with $\chi = 2\Delta s$ ("New algorithm"). (c) comparison between the V_G profiles reconstructed at different MC times (color lines), and the reference profile $F(M)$ (black line).

overdamped Langevin process in a square well. A flat free energy profile ($F(s) = 0$) has been employed with reflecting boundaries at -1 and 1. The metadynamics algorithm has been used to reconstruct the free energy profile. For comparison, a trajectory was also generated without the metadynamics bias. In this case the free-energy profile ($F_u(s,t)$) was estimated as:

$$F_u(s,t) = -\beta^{-1} \log\left(\mathcal{B}(s,t)\right) \tag{1.37}$$

where $\mathcal{B}(s,t)$ is the histogram of the visited positions up to time t. This corresponds to an *ideal* umbrella sampling simulation, in which the free-

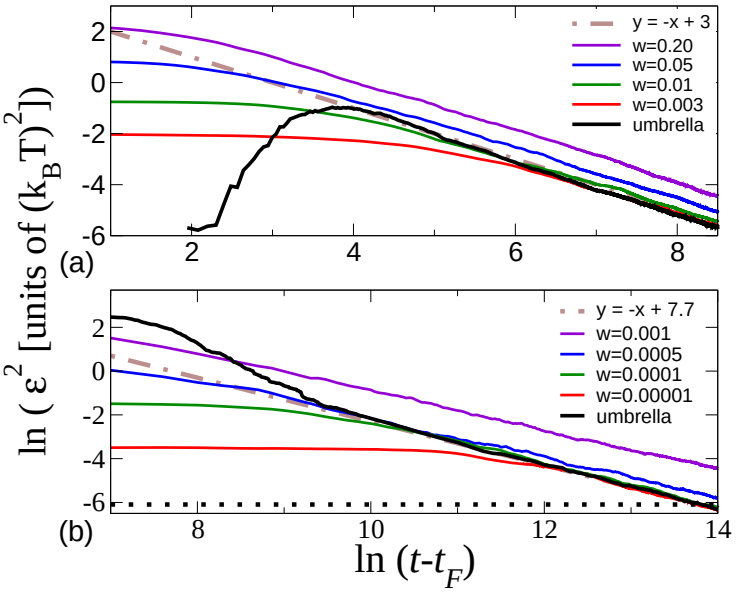

Figure 1.4: Free energy squared error as a function of simulation time t after the filling time t_F in logarithmic scale, for two different cases: (a) Langevin dynamics in a square well performed with $\beta = 1$, $D = 0.01$, $\Delta s = 0.025$ and $\chi = 2\Delta s$. The free energy is computed by umbrella sampling (black line) and metadynamics with four values of the Gaussian high $w = (0.20, 0.05, 0.01, 0.003)$. (b) 16×16 two-dimensional Ising model, calculated for $\beta = 1/1.86$, $\Delta s = 1.4 \cdot 10^{-2}$ and $\chi = 2\Delta s$. The free energy is computed by umbrella sampling (black line) and metadynamics with four values of the Gaussian high $w = (1.0 \cdot 10^{-3}, 5.0 \cdot 10^{-4}, 1.0 \cdot 10^{-4}, 1.0 \cdot 10^{-5})$ (color lines), taking as a reference an accurate umbrella sampling calculation. The dotted line is the estimated error in the reference F_{ref}, $\log(\epsilon^2) \simeq -6.1$.

energy is perfectly compensated by the bias (see section 1.5) [14]. The error of the reconstructed free energy at a given simulation time t was calculated as:

$$\varepsilon^2(t) = \left\langle \frac{1}{2} \int_{-1}^{1} \left(F_{rec}\left(s', t\right) - F_{ref}\left(s'\right) \right)^2 ds' \right\rangle \tag{1.38}$$

where, $F_{rec} = -\overline{V_G}$ for the metadynamic case, $F_{rec} = F_u$ for umbrella sampling and $F_{ref}(s) = 0$ for both cases. The average was taken over 100 statistically independent runs.

In Fig. 1.4-(a) $\varepsilon(t)^2$ is plotted as a function of simulation time in logarithmic scale. We see from the figure that the error of metadynamics, after an initial transient that increases when w is reduced, decreases with the same law of an ideal umbrella sampling, namely with the inverse square root of t :

$$\varepsilon \sim 1/\sqrt{t}. \tag{1.39}$$

Remarkably, for large t the error depends weakly on w and for $w \lesssim 0.05$, it is practically indistinguishable from the ideal umbrella sampling case. This is not a trivial result, since it was demonstrated that the error on a *single* profile V_G grows with $\sqrt{w}$ [6]. This corresponds to the error observed at $t = 0$ (*i.e.*, at filling time). The behavior observed in Fig. 1.4. can be rationalized by assuming that profiles obtained with large w have large errors, but decorrelate more quickly. The accuracy gained from fast decorrelation approximately compensates the accuracy lost due to large w. Indeed, for small w, taking the average between different profiles does not improve the accuracy, as the V_G profiles are strongly correlated. This is the origin of the plateau observed in the error curves for small time; consistently the plateau becomes longer for small w.

To investigate the effect of a violation of adiabatic separation on these results, we repeated all the analysis for the two-dimensional Ising model. In this case, as a reference, we performed umbrella sampling using as a bias the same $F_{ref} = F(M)$ of Fig. 1.3. The error as a function of simulation time is shown in Fig 1.4-(b). Clearly, also in this case the error decays to zero following the same law of the ideal umbrella sampling (Eq. (1.39)). Moreover, like in the metadynamics simulation on the Langevin system, the decay law (Eq. (1.39)) depends weakly on the height w of the Gaussians.

In summary, we have shown that the history-dependent potential of metadynamics, after a transient, fluctuates around a well-defined average that, for the system considered in this work, is a good approximation of the negative of the free energy. Stationary conditions can be reached thanks to

a novel procedure that eliminates the systematic errors at the boundaries generated by finite-width Gaussians. By applying this technique to a two-dimensional Ising model we showed that a stationary state is reached even for a system which lacks adiabatic separation between the biased CV and the remaining degrees of freedom. The error of the algorithm in reconstructing the equilibrium free-energy, after a transient, decays like umbrella sampling performed in optimal conditions. Another important result is that this decay law on the error holds independently on the filling speed, determined by w. The numerical evidence presented here does not exclude that systematic errors might appear when looking at fine details of the free-energy surfaces, possibly due to the violation of adiabatic separation and/or to residual effects of the boundaries. However, these errors, if present, are so small ($\ln(\epsilon^2) \leq -6.1 \Rightarrow \epsilon < e^{-3}\ k_B T$) that are not expected to affect the validity of the approach in most practical applications [15].

Chapter 2

Calculating Thermodynamics Properties: The Quantum Case.

2.1 Introduction

In this chapter we describe some stochastic techniques to calculate the thermodynamics properties of *quantum* systems. We start by introducing the well known path integral Monte Carlo (PIMC) method. Next we present the stochastic series expansion (SSE) method and we describe how it is applied to a specific example the quantum Ising model (QIM). We also show how to integrate the Wang-Landau (WL) method with the SSE (WL-SSE) and with PIMC (WL-PIMC) for applications to quantum systems.

In the last part we extend the metadynamics-based MC method, introduced in the previous chapter, to quantum systems. We adopt the path-integral formulation of MC that is applicable also to off-lattice quantum problems. We illustrate this approach by applying it again to the quantum Ising model where we reconstruct the free energy as a function of three CVs, the magnetization per spin $M_{\overline{\mathbf{X}}}$, the potential energy per spin $V_{\overline{\mathbf{X}}}$ and the kinetic

energy per spin $K_{\overline{\mathbf{X}}}$. As we will show, a calculation performed at a single point in parameter space is sufficient to generate the free energy in a whole region around that point. The method is tested by comparing its efficiency against the state-of-the-art WL-SSE method [10], or a WL over a standard PIMC [7]: we prove that our approach is at least as good as the WL-SSE on a lattice quantum problem, but is physically more transparent and unlike WL-SSE easily generalizable to off-lattice models.

2.2 The Path Integral (PI) Method

2.2.1 Density matrix product property and the Trotter formula

Let us suppose that we have a system with a Hamiltonian that we can split in two parts

$$\hat{H} = \hat{K} + \hat{V} \tag{2.1}$$

where $\hat{K}$ and $\hat{V}$ are respectively the kinetic and potential energy operators which in general do not commute. The *product property* of the density matrix $e^{-\beta\hat{H}}$ is the basis of the path integral (PI) method. This property states that the product of two density matrices is a density matrix:

$$e^{-(\beta_1+\beta_2)\hat{H}} = e^{-\beta_1\hat{H}} e^{-\beta_2\hat{H}}. \tag{2.2}$$

Applying the product property Q times to the density matrix $e^{-\beta\hat{H}}$ we have that,

$$e^{-\beta\hat{H}} = \underbrace{e^{-\tau\hat{H}} \dots e^{-\tau\hat{H}}}_{Q \text{ times}} \tag{2.3}$$

where $\tau = \beta/Q$ is the *time step*. For large Q, it is possible to write a sufficiently accurate approximation of the density matrix that can be used to explicitly construct the PI. According to the Baker-Campbell-Hausdorff formula [25] we have:

$$e^{-\tau(\hat{K}+\hat{V})+\tau^2\hat{\mathcal{G}}} = e^{-\tau\hat{K}} e^{-\tau\hat{V}} \tag{2.4}$$

where the operator $\hat{\mathcal{G}}$ is

$$\hat{\mathcal{G}} = \frac{1}{2}\left\{\left[\hat{K}, \hat{V}\right]\right\} + o(\tau).$$

As $\tau \to 0$ the commutator terms which are of the order τ^2 (see Eq. (2.4)) become smaller than the other terms and can be neglected. This is known as the *primitive approximation*:

$$e^{-\tau(\hat{K}+\hat{V})} \approx e^{-\tau\hat{K}} e^{-\tau\hat{V}} \tag{2.5}$$

Hence if τ is small enough, we can approximate the exact density matrix with the product of the density matrices of $\hat{K}$ and $\hat{V}$ alone. According to the Trotter formula:

$$e^{-\beta(\hat{K}+\hat{V})} = \lim_{Q\to\infty}\left[e^{-\frac{\beta}{Q}\hat{K}} e^{-\frac{\beta}{Q}\hat{V}}\right]^Q. \tag{2.6}$$

The error made in this approximation for finite Q, does not propagate. The Trotter formula holds if the three operators $\hat{K}$, $\hat{V}$ and $\hat{K}+\hat{V}$ are self-adjoint and if their spectrum is bounded from below [26]. A proof for the Trotter formula for Hermitian matrices is given in Appendix A.

2.2.2 Quantum Ising model (QIM)

Consider as a specific example the quantum Ising model (QIM) described by the following Hamiltonian:

$$\hat{H}_{\mathrm{QIM}} = -J\sum_{\langle ij\rangle}^{N} \hat{\sigma}_i^z \hat{\sigma}_j^z - h\sum_{i}^{N} \hat{\sigma}_i^z - \Gamma\sum_{i}^{N} \hat{\sigma}_i^x, \tag{2.7}$$

where $J > 0$ is an exchange constant, h is the strength of the magnetic field parallel to the Ising axis ($\hat{z}$), $\Gamma > 0$ is the strength of the transverse magnetic field, $i, j = 1 \ldots N$ and N is the total number of spins. The sum $\langle ij\rangle$ is taken over pairs of nearest-neighbor sites i, j. The operators $\hat{\sigma}_i^{x,y,z}$, are the Pauli matrices. We chose the basis where the $\hat{\sigma}_i^z$ is diagonal. In this basis these matrices have the form:

$$\hat{\sigma}^z = \begin{pmatrix} 1 & 0 \\ 0 & -1 \end{pmatrix}, \quad \hat{\sigma}^y = \begin{pmatrix} 0 & -i \\ i & 0 \end{pmatrix}, \quad \hat{\sigma}^x = \begin{pmatrix} 0 & 1 \\ 1 & 0 \end{pmatrix}. \tag{2.8}$$

The eigenvalue of $\hat{\sigma}_i^z$ are denoted by σ_i, so σ_i takes the values ± 1 ($|\uparrow\rangle_i$, $|\downarrow\rangle_i$). The term including Γ represents a kinetic energy which does not commute with the other two terms, inducing transitions between the $|\uparrow\rangle$ and $|\downarrow\rangle$ states of each single spin, so turning the model from classical to quantum. Again we are interested in calculating the thermodynamics properties of this quantum system that can be obtained through its partition function, defined as:

$$Z_{\text{QIM}} = \sum_{\mathbf{X}} \langle \mathbf{X} | e^{-\beta \hat{H}_{\text{QIM}}} | \mathbf{X} \rangle \tag{2.9}$$

The average value of any operator $\left\langle \hat{O} \right\rangle$ can be then calculated as:

$$\left\langle \hat{O} \right\rangle = \frac{1}{Z_{\text{QIM}}} \sum_{\mathbf{X}} \langle \mathbf{X} | \hat{O} e^{-\beta \hat{H}_{\text{QIM}}} | \mathbf{X} \rangle \tag{2.10}$$

Solving exactly Eq. (2.9) is a difficult task for most of quantum systems, including the simple example of the QIM. The path integral technique is an approximate solution of Eq. (2.9) that allows the stochastic calculation of the average value in Eq. (2.10) as it is shown in the next section.

2.2.3 Quantum Ising model path integral representation

Applying the *primitive approximation* Eq. (3.19) to the QIM leads to the path integral representation. We first write the Hamiltonian as the sum of two terms.

$$\hat{H}_{\text{QIM}} = \hat{V} + \hat{K}$$

with

$$\hat{V} = -J \sum_{\langle ij \rangle} \hat{\sigma}_i^z \hat{\sigma}_j^z - h \sum_i \hat{\sigma}_i^z, \quad \hat{K} = -\Gamma \sum_i \hat{\sigma}_i^x,$$

where $\hat{V}$ is the potential energy, and $\hat{K}$ is the kinetic energy. Then we write the canonical partition function for the QIM, Z_{QIM}, using the product property:

$$Z_{\text{QIM}} = \sum_{\mathbf{X}} \langle \mathbf{X} | e^{-\beta \hat{H}_{\text{QIM}}} | \mathbf{X} \rangle = Tr \left(e^{-\beta \hat{H}_{\text{QIM}}/Q} \right)^Q = Tr \left(e^{-\beta(\hat{K}+\hat{V})/Q} \right)^Q \tag{2.11}$$

where $\mathbf{X} = \{\sigma_{i=1\cdots N}\}$ is a configuration of all N spins. Inserting the identity operator $\hat{\mathbf{1}} = \sum_{\mathbf{X}_q} |\mathbf{X}_q\rangle \langle \mathbf{X}_q|$ in Eq. (2.9) we obtain:

$$Z_{\mathrm{QIM}} = \sum_{\overline{X}} \langle \mathbf{X}_0 | \, e^{-\beta(\hat{K}+\hat{V})/Q} \, |\mathbf{X}_1\rangle \ldots \langle \mathbf{X}_{Q-1}| \, e^{-\beta(\hat{K}+\hat{V})/Q} \, |\mathbf{X}_Q\rangle \, . \tag{2.12}$$

Here $\overline{\mathbf{X}} = \{\sigma_{i=1\cdots N;q=1\cdots Q}\}$. The extra index q labels the Q Trotter slices and $\mathbf{X}_0 = \mathbf{X}_Q$. We shall now use the *primitive approximation* Eq. (3.19) (see section 2.2.1) obtaining an approximate expression of Z_{QIM} whose error is proportional to $o(\tau^2)$. The generic density matrix element, is:

$$\langle \mathbf{X}_{q-1}| \, e^{-\tau(\hat{K}+\hat{V})} \, |\mathbf{X}_q\rangle = \langle \mathbf{X}_{q-1}| \, e^{-\tau\hat{K}} \, |\mathbf{X}_q\rangle \, e^{-\tau V(\mathbf{X}_q)} \tag{2.13}$$

since the potential energy is diagonal in the chosen spin basis. Now it is necessary to calculate the average of the kinetic energy operator between two consecutive Trotter slices

$$\begin{aligned} \langle \mathbf{X}_{q-1}| \, e^{-\tau\hat{K}} \, |\mathbf{X}_q\rangle &= \langle \mathbf{X}_{q-1}| \exp\left(\tau\Gamma \sum_{i=1}^{N} \hat{\sigma}_i^x\right) |\mathbf{X}_q\rangle \\ &= \prod_{i=1}^{N} \langle \mathbf{X}_{q-1}| \exp\left(\tau\Gamma\hat{\sigma}_i^x\right) |\mathbf{X}_q\rangle \end{aligned} \tag{2.14}$$

Using the definition of the exponential of an operator and the property of $\hat{\sigma}_i^x$

$$(\hat{\sigma}_i^x)^n \, |\uparrow\rangle = \begin{cases} |\uparrow\rangle & \text{if} \quad n = 2k \\ |\downarrow\rangle & \text{if} \quad n = 2k+1 \end{cases} \qquad k = 0, 1, 2, \ldots$$

$$(\hat{\sigma}_i^x)^n \, |\downarrow\rangle = \begin{cases} |\downarrow\rangle & \text{if} \quad n = 2k \\ |\uparrow\rangle & \text{if} \quad n = 2k+1 \end{cases} \qquad k = 0, 1, 2, \ldots \tag{2.15}$$

we have that the kinetic density matrix elements are

$$\begin{aligned} \langle\uparrow| \exp\left(\tau\Gamma\hat{\sigma}_i^x\right) |\uparrow\rangle &= \langle\downarrow| \exp\left(\tau\Gamma\hat{\sigma}_i^x\right) |\downarrow\rangle = \cosh\left(\tau\Gamma\right) \\ \langle\uparrow| \exp\left(\tau\Gamma\hat{\sigma}_i^x\right) |\downarrow\rangle &= \langle\downarrow| \exp\left(\tau\Gamma\hat{\sigma}_i^x\right) |\uparrow\rangle = \sinh\left(\tau\Gamma\right) \end{aligned} \tag{2.16}$$

which can be written as an Ising-like interaction between the spin σ and σ'

$$\langle\sigma| \exp\left(\tau\Gamma\hat{\sigma}_i^x\right) |\sigma'\rangle = Ce^{B\sigma\sigma'} \tag{2.17}$$

where

$$B = -\frac{1}{2}\ln\,\tanh\left(\tau\Gamma\right) \qquad C^2 = \frac{1}{2}\sinh\left(2\tau\Gamma\right).$$

Collecting all the ingredients we get the generic density matrix element

$$\begin{aligned}\left\langle \mathbf{X}_{q-1}\right| e^{-\tau(\hat{K}+\hat{V})}\left|\mathbf{X}_{q}\right\rangle &= C^{N} e^{J^{\perp}\tau\sum_{i}\sigma_{i,q}\sigma_{i,q+1}} \times \\ & \quad e^{J\tau\sum_{\langle ij\rangle}\sigma_{i,q}\sigma_{j,q}} e^{h\tau\sum_{i}\sigma_{i,q}} \end{aligned} \tag{2.18}$$

where

$$J^{\perp} = -\frac{1}{2\tau}\ln\,\tanh\left(\tau\Gamma\right) > 0 \tag{2.19}$$

The $J^{\perp}$ term can be interpreted as a ferromagnetic Ising-like coupling between the Trotter replicas of the same spin which are nearest-neighbors ($q-1$ and q) along the Trotter direction. Inserting Eq. (2.18) into Eq. (2.12) we get the approximate expression for the partition function Z_{QIM}:

$$Z_{\mathrm{QIM}} \approx C^{NQ} \sum_{\overline{\mathbf{X}}} e^{-\beta A_{\mathrm{QIM}}(\overline{\mathbf{X}})} \tag{2.20}$$

where

$$\begin{aligned} A_{\mathrm{QIM}}(\overline{\mathbf{X}}) &= H_{\mathrm{QIM}}^{d+1} = \sum_{q=1}^{Q}\left(A_{q}^{kin} + A_{q}^{pot}\right) \\ &= -\frac{1}{Q}\sum_{q=1}^{Q}\left(J\sum_{\langle ij\rangle}^{N}\sigma_{i,q}\sigma_{j,q} + J^{\perp}\sum_{i}^{N}\sigma_{i,q}\sigma_{i,q+1} + h\sum_{i}^{N}\sigma_{i,q}\right). \end{aligned} \tag{2.21}$$

Here A_{q}^{kin} and A_{q}^{pot} are respectively the kinetic and potential action of a *link* (a pair of time slices $(\mathbf{X}_{q-1}, \mathbf{X}_{q})$ separated by time τ) defined as minus the logarithm of the exact density matrix:

$$\begin{aligned} A_{q}^{kin}(\mathbf{X}_{q-1}, \mathbf{X}_{q}, \tau) &\equiv -\ln\left[\left\langle \mathbf{X}_{q-1}\right| e^{-\tau\hat{K}}\left|\mathbf{X}_{q}\right\rangle\right] \\ A_{q}^{pot}(\mathbf{X}_{q-1}, \mathbf{X}_{q}, \tau) &\equiv -\ln\left[\left\langle \mathbf{X}_{q-1}\right| e^{-\tau\hat{V}}\left|\mathbf{X}_{q}\right\rangle\right] \end{aligned} \tag{2.22}$$

The total action $A_{\mathrm{QIM}}(\overline{\mathbf{X}})$ represents the Hamiltonian of a classical $(d+1)$-dimensional anisotropic Ising system at a temperature QT. The system has uniform coupling J along the original d-dimensional lattice bounds, and $J^{\perp}$

along the extra Trotter dimension. Thus the PI technique maps the quantum problem in d-dimensions into a $(d+1)$-dimensional classical problem. This maps allows the application of the Metropolis MC technique to calculate average values, in a method called PIMC. The WL and the metadynamics-based MC scheme proposed in the previous chapter, can be also extended to calculate the thermodynamics properties of a quantum system, as we will show in the following sections.

Calculating averages

An ensemble of paths generated according to the partition function Eq. (2.20) can be used to compute expectation values. The thermodynamic estimator of the internal total energy (E) is obtained by differentiating the logarithm of the partition function with respect to the inverse temperature,

$$E = \left\langle \hat{H} \right\rangle = -\frac{d \ln [Z]}{d\beta} \tag{2.23}$$

obtaining for the QIM that

$$E = E_0 - \left\langle \frac{1}{Q} \sum_{q=1}^{Q} \left(J \sum_{\langle ij \rangle}^{N} \sigma_i^q \sigma_j^q + J_1^{\perp} \sum_{i}^{N} \sigma_i^q \sigma_i^{q+1} + h \sum_{i}^{N} \sigma_i^q \right) \right\rangle \tag{2.24}$$

where

$$E_0 = -N\Gamma \coth (2\tau\Gamma), \quad J_1^{\perp} = -\Gamma \operatorname{sinh}^{-1} (2\tau\Gamma), \quad \langle \cdot \rangle = 1/Z \sum (\cdot) e^{-\beta A},$$

Z is given by Eq. (2.20) and A by Eq. (2.21). The average potential energy $\left\langle \hat{V} \right\rangle$ can be calculated as $\left\langle \hat{V} \right\rangle = -\frac{1}{\beta} \left(J \frac{d \ln[Z]}{dJ} + h \frac{d \ln[Z]}{dh} \right)$ giving:

$$\left\langle \hat{V} \right\rangle = - \left\langle \frac{1}{Q} \sum_{q=1}^{Q} \left(J \sum_{\langle ij \rangle}^{N} \sigma_i^q \sigma_j^q + h \sum_{i}^{N} \sigma_i^q \right) \right\rangle . \tag{2.25}$$

For the kinetic energy we have $\left\langle \hat{K} \right\rangle = -\frac{\Gamma}{\beta} \frac{d \ln[Z]}{d\Gamma}$

$$\left\langle \hat{K} \right\rangle = E_0 - \left\langle \frac{J_1^{\perp}}{Q} \sum_{q=1}^{Q} \sum_{i}^{N} \sigma_i^q \sigma_i^{q+1} \right\rangle \tag{2.26}$$

Note that $\left\langle \hat{K} \right\rangle \to 0$ as $\Gamma \to 0$ and we recover the classical limit.

2.3 Free Energy Extrapolation.

In section 1.4 we showed how to calculate the average value of a collective variable using the free energy as a function of this collective variable (see Eq. (1.13)). This equation is also valid in the quantum case within the PI representation, but now the weight is $W(\overline{\mathbf{X}}) = e^{-\beta A(\overline{\mathbf{X}})}$. The second important result of section 1.4 was the possibility of obtaining $F(E)_{\beta'}$ as a function of an already known free energy $F(E)_{\beta}$, the total energy E and the initial and final temperatures (β, β'). This results allows to calculate the average value of E for any temperature. Thus we are interested in doing the same for the quantum case.

In the demonstration done in section 1.4 there were some points that need to be highlighted: i) the extrapolation parameter, the temperature, appears in the argument of the exponential; ii) the selected collective variable (E) does not depend explicitly on this parameter; iii) this allows to write the free energy as the sum of terms including one that does not depend on the selected parameter. So by analogy, to perform a temperature extrapolation ,in the case of the QIM, it is necessary to select at least two collective variables, the potential and the kinetic energies (note that $J^{\perp}(\beta)$ depend on β see Eq. (2.19) and Eq. (2.21)). To make extrapolations also in Γ and h we need to select three collective variables: the classical interaction energy per spin $V_{\overline{\mathbf{X}}} = -(NQ)^{-1} \sum_q \sum_{\langle ij \rangle} \sigma_{i,q}\sigma_{j,q}$, the quantum "kinetic energy" per spin, $K_{\overline{\mathbf{X}}} = -(NQ)^{-1} \sum_{i,q} \sigma_{i,q}\sigma_{i,q+1}$, and the magnetization per spin $M_{\overline{\mathbf{X}}} = (NQ)^{-1} \sum_{i,q} \sigma_{i,q}$.

In the QIM case, where the partition function is given by Eq. (2.20) and the action can be written using Eq. (2.39): the free energy (Eq. (1.28)) as a

function of these three CVs has the form:

$$F(M,V,K) = -\frac{1}{\beta}\ln\left[C^{NQ}(\beta)\sum_{\overline{X}} e^{-N\beta\left(JV_{\overline{\mathbf{X}}}+J^{\perp}(\beta)K_{\overline{\mathbf{X}}}-hM_{\overline{\mathbf{X}}}\right)} \times \delta(M-M_{\overline{\mathbf{X}}})\delta(V-V_{\overline{\mathbf{X}}})\delta(K-K_{\overline{\mathbf{X}}})\right]. \quad (2.27)$$

Let us suppose that we know the free energy for a value of β and we want to know it for an arbitrary value β'. To do this we use the procedure described in section 1.4. We have:

$$\beta F(M,V,K)_{\beta} = -\ln\left[C(\beta)^{NQ}e^{-N\beta\left(JV+J^{\perp}(\beta)K-hM\right)} \times \sum_{\overline{\mathbf{X}}}\delta(M-M_{\overline{\mathbf{X}}})\delta(V-V_{\overline{\mathbf{X}}})\delta(K-K_{\overline{\mathbf{X}}})\right] \quad (2.28)$$

Using the logarithm properties we obtain

$$\beta' F(M,V,K)_{\beta} = -NQ\ln[C(\beta)] + N\beta\left(JV+J^{\perp}(\beta)K-hM\right) - \ln\left[g(V,K,M)\right] \quad (2.29)$$

where $g(V,K,M)$ is the generalized multi-dimensional density of states,

$$g(V,K,M) = \sum_{\overline{\mathbf{X}}}\delta(M-M_{\overline{\mathbf{X}}})\delta(V-V_{\overline{\mathbf{X}}})\delta(K-K_{\overline{\mathbf{X}}}), \quad (2.30)$$

that does not depend on β,h or Γ. Doing the same for the case of β', and subtracting Eq. (2.29) we finally obtain the new free energy value:

$$F(V,K,M)_{\beta'} = \frac{\beta}{\beta'}\left[F(V,K,M)_{\beta} - N\left(JV+J^{\perp}_{\beta}K-hM\right)\right] + N\left(JV+J^{\perp}_{\beta'}K-hM\right) + \frac{NQ}{\beta'}\ln\left[\frac{C(\beta)}{C(\beta')}\right] \quad (2.31)$$

This equation tell us that if we know the free energy at a temperature β we can calculate it at any temperature β'. Exactly the same derivation can be

done for obtaining the three dimensional free energy as a function of other parameters (*i.e.*, Γ and h). For Γ we have:

$$F(V,K,M)_{\Gamma'} = F(V,K,M)_{\Gamma} + N\left(J_{\Gamma'}^{\perp} - J_{\Gamma}^{\perp}\right)K + \frac{NQ}{\beta}\ln\left[\frac{C(\Gamma)}{C(\Gamma')}\right], \quad (2.32)$$

and for h,

$$F(V,K,M)_{h'} = F(V,K,M)_{h} - N\left(h' - h\right)M. \quad (2.33)$$

By logarithmic integration of $F(V,K,M)$ with respect to one or more variables we get the free-energy as a function of a reduced number of CVs. For instance:

$$F(M) = -\frac{1}{\beta}\ln\left[\int dV dK\; e^{-\beta F(M,V,K)}\right]. \quad (2.34)$$

To calculate the average value of the total energy (E) using the three dimensional free energy $F(M,V,K)$ we rewrite the equation (2.24) as:

$$E = E_0 + NJ\langle V\rangle - NJ_1^{\perp}\langle K\rangle - Nh\langle M\rangle \quad (2.35)$$

then we calculate the potential average value using the expression:

$$\langle V\rangle = \frac{\sum_{VKM} V e^{-\beta F(V,K,M)}}{\sum_{VKM} e^{-\beta F(V,K,M)}} \quad (2.36)$$

and similarly for $\langle K\rangle$ and $\langle M\rangle$. Thus with Eqs. (2.31)-(2.33) we already know how to do free energy extrapolations in the quantum case. So we just have to extend the WL and the Metadynamic techniques to calculate the free energy of quantum systems as a function of a small number of CVs.

2.4 Wang-Landau Mapping Using the PI Representation

The discussion of section 1.6 applies to classical systems: How should one proceed for a quantum system? [7] Consider, to fix ideas, our example of the QIM (Eq. (2.7)). The first step consists in rewriting the partition function in a form similar to Eq. (1.24); that is, as the sum of the product of two functions

where one of them does not depend on temperature and the other can be expressed in terms of elementary functions (*e.g.*, e^x). With this purpose we rewrite the action of the system (Eq. (2.21)) as a function of the three CVs, $V_{\overline{\mathbf{X}}}, K_{\overline{\mathbf{X}}}, M_{\overline{\mathbf{X}}}$,

$$A_{\mathrm{QIM}}(\overline{\mathbf{X}}) = N\left[JV_{\overline{\mathbf{X}}} + J^{\perp}K_{\overline{\mathbf{X}}} - hM_{\overline{\mathbf{X}}}\right]. \tag{2.37}$$

Then using the Eqs. (2.20),(2.30),(2.37) and the properties of $\delta(\bullet)$ function we can easily rewrite:

$$Z_{\mathrm{QIM}} \approx \sum_{V,K,M} g(V,K,M)\; e^{-\beta\overline{A}(V,K,M)} \tag{2.38}$$

where as shown in the previous section $g(V,K,M)$ does not depend on β and

$$\overline{A}(V,K,M) = N\left[JV + J^{\perp}K - hM - (Q/\beta)\ln C\right]. \tag{2.39}$$

For $h = 0$ the relevant CVs are two, V and K. Using the WL idea to reconstruct Z_{QIM} for all values of T and Γ requires now sampling a *two-dimensional* density of states $g(V,K) = \sum_M g(V,K,M)$ in terms of which,

$$Z_{\mathrm{QIM}} \propto \sum_{V,K} g(V,K) e^{-\beta N(JV+J^{\perp}K)}. \tag{2.40}$$

We can apply the WL procedure explained in section 1.6 to generate $g(V,K)$.

2.5 The Stochastic Series Expansion (SSE) Method

The Stochastic Series Expansion (SSE) [8] is a quantum MC simulation scheme for spin and lattice systems. Instead of the Trotter decomposition of the operator $\exp(-\beta\hat{H})$ explained before (see Section 2.2.1), the SSE method uses the power-series expansion of $\exp(-\beta\hat{H})$ to obtain a solution of Eq. (2.9) allowing the calculation of average values with the Metropolis MC method [1]. It is a generalization of the Handscomb's method [27] and it can be applied also when the trace of the Hamiltonian cannot be calculated analytically.

2.5.1 Quantum mechanical stochastic series expansion

In the SSE method the exponential operator in the definition of the partition function (Eq. (2.9)) is estimated as a Taylor expansion and the trace is expressed as a sum over a complete set of states in a suitable basis $|\mathbf{X}\rangle$;

$$Z = \sum_{\{\mathbf{X}\}} \sum_{n=0}^{\infty} \frac{\beta^n}{n!} \langle \mathbf{X} | (-\hat{H})^n | \mathbf{X} \rangle \tag{2.41}$$

Suppose that the Hamiltonian of the system can be written as:

$$\hat{H} = -\sum_{i,j} \hat{H}_{i,j} \tag{2.42}$$

where the index j refers to an operator type *e.g.*, $j = 0$ off-diagonal operator, $j = 1, \ldots, d$, where d is the dimensionality, is a diagonal operator at a lattice site that is the nearest-neighbor of site i and $j = d + 1$ a constant added to the Hamiltonian (see Eqs. (2.47)-(2.50)). The powers of the Hamiltonian are written as a sum over all possible products ("strings") of the operators $\hat{H}_{i,j}$.

$$\begin{aligned} (-\hat{H})^n &= \left(\sum_{i,j} \hat{H}_{i,j} \right)^n = \left(\sum_{i,j} \hat{H}_{i,j} \right)_n \underbrace{\cdots}_{\text{times}} \left(\sum_{i,j} \hat{H}_{i,j} \right) \\ &= \sum_{j_1,i_1} \cdots \sum_{i_n,j_n} \hat{H}_{i_1,j_1} \cdots \hat{H}_{i_n,j_n} = \sum_{\{i_k,j_k\}} \prod_{k=1}^{n} \hat{H}_{i_k,j_k} \end{aligned} \tag{2.43}$$

The operators $\hat{H}_{i,j}$ do not all commute with each other. The order of the operators in the string is therefore important. The Taylor expansion is truncated at some cut-off L which is chosen sufficiently large for the truncation error to be negligible. To simplify the MC sampling it is useful to deal with strings of the same length L. This is done by introducing an identity operator $\hat{H}_{0,0} = 1$ that is not part of the Hamiltonian, written with the same notation as for the other terms of the Hamiltonian, with indices $i = j = 0$. The unit operator $\hat{H}_{0,0}$ is used to increase the length of all the strings with $n < L$, constructing a computationally simpler updating scheme where the operator list has a fixed length L. Allowing for all the $L!/((L-n)!n!)$ possible placements of unit operators in the string and substituting Eq. (2.43)

into Eq. (2.41) the partition function can be written as,

$$Z = \sum_{\{\mathbf{X}\}} \sum_{\mathcal{X}_L} W(\mathbf{X}, \mathcal{X}_L) \tag{2.44}$$

where $\mathcal{X}_L = \{[i_1, j_1], \cdots, [i_L, j_L]\}$ and,

$$W(\mathbf{X}, \mathcal{X}_L) = \frac{\beta^n (L-n)!}{L!} \langle \mathbf{X} | \prod_{k=1}^{L} \hat{H}_{i_k, j_k} | \mathbf{X} \rangle . \tag{2.45}$$

If all terms are positive $W(\mathbf{X}, \mathcal{X}_L)$ can be interpreted as a probability weight and the MC method explained in chapter one can be used to generated configurations distributed with the probability $P(\mathbf{X}, \mathcal{X}_L) = W(\mathbf{X}, \mathcal{X}_L)/Z$. The presence of negative terms is referred to as "sign problem" [24]. Fortunately there are several classes of Hamiltonians for which positive definiteness can be achieved: this is the case of the QIM.

2.5.2 Stochastic series expansion applied to the QIM

The Hamiltonian of the QIM (Eq. (2.7)) in the absence of the parallel magnetic field ($h = 0$) is given by:

$$\hat{H}_{\mathrm{QIM}}^{h=0} = -J \sum_{\langle ij \rangle}^{N} \hat{\sigma}_i^z \hat{\sigma}_j^z - \Gamma \sum_{i=1}^{N} \hat{\sigma}_i^x \tag{2.46}$$

To apply the SSE to this system we need to express the Hamiltonian in the form (2.42). This is done by defining the following operators:

$$\hat{H}_{0,0} = 1, \tag{2.47}$$

$$\hat{H}_{i,0} = \Gamma \hat{\sigma}_i^x = \Gamma(\hat{\sigma}_i^+ + \hat{\sigma}_i^-), \tag{2.48}$$

$$\hat{H}_{i,j} = J(1 + \hat{\sigma}_i^z \hat{\sigma}_j^z), \qquad j = 1, \ldots, d. \tag{2.49}$$

$$\hat{H}_{i,d+1} = \Gamma, \tag{2.50}$$

where $j = 1, \ldots, d$ labels the nearest-neighbors of the spin in site $i = 1, \ldots, N$ located at the positive directions of the system axis, to avoid double counting.

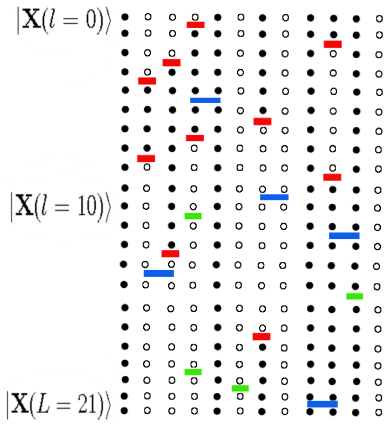

Figure 2.1: An SSE configuration for a 12-site one-dimensional system. Here the truncation $L = 21$, and the expansion order of the term (*i.e.*, the number of Hamiltonian operators present) $n = 20$. The solid and open circles represent the spins $\sigma_i^z(l) = \pm 1$, with the propagation index $l = 0, \ldots, L$ corresponding to the different 12-spin rows. The red and green short horizontal bars represent spin-flip operators $\hat{H}_{i,0}$ and constants $\hat{H}_{i,d+1}$, respectively. The longer blue lines represent Ising operators $\hat{H}_{i,j}$ acting on the spins at the line-ends.

Up to a constant, the Hamiltonian (2.46) can be written as:

$$\hat{H}_{\mathrm{QIM}}^{h=0} = -\sum_{i=1}^{N}\sum_{j=0}^{d+1}\hat{H}_{i,j}. \tag{2.51}$$

The constants $H_{i,d+1}$ are introduced for a practical purpose that will become clear below. Because of the constants added to $\hat{H}_{i,j}$ in (2.49), the eigenvalues of these operators are $2J$ and 0. All non-zero terms in (2.45) are therefore positive and can be used as relative probabilities.

It is useful to define states $|\mathbf{X}(l)\rangle = |\sigma_1^z(l), \ldots, \sigma_N^z(l)\rangle$ obtained by propagating $|\mathbf{X}\rangle = |\mathbf{X}(0)\rangle$ by the first l operators in $\mathcal{X}_L$ (see Eq. (2.44));

$$|\mathbf{X}(l)\rangle = \varrho \prod_{k=1}^{l} \hat{H}_{i_k,j_k} |\mathbf{X}\rangle\,, \tag{2.52}$$

where ϱ is a normalization factor. A non-vanishing matrix element in Eq. (2.45) then corresponds to the periodicity condition $|\mathbf{X}(L)\rangle = |\mathbf{X}(0)\rangle$, which re-

quires that for each site i there is an even number (or zero) of spin flipping operators $\hat{H}_{i,0}$ in $\mathcal{X}_L$. The definition of Eq. (2.49) implies that the Ising operators $\hat{H}_{i,j}$ may act only on states with $\sigma_i^z = \sigma_j^z$ ($\hat{H}_{i,j} = 0$ if $\sigma_i^z \neq \sigma_j^z$). There are no other constraints. A SSE configuration is illustrated in Fig. 2.1. The vertical direction in this representation will be referred to as the SSE *propagation direction*.

Local updates

The sampling of Eq. (2.44) can be carried out using simple operator substitutions of the types

$$\hat{H}_{0,0,l} \longleftrightarrow \hat{H}_{i,j,l} \qquad i,j \neq 0, \tag{2.53}$$

$$\hat{H}_{i,d+1,l_1}\hat{H}_{i,d+1,l_2} \longleftrightarrow \hat{H}_{i,0,l_1}\hat{H}_{i,0,l_2}, \quad i \neq 0, \tag{2.54}$$

where the subscript l indicates the position ($l = 1, \ldots, L$) of the operator in the sequence $\mathcal{X}_L$. The power n is changed by ± 1 in the *diagonal update* (2.53) and is unchanged in the *off-diagonal update* (2.54). In the diagonal update the Ising terms $\hat{H}_{i,j}$ and the constants $\hat{H}_{i,d+1}$ are sampled. The constants are used in the off-diagonal update as a means of achieving easy insertions and removals of two spin-flipping operators $\hat{H}_{i,0}$. With the value Γ chosen for the constant in (2.50), the operator replacements do not change the weight of the SSE configuration and the move is accepted with probability one. However, the off-diagonal update also leads to spin flips in the propagated states between l_1 and l_2; $\sigma_i^z(l_1), \ldots, \sigma_i^z(l_2 - 1) \rightarrow -\sigma_i^z(l_1), \ldots, -\sigma_i^z(l_2 - 1)$. $l_1 > l_2$ also has to be considered, leading to flipped $\sigma_i^z(l_1), \ldots, \sigma_i^z(l - 1)$ $\sigma_i^z(0), \ldots, \sigma_i^z(l_2 - 1) \rightarrow -\sigma_i^z(l_1), \ldots, -\sigma_i^z(L - 1) - \sigma_i^z(0), \ldots, -\sigma_i^z(l_2 - 1)$. The off-diagonal update (2.54) is allowed if (and only if) no Ising operators $\hat{H}_{i,j}$ acting on site i are present in $\mathcal{X}_L$ between positions l_1 and l_2 [9].

The diagonal update (2.53) is attempted successively for all $l = 1, \ldots, L$. In the course of this process, the spin state is propagated by flipping spins σ_i^z as off-diagonal operators $\hat{H}_{i,0}$ are encountered in $\mathcal{X}_L$, so that the states

$|\mathbf{X}(l)\rangle$ are generated successively. For an $\hat{H}_{i,j} \to \hat{H}_{0,0}$ update, *i.e.*, removing a Hamiltonian operator, there are no constraints and the update should be accepted with some non-zero probability [9]. In the case of $\hat{H}_{0,0} \to \hat{H}_{i,j}$, *i.e.*, inserting an operator from the Hamiltonian, there are constraints, and the update may not be allowed for all a, b (*e.g.*, $\sigma_i^z \neq \sigma_j^z$). However, initially it is assumed that any $\hat{H}_{i,j}$ would be allowed. Under this assumption, the acceptance probabilities for the diagonal update are given by

$$P(\hat{H}_{0,0} \to \hat{H}_{i,j}) = \frac{\beta N(\Gamma + 2Jd))}{L - n}, \tag{2.55}$$

$$P(\hat{H}_{i,j} \to \hat{H}_{0,0}) = \frac{L - n + 1}{\beta N(\Gamma + 2Jd)}, \tag{2.56}$$

where $P > 1$ should be interpreted as probability one. These probabilities are simply obtained from the ratio of the new and old prefactor in Eq. (2.45) when $n \to n \pm 1$;

$$\beta^{\pm 1} \frac{[L - (n \pm 1)]!}{(L - n)!}, \tag{2.57}$$

and the ratio between the matrix element 1 for the $\hat{H}_{0,0}$ operator and the total number of possible diagonals operators to choose, N can be chosen with probability Γ and dN with probability $2J$. Staying with the assumption that any $\hat{H}_{i,j}$ is allowed in the update $\hat{H}_{0,0} \to \hat{H}_{i,j}$, the probability of an operator with the first index i is uniform and i can be selected randomly between 1 and N, $P(i) = 1/N$. The relative probability of choosing one of the $d + 1$ operators with the second index $j \neq 0$, given that the index i was already selected, is $P(j) = h_{i,j}/(\Gamma + 2Jd)$, where $h_{i,j}$ is the non-zero matrix element corresponding to $\hat{H}_{i,j}$ (*i.e.*, Γ for $j = 1$ and $2J$ else).

The operator $\hat{H}_{i,j}$ generated as above may or may not be allowed in the current spin configuration $|\mathbf{X}(l)\rangle$. If $\sigma_i^z(l) = \sigma_j^z(l)$, $\hat{H}_{i,j}$ is inserted at position l. Otherwise, the process for generating $\hat{H}_{i,j}$ has to be repeated, until an allowed operator has been generated. The reject-and-repeat step leads to the correct probabilities for selecting among all the allowed diagonal operators $\hat{H}_{i,j}$. Typically, an allowed operator is generated quickly, since the

interactions favor the allowed spin alignment. Note that the constants $\hat{H}_{i,j}$ are always allowed (for $\Gamma > 0$), so there is no risk of a not terminating search [9].

2.6 Wang-Landau Mapping Using the SSE Representation

A convenient ("*state-of-the-art*") route to compute the thermodynamic properties of quantum systems is based on the SSE [8, 9] introduced in section 2.5.1 and involves using a WL approach to reconstruct the coefficients $g(n) = \mathrm{Tr}(-\hat{H})^n$ of a high-temperature expansion of the partition function,

$$Z = \sum_n (\beta^n / n!) g(n). \tag{2.58}$$

Comparing Eqs. (2.58) and (2.44), we see that it is possible to obtain $g(n)$ by counting the number of times a configuration with n nonunit operators is observed during a simulation at an inverse temperature $\beta = 1$ using the WL method (see section 1.6) [10]. The only change is that now in the acceptance probabilities from SSE algorithm (Eqs. (2.55) and (2.56)) we have to set $\beta = 1$ and to include an additional factor $g(n)/g(n')$ for any move that change the number of nonunit operators from n to n' [10]. In the case of the QIM we have:

$$P(\hat{H}_{0,0} \to \hat{H}_{i,j}) = \frac{g(n) N (\Gamma + 2Jd)}{g(n+1)(L-n)}, \tag{2.59}$$

$$P(\hat{H}_{i,j} \to \hat{H}_{0,0}) = \frac{g(n)(L-n+1)}{N g(n-1)(\Gamma + 2Jd)}, \tag{2.60}$$

This method is efficient because, to obtain the partition function of a quantum system, we just have to reconstruct a one-dimensional function $g(n)$, contrary to the previous case where a two-dimensional density of states $g(V, K)$ had to be found (see section 2.4). Nevertheless the SSE approach is particularly suited to treat quantum spin systems and other lattice quantum

problems, but is in general not straightforward, for instance, for quantum problems on the continuum, where the matrix elements required for the SSE can not be easily computed.

2.7 Extension of the Metadynamics-Based MC Method to Quantum Systems

Given the classical-like PI expression for the partition function of a quantum model, for instance the QIM case $Z \approx \sum_{\overline{\mathbf{X}}} e^{-\beta A(\overline{\mathbf{X}})}$, see Eq. (2.20), we first define a small number a of CVs $s_i(\overline{\mathbf{X}})$, $i = 1 \dots a$, which appear in the action $A(\overline{\mathbf{X}}) = A(\mathbf{s}(\overline{\mathbf{X}}))$: in the QIM case there are three physically meaningful CVs (see section 2.3), the potential energy $s_1 = V$, the kinetic energy $s_2 = K$ and the magnetization $s_3 = M$, in terms of which the action is $\overline{A}(\mathbf{s}) = N\left[JV + J^{\perp}K - hM - (Q/\beta)\ln C\right]$ (see Eq. (2.39)).

Next, we perform a Metropolis walk in configuration space $\{\overline{\mathbf{X}}\}$ in which the transition probability from $\overline{\mathbf{X}}$ to $\overline{\mathbf{X}}'$ is modified adding to the action a history-dependent potential $V_G(\mathbf{s}(\overline{\mathbf{X}}), t)$:

$$P_A(\overline{\mathbf{X}} \to \overline{\mathbf{X}}', t) \equiv \min\left[1, e^{-\beta\left(\Delta A(\overline{\mathbf{X}}) + \Delta V_G(\overline{\mathbf{X}}, t)\right)}\right] \tag{2.61}$$

where $\Delta A(\overline{\mathbf{X}}) = A(\overline{\mathbf{X}}') - A(\overline{\mathbf{X}})$ is the change in action and $\Delta V_G(\overline{\mathbf{X}}, t) = V_G(\mathbf{s}(\overline{\mathbf{X}}'), t) - V_G(\mathbf{s}(\overline{\mathbf{X}}), t)$ is the change in the history-dependent potential. Whether or not a move is accepted, we update V_G by adding to it a small localized repulsive potential (a Gaussian in normal metadynamics [5]).

We store the potential V_G by grid-discretizing the CVs-space and keeping track of $V_G(\mathbf{s}^k, t)$ only at grid points $\mathbf{s}^k$. Then, to speed up the calculation and avoid systematic errors near the boundary we use a non-uniform grid (see Fig.2.2). Far from the boundary we use a coarse grid while near the boundaries we use a grid including all the possible discrete values of the CVs.

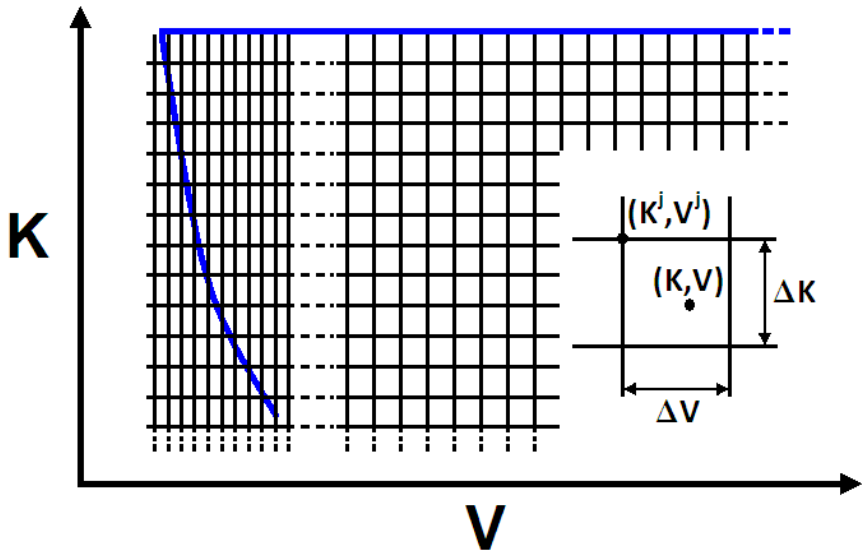

Figure 2.2: Grids used to store the history-dependent potential V_G in the kinetic K and potential V energy space. A thinner grid in V direction is used near the curved boundary.

As an example in Fig.2.2 we show a diagram of the grids used for the CVs K and V. As can be seen the boundary of the CVs space is not straight in the K direction making the application of the method explained in the previous chapter difficult. Here we have the advantage that during the simulation the variation of K was small $0.8 < K \leq 1.0$ and we use a grid including all the possible values of K. In the V direction instead we use a grid spacing of 10 energy levels far from the boundaries $-1.8 < V < 1.8$ and thinner grid of 1 energy level near the boundaries $-2 < V < -1.8$ and $1.8 < V < 2$. The value of V_G at a generic point $\mathbf{s}(\overline{\mathbf{X}})$ is then calculated by a linear interpolation:

$$V_G(\mathbf{s}(\overline{\mathbf{X}}),t) = \sum_{j=1}^{2^a} V_G(\mathbf{s}^j,t) \prod_{i=1}^{a} \left(1 \pm \frac{s_i^j - s_i(\overline{\mathbf{X}})}{\Delta s_i}\right) \tag{2.62}$$

where the $(+)$ sign is used if $s_i^j \leq s_i(\overline{\mathbf{X}})$ and the $(-)$ sign otherwise, Δs_i is the spacing of the grid in the s_i direction and $\mathbf{s}^j$, $j = 1, 2, \ldots, 2^a$ are the points of the grid nearest-neighbors of $\mathbf{s}(\overline{\mathbf{X}})$ (see Fig.2.2). In this scheme,

the potential V_G is updated on the neighboring grid-points $\mathbf{s}^j$ as:

$$V_G(\mathbf{s}^j, t+1) = V_G(\mathbf{s}^j, t) + w \prod_{i=1}^{a} \left(1 \pm \frac{s_i^j - s_i(\overline{\mathbf{X}})}{\Delta s_i} \right) , \qquad (2.63)$$

where w is a parameter that determines the speed of the free energy reconstruction. Therefore, like in WL, the acceptance changes every time a move is accepted or rejected, and the "walk" in configuration space is intrinsically non-Markovian (it depends on the history). At the beginning of the simulation the potential $V_G(\mathbf{s}^{(k)}, t = 0)$, stored on the grid, is set to zero. Then, as the system moves in configuration space, V_G is updated at each move as in Eq. (2.63).

After a sufficient time, V_G will approximately compensate the underlying F profile [6]. As shown in the previous chapter a further improvement can be obtained by taking as estimator of the F not just a single profile V_G, but the arithmetic average of all the profiles $\overline{V_G}(s,t)$ between a "filling" time t_F and the total simulation time t_{tot} (see Eq. (1.36)). This reduces the error of the method, which drops fast to zero for large $t_{tot} - t_F$ as $\varepsilon \sim 1/\sqrt{t_{tot} - t_F}$ [15].

2.8 Results and Discussion

Fig. 2.3 shows $F(M)$ for the QIM on a 8×8 lattice ($N = 64$ spins), with $Q = 30$ Trotter slices at two different points in parameter space. The agreement between the reference $F(M)$ and that calculated from $F(V, K, M)$ is good, even if we extrapolate the $F(V, K, M)$ from the ordered to the disordered side (or viceversa) of the phase transition line. Thus with a single calculation of $F(V, K, M)$ at a point (T, Γ, h) in parameter space, we can get reliable information for $F(V, K, M)$ in a whole neighborhood of that point (see inset). As a reference for the comparison we use the results of an accurate umbrella sampling calculation (see section 1.5) [14].

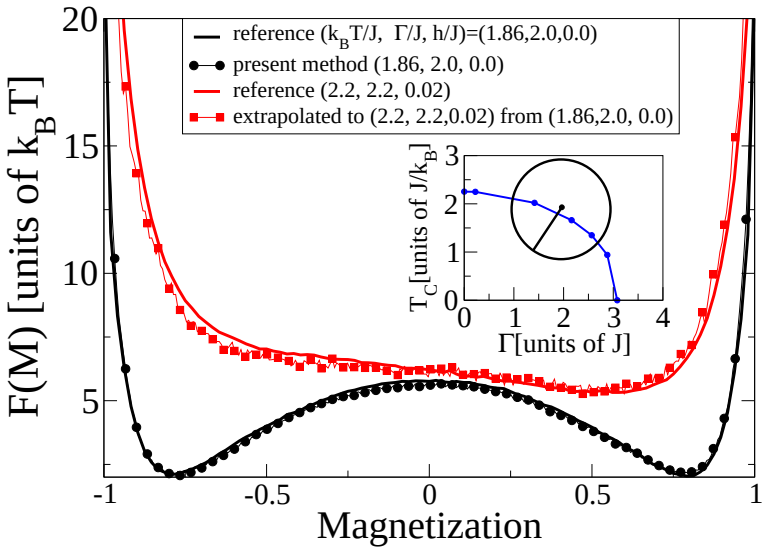

Figure 2.3: Free energy profile for the 8×8 QIM, as a function of the magnetization for two different set of parameters. The results at $(k_BT = 1.86, \Gamma = 2.0, h = 0)$ (in units of J) were obtained by first calculating $F(V, K, M)$, and then performing a logarithmic integration, Eq. (2.34), to calculate $F(M)$. The results at $(k_BT = 2.2, \Gamma = 2.2, h = 0.02)$ were instead obtained by extrapolating the previous $F(V, K, M)$ using Eqs. (2.31)-(2.33), and then integrating to obtain $F(M)$. As a reference for the comparison we use the results of an accurate umbrella sampling calculation [14] (solid line). The inset shows the phase diagram of the model and the circle represents the size of the extrapolation region.

To test the efficiency of the proposed method we compare it with a SSE-WL simulation [10, 9], as well as with a direct application of WL to PIMC in which the two-dimensional $g(V, K)$ is calculated.

For the same system of Fig. 2.3 we estimate T_c (conventionally defined as the temperature at which the specific heat, $C_v = \beta(\langle E^2\rangle - \langle E\rangle^2)/T$, reaches its maximum value) as a function of the MC time with the three methods. The results are shown in Fig. 2.4. As a reference, we also computed T_c by a very long PIMC calculation (red line with error bars in Fig. 2.4).

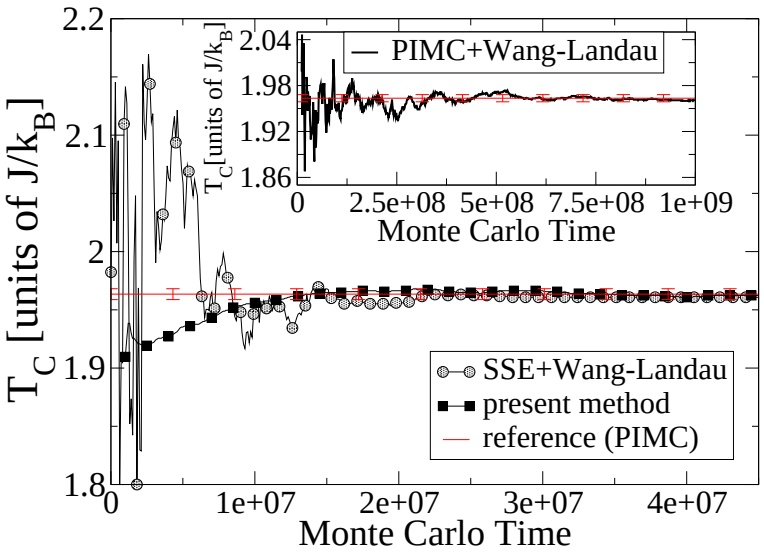

Figure 2.4: Critical temperature (T_c) for a 8×8 QIM, as a function of the MC time, calculated using three different methods: SSE-WL (solid circles), our method (solid squared) and the PIMC-WL algorithm (inset). The reference (red line with error bars) is obtained by a long PIMC simulation.

In the SSE+WL calculation the histogram is considered "flat" when for all the values of n the histogram is larger than 95 % of its average [28] (the limit of 80 % suggested in Ref [2] leads, for this specific system, to systematic errors, data not shown). Instead, for PIMC-WL the 80 % limit is sufficient to reach convergence. The specific heat for our method was calculated computing a $F(V, K)$ at $k_B T/J = 1.8$ and $\Gamma/J = 2.0, h/J = 0.0$ and extrapolating in temperature according to Eq. (2.31). The grid spacing in the V and K directions was of 10 and 1 energy levels respectively. However we needed a finer grid spacing of 1 also for V for states too close to the parameter boundary values $V \approx -2$ or $V \approx 2$, where systematic errors may otherwise arise (see sections 1.9 and 2.7).

In order to extrapolate the free energy in a meaningful temperature interval $\Delta T \sim \pm J/k_B$ including the peak of the specific heat, it is necessary to obtain

quickly a large maximum value of $V_G \sim 80 k_B T/J$ for the system considered here. This is accomplished by starting the simulation with $w = 8 \cdot 10^{-3}$ and decreasing it up to 10^{-4} in $2 \cdot 10^6$ MC steps (t_F in Eq. (1.36)), then w is not changed anymore, and the free energy is estimated using Eq. (1.36). It is clear from the previous discussion that the optimal "filling" protocol is system-dependent.

As shown in Fig. 2.4, using our approach we can obtain T_c within the PIMC error bar, with an efficiency similar to the SSE+WL algorithm. The PIMC+WL method is, by comparison, an order of magnitude slower (Fig. 2.4, inset). The efficiency of the approach presented here is strongly influenced by the temperature where the reconstruction is performed, which should not be too far from T_c ($\sim 10\%$ smaller in our example). However, T_c can always be estimated *approximately, e.g.*, by performing a preliminary calculation on a system of smaller size.

Fig. 2.5 shows the specific heat as a function of T for a larger system, $N = 32 \times 32$, with $Q = 100$ Trotter slices, calculated with PIMC and with the present method. Also in this case we computed $F(V, K)$ and extrapolated in temperature according to Eq. (2.31), with a grid spacing of 150 and 10 energy levels in V and K directions respectively (no need to reduce the grid spacing near the parameter boundaries since the free energy is very high there, more than 300 $k_B T$ bigger than the value on the minimum). In this case w was decreased from 10^{-1} to 5×10^{-3} in 1.1×10^6 MC steps. After this time the free energy was estimated using Eq. (1.36). As shown in Fig. 2.5, our approach reproduces the specific heat accurately between 1 and $3 k_B T/J$. In the inset we show how T_c converges as a function of the MC time. Remarkably, even for this much larger 32×32 system the convergence of T_c needs roughly the same order of magnitude of MC steps of those needed for the small 8×8 system: thus, the computational cost grows only linearly with the system size.

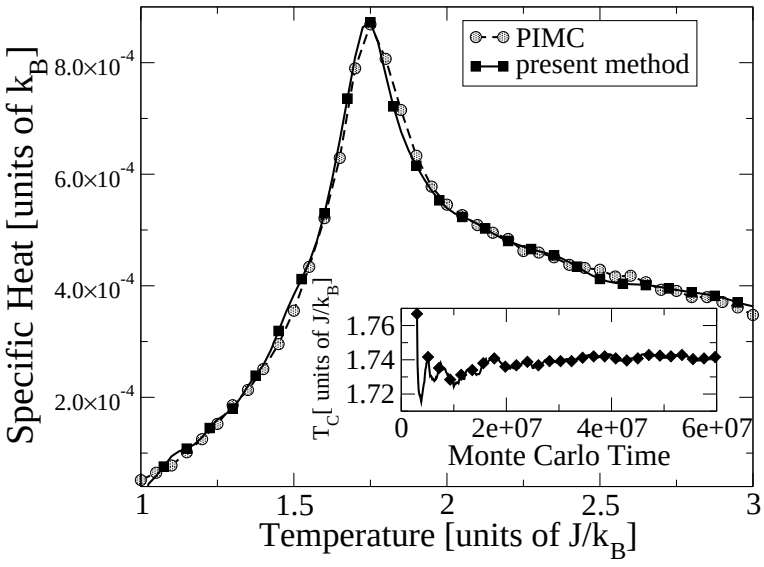

Figure 2.5: Specific heat as a function of the temperature for the 32×32 QIM using two different methods, the PIMC technique (solid circles) and the proposed method (solid squares). The inset shows how the estimate of T_c evolves as a function of the MC time using the present scheme.

In conclusion, we introduced an efficient history-dependent Monte Carlo scheme to calculate the free energy landscape of quantum systems in an accurate manner. The proposed approach was tested on a two-dimensional quantum Ising model, where we reconstruct the free energy as a function of two and three collective variables. This allows reproducing the thermodynamic properties in a whole neighborhood of the point in parameter space at which the calculation is performed. The number of MC steps that are necessary to estimate T_c grows only linear with the system size. The efficiency in estimating T_c is similar to that of SSE+WL, the state-of-the-art approach. Based on path-integral MC, our method can however be directly applied to continuous, off-lattice quantum problems, where SSE would be harder to implement.

Chapter 3

Re-entrant Phase Line in Solid Hydrogen Deuterium

3.1 Introduction

The solid hydrogen compounds H_2, D_2 and HD are quantum molecular solids that exhibit complex phase diagrams in which the symmetry of the low-pressure quantum rotor states of the molecules gives way to a high-pressure anisotropic molecular crystal phase, generally called the "broken symmetry phase" (BSP) [16],[17],[18]. In hydrogen and deuterium the transition pressure of the BSP line increases with increasing temperature [17],[16] and is well understood (see Fig. 3.1 (a)). In HD this line is re-entrant and the transition pressure first decreases and then increases with increasing temperature (see Fig. 3.1 (b)) [18]; this behavior is still in need of quantitative and qualitative understanding. Existing theoretical studies of the re-entrant behavior of the BSP have been mainly done within the mean-field approximation [19],[20]. A recent attempt to study the re-entrant behavior in solid HD using standard path integral Monte Carlo (PIMC) was made in Ref. [21] where the authors consider asymmetric rotors with centers fixed on a face centered cubic (FCC) lattice and the electronic quadrupole-quadrupole interaction as the anisotropic interaction potential. The results were only of

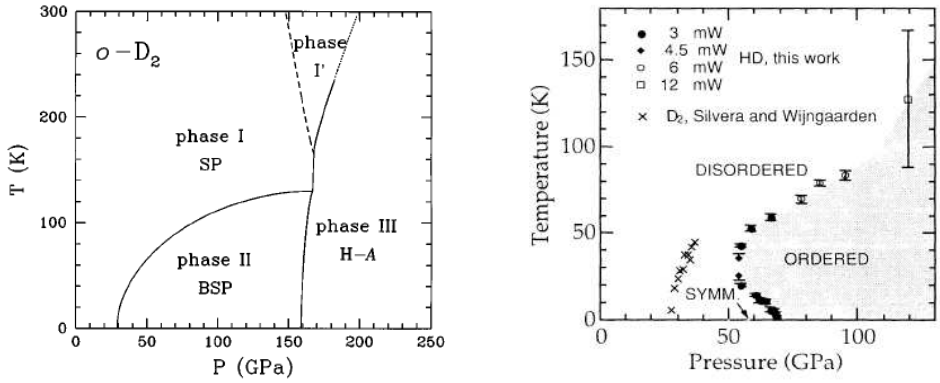

(a) Fig.1 of Ref. [22]. Schematic experimental phase diagram for *ortho*-D_2.

(b) Fig.2 of Ref. [18]. The phase line for orientational order in HD.

Figure 3.1: Phase diagrams of (a) *ortho*-D_2 and (b) HD

qualitative value.

In this chapter we address this problem using a more accurate approach. We start describing the interaction potential of two isolated H_2 molecules, and how to use this pair potential in the molecular solid. We develop the theory of path integral (PI) representation of rotors, considering in particular the constant-pressure ensemble where temperature and pressure are controlled parameters, while the volume is calculated directly in the equilibrated simulation cell. The isotropic part of the interaction potential is tested by reproducing, within PIMC, the well known *ortho*-D_2 (see Appendix C) equation of state.

Finally we apply our metadynamics-based MC method to the HD system in the hexagonal closed-packed (HCP) lattice to find the classical configuration of the molecules for which the interaction potential energy is minimum, obtaining a new structure with the same characteristics of the result given earlier by Surh *et al.*, [22] but with different molecular orientations. Before applying our metadynamics-based MC method to the quantum solid HD we calculate the re-entrant phase line of the BSP to test both our PIMC algo-

rithm and the interaction potential between the molecules. This calculation is done by using two order parameters, a lattice biased order parameter where the new structure is used as reference, and an order parameter related to the quadrupolar tensor of a single molecule. We obtain the unusual re-entrant behavior of the phase line at a pressure of $\approx$ 65 GPa for an HCP lattice, close to the experimental value. The stage is now ready for the application of the proposed metadynamics-based MC method to calculate the free energy of this quantum system: this future study will shed light on the physics of the quantum rotational melting at the physical root of the re-entrance in the phase diagram.

3.2 The Pair Interaction Potential

The interaction potential between two hydrogen molecules H_2 - H_2 can be written as [29]:

$$\begin{aligned} V^{pair}(\mathbf{r}_1,\mathbf{r}_2,\mathbf{R}_{12}) &= \sum_{l_1,l_2,l} B_{l_1 l_2 l}(r_1,r_2,R_{12}) \sum_{\xi_{l_1},\xi_{l_2},\xi_l} (l_1,\xi_{l_1},l_2,\xi_{l_2}|l_1,l_2,l,\xi_l) \times \\ &\times\ Y_{l_1}^{\xi_{l_1}}(\mathbf{r}_1) Y_{l_2}^{\xi_{l_2}}(\mathbf{r}_2) Y_l^{\xi_l *}(\mathbf{R}_{12}) \end{aligned} \tag{3.1}$$

where $(l_1,\xi_{l_1},l_2,\xi_{l_2}|l_1,l_2,l,\xi_l)$ are the Clebsch-Gordan coefficients [30], $\mathbf{r}_1,\mathbf{r}_2$ specify the relative coordinates of the diatomic molecules, $\mathbf{R}_{12}$ connects the midpoints between two nuclei in the two molecules, r_1, r_2, R_{12} are respectively their modulus value (see Fig. 3.2) and (*) means complex conjugate. This formula is obtained by expansion of the function $1/r$ in terms of spherical harmonics and considering the symmetry of the system [31]. In the sum only terms with $\xi_{l_1} = -\xi_{l_2} = \xi$ occur due to the invariance of the interaction energy under rotations. The sum in Eq. (3.1) is also restricted to even values of l_1 and l_2 provided R_{12} connects the midpoints of the molecules as in Fig. 3.2 [30].

Generally $V^{pair}(\mathbf{r}_1,\mathbf{r}_2,\mathbf{R}_{12})$ is written as the sum of an isotropic and anisotropic

potential:

$$V^{pair}(\mathbf{r}_1, \mathbf{r}_2, \mathbf{R}_{12}) = V^{pair}_{iso}(R_{12}) + V^{pair}_{ani}(\mathbf{r}_1, \mathbf{r}_2, \mathbf{R}_{12}). \tag{3.2}$$

In the ground state of low-pressure solid H_2, molecules are in the rotational state $l = 0$ or $l = 1$ (see Appendix C) and matrix elements of V^{pair} within the ground manifold vanish for terms with l_1 or $l_2 > 2$: then just six terms mainly contribute to Eq. (3.1), the isotropic potential V^{pair}_{iso} ($l_1 = l_2 = l = 0$) and five terms corresponding to V^{pair}_{ani} [32]. In the Eq. (3.1) $V^{pair}_{iso}(R_{12}) = B_{0,0,0}(R_{12})$ is the leading term in this expansion and does not depend on the orientation of the molecules because $Y_{0,0}$ is a constant. The anisotropic part of the potential V^{pair}_{ani} is calculated by using all the others terms in the expansion that can be written as follows:

Two identical terms corresponding to $l_1 = 2$, $l_2 = 0$ and $l = 2$ or $l_1 = 0$, $l_2 = 2$ and $l = 2$ ($B_{202} = B_{022}$),

$$V^{int} = B_{202}(r_1, r_2, R_{12}) Y^0_0 Y^0_2(\mathbf{R}_{12})(Y^0_2(\mathbf{r}_1) + Y^0_2(\mathbf{r}_2)) \tag{3.3}$$

This term arises from the sum of the interaction between an anisotropic charge distribution (Y^0_2) on one molecule with the spherical part (Y^0_0) of the other. The remaining three terms arise from charge overlap and exchange referred to as valence forces:

$$V^v = B_{220}(r_1, r_2, R_{12}) Y^0_0(\mathbf{R}_{12}) \sum_{\xi_{l_1}, \xi_{l_2}} (2, \xi_{l_1}, 2, \xi_{l_2} | 2, 2, 0, 0) Y^{\xi_{l_1}}_2(\mathbf{r}_1) Y^{\xi_{l_2}}_2(\mathbf{r}_2), \tag{3.4}$$

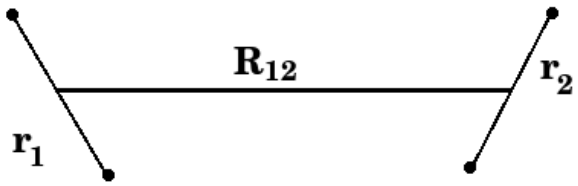

Figure 3.2: The standard set of variables for a pair of homonuclear, diatomic molecules.

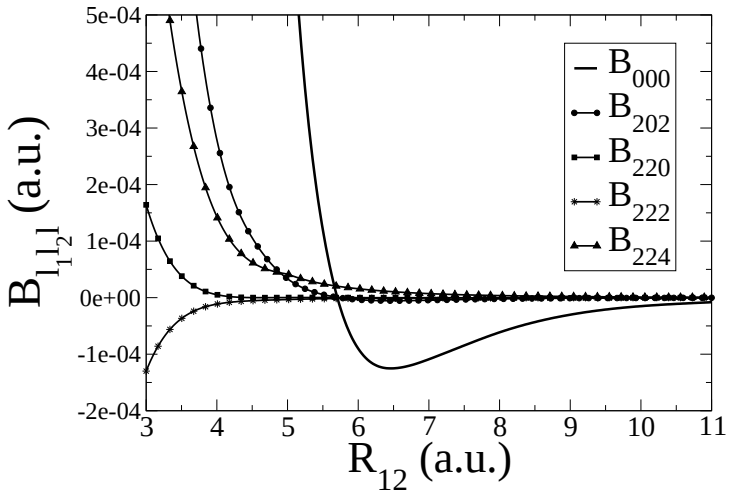

Figure 3.3: The relevant coefficients ($B_{l_1 l_2 l}$) of the gas pair potential (V^{pair}) of Ref [32] as a function of the intermolecular separation R_{12} for r_1 and r_2 fixed at the ground state vibrationally averaged distance ($r_0 = 1.449$ a.u.). See also Ref. [33]

.

anisotropic forces:

$$V^{anf} = B_{222}(r_1, r_2, R_{12}) \sum_{\xi_{l_1}, \xi_{l_2}, \xi_l} (2, \xi_{l_1}, 2, \xi_{l_2} | 2, 2, 2, \xi_l) Y_2^{\xi_{l_1}}(\mathbf{r}_1) Y_2^{\xi_{l_2}}(\mathbf{r}_2) Y_2^{\xi_l *}(\mathbf{R}_{12}), \tag{3.5}$$

and the permanent electric quadrupole-quadrupole (EQQ) interactions [29]:

$$V^{EQQ} = B_{224}(r_1, r_2, R_{12}) \sum_{\xi_{l_1}, \xi_{l_2}, \xi_l} (2, \xi_{l_1}, 2, \xi_{l_2} | 2, 2, 4, \xi_l) Y_2^{\xi_{l_1}}(\mathbf{r}_1) Y_2^{\xi_{l_2}}(\mathbf{r}_2) Y_4^{\xi_l *}(\mathbf{R}_{12}). \tag{3.6}$$

The most recent calculation of the pair potential coefficients $B_{l_1,l_2,l}$ reported in the literature is by Diep *et al.*, [34]. The isotropic potential B_{000} and leading coefficients of the anisotropic potential, (B_{224} Eq. (3.6), $B_{202} = B_{022}$ Eq. (3.3), see also Fig. 3.3) were accurately calculated using first principles [34]. The remaining coefficients (B_{220} Eq. (3.4) and B_{222} Eq. (3.5)) were reported by others authors [32], [35]. In Fig. 3.3 we plot the relevant coeffi-

cients ($B_{l_1 l_2 l}$) of the pair potential (V^{pair}) reported by Burton *et al.*, Ref [32], as a function of the intermolecular separation R_{12} for r_1 and r_2 fixed at the ground state vibrationally averaged distance ($r_0 = 1.449$ a.u.) see also Refs. [33],[34], [36]. From the figure we can see that the EQQ contribution B_{224} is the anisotropic leading coefficient at low pressures but at high pressures the anisotropic interaction coefficient B_{202} takes over.

3.3 The Solid Isotropic Interaction Potential

Before starting the calculations using the PIMC method, to obtain the phase diagram of HD, we need a reliable interaction potential between the molecules in the solid phase $V^s = V^s_{iso} + V^s_{ani}$. In the literature most of the semi-empirical forms of the isotropic components (V^s_{iso}) that have been established for solid hydrogen are of the Lennard-Jones type [29]. In case of low pressure, Silvera [29] recommended the use of the potential proposed by Silvera and Goldman [37] $V^{SG}(R_{12})$ given by the equation:

$$V^{SG}(R_{12}) = \exp\left[\eta - \vartheta R_{12} - \nu R_{12}^2\right] - \Upsilon(R_{12}) \left(\sum_{i=6,8,10} \frac{C_i}{R_{12}^i} - \frac{C_9}{R_{12}^9} \right) \quad (3.7)$$

with

$$\begin{aligned} \Upsilon(R_{12}) &= \exp\left[-\left(\frac{1.28 R_m}{R_{12}} - 1 \right)^2 \right] \text{ for } \quad \mathrm{R_{12} < 1.28 R_m} \\ &= 1 \qquad\qquad\qquad\qquad\quad \text{for } \quad \mathrm{R_{12} > 1.28 R_m} \end{aligned}$$

Table 3.1: Parameters values (in atomic units) for the isotropic part of the interaction potential between two H_2 molecules, from Ref. [37] and Ref. [38].

η	ϑ	ν	C_6	C_8	C_9	C_{10}	R_m
1.713	1.5671	0.00993	12.14	215.2	143.1	4813.9	6.444

a_1	a_2	R_c
4.213×10^{-4}	-8.045×10^{-5}	5.291

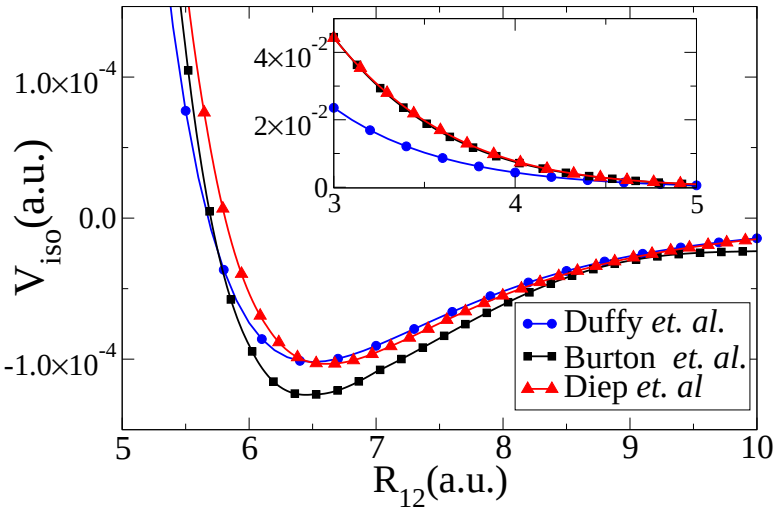

Figure 3.4: The isotropic potential for the solid hydrogen (V^s_{iso}) given by Eq.(3.8) [38] (circles) together with the isotropic pair interaction potential reported by Burton *et al.* ($B^{\rm Burton}_{000}$), Ref. [32] (squares) and by Diep *et al.* ($B^{\rm Diep}_{000}$), Ref. [34] (triangles). Inset repulsive part of the previous potentials.

where the parameters values are given in Table 3.1 and R_m is the potential minimum when $C_9 = 0$ [37]. This potential is designed to represent pair interactions plus many-body effects, accounted for by the C_9 term [29],[37].

To fit high pressure thermodynamic data Hemley *et al.*, [39] showed that additional corrections to the potential V^{SG} are needed. In particular, they found that the V^{SG} potential needs to be softened even more in the dense solid environment, due to enhanced many-body short-range contributions. Based on this correction, Duffy *et al.*, [38] developed a new form of the isotropic potential that fit both static compression and sound velocity data [38]. They proposed an *ad-hoc* short-range correction to the V^{SG} potential

of the form,

$$\begin{aligned} V^s_{iso}(R_{12}) &= V^{SG}(R_{12}) + V^{SR}(R_{12}) \qquad \text{where} \qquad (3.8) \\ V^{SR}(R_{12}) &= a_1(R_{12}-R_c)^3 + a_2(R_{12}-R_c)^6 \quad R_{12} \le R_c \\ &= 0 \qquad\qquad\qquad\qquad\qquad\quad R_{12} > R_c \qquad (3.9) \end{aligned}$$

with parameter values for this correction also listed in Table 3.1 [38].

In Fig. 3.4 we plot the isotropic potential for solid hydrogen V^s_{iso} given by Eq. (3.8) (circles) together with the isotropic pair interaction potential reported by Burton *et al.* (B^{Burton}_{000}), Ref. [32], (squares) and by Diep *et al.* (B^{Diep}_{000}), Ref. [34], (triangles). The well depth for V^s_{iso} and B^{Diep}_{000}, are very similar, while B^{Burton}_{000} has a deeper well. As we can see, V^s_{iso} is less repulsive than the isotropic pair interaction potentials (see Inset).

3.4 The Solid Anisotropic Interaction Potential

The anisotropic terms of the interaction potential have been subject of considerably less work. Since their contribution is negligible in low-pressure solids, their values cannot be directly tested against available experimental data. Within the Born-Oppenheimer approach, the local density approximation (LDA) can be used to calculate the total energy of any static ionic configuration and thus provide an effective potential for the molecules. However *ab initio.* total-energy calculations are too lengthy and their use in a PIMC simulation is inefficient. To avoid these problems some approximations for the interaction potential are necessary. For example in Ref. [40] it is shown that a density dependent renormalization of the gas pair potential V^{pair} [35], [33], [32].

$$V^s_{\text{Runge}}(\mathbf{r}_i, \mathbf{r}_j, \mathbf{R}_{ij}) \approx \eta \sum_{i<j} V^{pair}(\mathbf{r}_i, \mathbf{r}_j, \mathbf{R}_{ij}), \qquad (3.10)$$

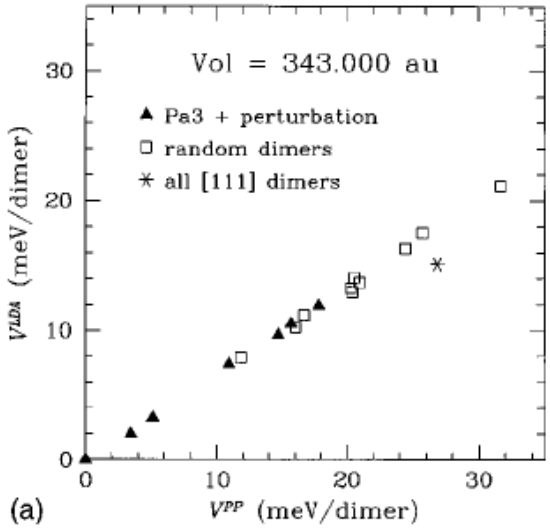

Figure 3.5: Fig.2 (a) of Ref. [22]. Comparison between total energies calculated using LDA (V^{LDA}) *vs.*, the LDA pair potential ($V^s_{Runge} = V^0$ Eq. (3.10)) of Ref. [35], [33], [32].

where $\eta \approx 0.61 + 0.31(R_{nn}/R^0_{nn} - 0.5)$, fits the LDA total energies results for a wide range of pressures on an FCC lattice (see Fig. 3.5). Here R^0_{nn} and R_{nn} are the nearest-neighbor distances at zero pressure and at pressure p, respectively. With this potential Runge *et al.* in Ref. [40] calculates the phase diagram of H_2 and D_2 in the fixed center rigid rotor approximation obtaining good agreement with the experiment for the D_2 phase line on an FCC lattice at low temperatures ($T < 50$K). The proposed potential was also used in Ref. [41] including the translational part of the Hamiltonian, with the difference that the authors of Ref. [41] uses V^s_{iso} for the isotropic part of the interaction potential, that is:

$$V^s_{\text{Cui}}(\mathbf{r}_i, \mathbf{r}_j, \mathbf{R}_{ij}) = V^s_{iso}(R_{12}) + \eta \sum_{i<j} V^{pair}_{ani}(\mathbf{r}_i, \mathbf{r}_j, \mathbf{R}_{ij}). \tag{3.11}$$

reporting in this manner the H_2 and D_2 phase line in the high temperature region ($T > 50$K) for an HCP lattice [41].

3.5 Path Integral Representation of Rotors

The Hamiltonian for Hydrogen-like molecular solids (*para*-H_2, *ortho*-D_2, HD see Appendix C) in the rigid-rotor approximation where the molecules have just translational and rotational degrees of freedom can be written as a sum of two terms:

$$\hat{H} = \hat{K} + \hat{V} \tag{3.12}$$

$$\hat{K} = K^{tra} + K^{rot} = -\lambda \sum_{i=1}^{N} \hat{\nabla}^2_{\mathbf{R}_{CM_i}} + B \sum_{i=1}^{N} \hat{L}_i^2 \tag{3.13}$$

$$\hat{V} = \sum_{i<j} V^s(\mathbf{\Omega}_i, \mathbf{\Omega}_j, \mathbf{R}_{CM_i}, \mathbf{R}_{CM_j}) \tag{3.14}$$

where N is the number of molecules, $\lambda = \frac{\hbar^2}{2M_T}$ with M_T the total mass of the molecule. $B = \frac{\hbar^2}{2\mathcal{I}}$ is the rotational constant with $\mathcal{I}$ the molecular moment of inertia, $\hat{\nabla}^2$ is the Laplacian operator, $\hat{L}$ is the angular momentum operator, $\mathbf{R}_{CM_i} = (m_2\mathbf{r}_{2i} + m_1\mathbf{r}_{1i})/M_T$ is the position of the center of mass of the ith molecule, $\mathbf{\Omega}_i = (\phi_i, \theta_i)$ and ϕ_i, θ_i are respectively the azimuth and inclination angles in a spherical coordinate system centered in one of the atoms of the molecule.

To obtain the PI representation we shall work in the *position basis* where the *particles are labeled*. Let us introduce the eigenstates of the position operator $\hat{\mathbf{R}}$, which form a complete, orthonormal set:

$$\hat{\mathbf{R}} \left|\mathbf{R}\right\rangle = \mathbf{R} \left|\mathbf{R}\right\rangle, \qquad \left\langle \mathbf{R}' \right| \left.\mathbf{R}\right\rangle = \delta(\mathbf{R}' - \mathbf{R}), \qquad \int d\mathbf{R} \left|\mathbf{R}\right\rangle \left\langle \mathbf{R}\right| = 1,$$

where $\mathbf{R} = \{\mathbf{R}_{CM_{i=1,\ldots,N}}, \mathbf{\Omega}_{i=1,\ldots,N}\}$. The density matrix operator $e^{-\beta\hat{H}}$ in the

position basis takes the form:

$$\begin{aligned}\rho(\mathbf{R}',\mathbf{R},\beta) &= \langle\mathbf{R}'|\, e^{-\beta\hat{H}}\,|\mathbf{R}\rangle\,. \\ &= \langle\mathbf{R}'|\, e^{-\beta\hat{H}} \underbrace{\sum_{\gamma} |\gamma\rangle\,\langle\gamma|}_{=1}\,|\mathbf{R}\rangle \\ &= \sum_{\gamma} e^{-\beta E_\gamma}\langle\gamma\,|\mathbf{R}\rangle\,\langle\mathbf{R}'|\,\gamma\rangle, \end{aligned} \tag{3.15}$$

where E_γ is the value of the energy eigenstate $|\gamma\rangle$. Putting $\mathbf{R}' = \mathbf{R}$ and integrating over $\mathbf{R}$, we get:

$$\int d\mathbf{R}\,\rho(\mathbf{R},\mathbf{R},\beta) = \sum_{\gamma} e^{-\beta E_\gamma} \underbrace{\langle\gamma|\int d\mathbf{R}\,|\mathbf{R}\rangle\,\langle\mathbf{R}|\,|\gamma\rangle}_{=1} = Z. \tag{3.16}$$

In the position representation the expectation value of any physical observable O becomes:

$$\langle\hat{O}\rangle = Z^{-1}\int d\mathbf{R}'d\mathbf{R}\,\rho(\mathbf{R}',\mathbf{R},\beta)\,\langle\mathbf{R}'|\,\hat{O}\,|\mathbf{R}\rangle\,. \tag{3.17}$$

The PI formula is derived by using the product property Q times (see section 2.2.1). Then from Eq. (2.2) we have:

$$\rho(\mathbf{R}',\mathbf{R},\beta) = \langle\mathbf{R}'|\left(e^{-\tau\hat{H}}\right)^{Q}|\mathbf{R}\rangle = \langle\mathbf{R}'|\underbrace{e^{-\tau\hat{H}}\cdots e^{-\tau\hat{H}}}_{Q\ \text{times}}|\mathbf{R}\rangle\,.$$

where $\tau = \beta/Q$ is the *time step*. Inserting again a complete set of states between each exponential, we obtain:

$$\begin{aligned}\rho(\mathbf{R}';\mathbf{R},\beta) &= \langle\mathbf{R}'|\, e^{-\tau\hat{H}}\int d\mathbf{R}_{Q-1}\,|\mathbf{R}_{Q-1}\rangle\,\langle\mathbf{R}_{Q-1}|\, e^{-\tau\hat{H}}\cdots \\ &\qquad \cdots\int d\mathbf{R}_1\,|\mathbf{R}_1\rangle\,\langle\mathbf{R}_1|\, e^{-\tau\hat{H}}\,|\mathbf{R}\rangle \\ &= \int d\mathbf{R}_1\cdots d\mathbf{R}_{Q-1}\,\langle\mathbf{R}'|\, e^{-\tau\hat{H}}\,|\mathbf{R}_{Q-1}\rangle\cdots \\ &\qquad \cdots\langle\mathbf{R}_1|\, e^{-\tau\hat{H}}\,|\mathbf{R}\rangle \\ &\equiv \int d\mathbf{R}_1\cdots d\mathbf{R}_{Q-1}\rho_{\mathbf{R}_0,\mathbf{R}_1}\cdots\rho_{\mathbf{R}_{Q-1},\mathbf{R}_Q}, \end{aligned} \tag{3.18}$$

where we have defined $\rho_{\mathbf{R}_{q-1},\mathbf{R}_q} = \rho(\mathbf{R}_{q-1},\mathbf{R}_q,\tau)$, with $\mathbf{R}_0 = \mathbf{R}$, $\mathbf{R}_Q = \mathbf{R}'$ and $\mathbf{R}_q = \{\overline{\mathbf{R}}_{CM_q}, \overline{\mathbf{\Omega}}_q\}$ with $\overline{\mathbf{R}}_{CM_q} = \{\mathbf{R}_{CM_{i=1,\ldots,N,q}}\}$ and $\overline{\mathbf{\Omega}}_q = \{\mathbf{\Omega}_{i=1,\ldots,N,q}\}$ is a vector containing all the particles positions in the Trotter slice q. Note that the integrals are *not* taken over the initial and final positions $\mathbf{R}_0$ and $\mathbf{R}_Q$.

3.5.1 Definition of the action

For τ small enough we can rewrite the density matrix operator using the *primitive approximation* (see section 2.2.1) as:

$$e^{-\tau(\hat{K}+\hat{V})} = e^{-\tau(\hat{K}^{tra}+\hat{K}^{rot}+\hat{V})} \approx e^{-\tau\hat{K}^{tra}} e^{-\tau\hat{K}^{rot}} e^{-\tau\hat{V}} \tag{3.19}$$

We now define the action of a *link* (a pair of time slices $(\mathbf{R}_{q-1},\mathbf{R}_q)$) separated by time τ as minus the logarithm of the density matrix:

$$A_q \equiv A(\mathbf{R}_{q-1},\mathbf{R}_q,\tau) \equiv -\ln\left[\rho(\mathbf{R}_{q-1},\mathbf{R}_q,\tau)\right] \tag{3.20}$$

There will be contributions to $A_q = (A_q^{kin} + A_q^{pot})$ coming from each term of the Hamiltonian. It is convenient to separate each of them. The kinetic action for the link q denoted A_q^{kin} is:

$$\begin{aligned} A_q^{kin} &\equiv -\ln\left[\rho_q^{kin}(\mathbf{R}_{q-1},\mathbf{R}_q,\tau)\right] = -\ln\left[\langle\mathbf{R}_{q-1}|\, e^{-\tau\hat{K}^{tra}} e^{-\tau\hat{K}^{rot}} \,|\mathbf{R}_q\rangle\right] \\ &= -\ln\left[\langle\overline{\mathbf{R}}_{CM_{q-1}}|\, e^{-\tau\hat{K}^{tra}} \,|\overline{\mathbf{R}}_{CM_q}\rangle\right] - \ln\left[\langle\overline{\mathbf{\Omega}}_{q-1}|\, e^{-\tau\hat{K}^{rot}} \,|\overline{\mathbf{\Omega}}_q\rangle\right] \\ &= A_q^{tra}\left(\overline{\mathbf{R}}_{CM_{q-1}},\overline{\mathbf{R}}_{CM_q},\tau\right) + A_q^{rot}(\overline{\mathbf{\Omega}}_{q-1},\overline{\mathbf{\Omega}}_q,\tau). \end{aligned} \tag{3.21}$$

For N distinguishable free particles confined in a box with periodic boundary conditions the translational action can be written as (see Appendix B.1):

$$A_q^{tra}\left(\overline{\mathbf{R}}_{CM_{q-1}},\overline{\mathbf{R}}_{CM_q},\tau\right) = \frac{3N}{2}\ln\left[4\pi\tau\lambda\right] + \sum_{i=1}^{N}\frac{\left[\mathbf{R}_{CM_{i,q-1}} - \mathbf{R}_{CM_{i,q}}\right]^2}{4\tau\lambda} \tag{3.22}$$

and for the rotational part we have: (see Appendix B.2),:

$$A_q^{rot}(\overline{\mathbf{\Omega}}_{q-1},\overline{\mathbf{\Omega}}_q,\tau) = -\sum_{i=1}^{N}\ln\left[\sum_{l=0}^{\infty}\frac{2l+1}{4\pi}P_l\left(\cos(\Theta_{i,q})\right)e^{-\tau Bl(l+1)}\right] \tag{3.23}$$

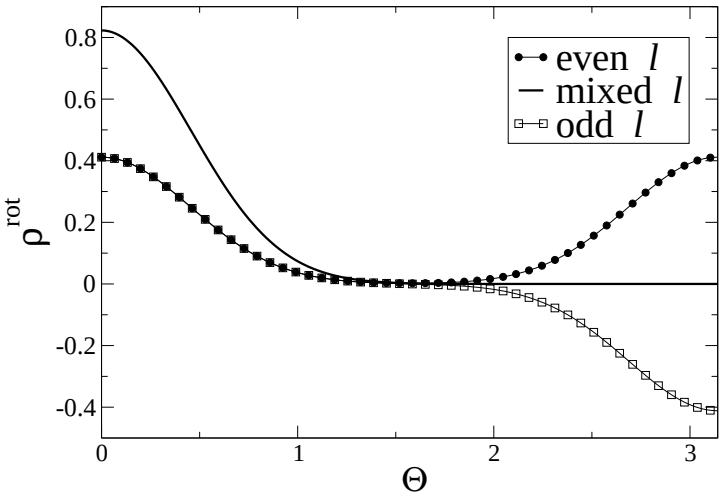

Figure 3.6: Rotational density matrix at a given site as a function of Θ for $\tau B = 0.1$ Eq. (3.24). Three cases are considered i) l even (solid circles) ii) l mixed (solid line) iii) l odd (open squares).

where $\cos(\Theta_{i,q}) = \mathbf{n}_{i,q-1} \cdot \mathbf{n}_{i,q}$, with $\mathbf{n}_{i,q} = (\cos(\phi_{i,q})\sin(\theta_{i,q}), \sin(\phi_{i,q})\sin(\theta_{i,q}), \cos(\theta_{i,q}))$, $P_l(\bullet)$ is the Legendre polynomial. The rotational density matrix at a given site $\rho^{rot}_{i,q}(\mathbf{\Omega}_{i,q-1}, \mathbf{\Omega}_{i,q}, \tau) = \rho^{rot}_{i,q}(\Theta_{i,q}, \tau)$ has hence the form [42]:

$$\rho^{rot}_{i,q}(\Theta_{i,q}, \tau) = \sum_{l=0}^{\infty} \frac{2l+1}{4\pi} P_l(\cos(\Theta_{i,q})) e^{-\tau B l(l+1)} \tag{3.24}$$

For finite temperatures, $\tau > 0$ and the sum obviously converges. Although $\rho^{rot}_{i,q}(\Theta_{i,q}, \tau)$ cannot be expressed analytically, it can be computed numerically to very high precision and then tabulated on a fine grid. Only one function needs to be stored at each effective temperature QT in order to compute the Boltzmann weight. In the Fig 3.6 we show $\rho^{rot}_{i,q}(\Theta_{i,q}, \tau)$ as a function of $\Theta_{i,q}$ for $\tau B = 0.1$ in three different cases: (i) the sum is limited to even l-values (symmetric rotational states) as would have to be done for simulation of *para*-H_2 and *ortho*-D_2 (see Appendix C); (ii) even and odd values of l are considered (non-symmetrical rotational states), as necessary in a simulation of heteronuclear molecules such as HD; (iii) the sum is restricted to odd values of l (anti-symmetric rotational states) as in the case of *ortho*-H_2 and *para*-D_2. In the even and mixed l-cases Eq. (3.24) always remains positive,

and hence can be interpreted as a probability, while in the odd l-case it is antisymmetric, leading to a sign problem [24].

The rest of the action is due to the interaction (potential) contribution:

$$A_q^{pot} \equiv A_q^{pot}(\mathbf{R}_{q-1}, \mathbf{R}_q, \tau) = A_q - A_q^{kin},$$

which in the primitive approximation reads

$$A_q^{pot} = \frac{\tau}{2}\left[V(\mathbf{R}_{q-1}) + V(\mathbf{R}_q)\right] \tag{3.25}$$

where we have symmetrized A_q^{pot} with respect to $\mathbf{R}_{q-1}$ and $\mathbf{R}_q$ to improve on accuracy [24]. Summarizing the path integral expression for the partition function is obtained by substitution of Eq. (3.18) and (3.20) into Eq. (3.16) leading to:

$$Z = \int d\overline{\mathbf{R}} e^{-\beta A(\overline{\mathbf{R}})} \tag{3.26}$$

with $A(\overline{\mathbf{R}}) = \beta^{-1}\sum_{q=1}^{Q} A_q(\mathbf{R}_{q-1}, \mathbf{R}_q)$, $\overline{\mathbf{R}} = \{\mathbf{R}_{q=1\cdots Q}\}$ and $\mathbf{R}_0 = \mathbf{R}_Q$. Periodic boundary conditions are imposed in the time-direction, as dictated by the trace in the quantum partition function. The average of any diagonal operator $\hat{O}(\mathbf{R})$ can be calculated using Eq. (3.17),

$$\begin{aligned} \left\langle \hat{O} \right\rangle &= \frac{1}{Z}\int d\overline{\mathbf{R}} \left[\sum_{q=1}^{Q} \frac{\hat{O}(\mathbf{R}_q)}{Q}\right] e^{-\beta A(\overline{\mathbf{R}})} \\ &= \left\langle \frac{1}{2Q}\sum_{q=1}^{Q}\left[\hat{O}(\mathbf{R}_{q-1}) + \hat{O}(\mathbf{R}_q)\right]\right\rangle \end{aligned} \tag{3.27}$$

The sum over the Trotter slices is obtained by applying the cyclic properties of the trace, meaning that $\left\langle \hat{O} \right\rangle$ does not depend on the selection of the first slice.

3.6 Constant Pressure Ensemble

An advantage of the MC method is that it can be readily adapted to the calculation of averages in any ensemble. As we are interested in studying the

temperature *vs.* pressure HD phase diagram, most of the calculations were performed in the constant-pressure ensemble (NpT) where N, p, T remain constant. In this ensemble the configurational average of an operator $\hat{O}$ is given by:

$$\langle \hat{O} \rangle = Z_{\mathrm{NpT}}^{-1} \int d\mathrm{v} \int \mathrm{d}\overline{\mathbf{R}}' \; \mathrm{O}(\overline{\mathbf{R}}')\mathrm{v}^{\mathrm{NQ}}\mathrm{e}^{-\beta \mathrm{pv}}\mathrm{e}^{-\beta \mathrm{A}(\overline{\mathbf{R}}')} \tag{3.28}$$

where Z_{NpT} is the appropriate configurational integral, v is the volume of the simulation cell and p is the pressure. Note that in this equation we use a set of scaled coordinates $\overline{\mathbf{R}}' = \{\mathbf{R}'_{CM_{i=1,\ldots,N,q=1,\ldots,Q}}, \mathbf{\Omega}_{i=1,\ldots,N,q=1,\ldots,Q}\}$ where

$$\mathbf{R}'_{CM_{i,q}} = L_{Box}^{-1}\mathbf{R}_{CM_{i,q}} \tag{3.29}$$

In this case the configurational integral in Eq. (3.28) is over the unit cube and the additional factor of v^{NQ} comes from the volume element $d\overline{\mathbf{R}} = \mathrm{v}^{\mathrm{NQ}}\mathrm{d}\overline{\mathbf{R}'}$ [43]. The Metropolis scheme is implemented by generating a Markov chain (see Sections 1.3.1) of states which has a limiting distribution proportional to:

$$\exp\left[-\beta\left(\mathrm{pv} + \mathrm{A}(\overline{\mathbf{R}}') - \frac{\mathrm{NQ}}{\beta}\ln[\mathrm{v}]\right)\right] \tag{3.30}$$

A new state is generated by displacing a molecule randomly and/or making a random volume change. One important difference between this ensemble and the canonical ensemble is that when a move involves a change in volume the density of the solid changes. In this case the potential energy in the initial and final states are different and must be recalculated for the new state, which is computationally more expensive than changing the configuration of just one molecule.

As we are working in the rigid-rotor approximation, the intermolecular distance must not change when applying to the system a volume move. This implies that $\mathbf{r}'_{2i,q} - \mathbf{r}'_{1i,q} = \mathbf{r}_{2i,q} - \mathbf{r}_{1i,q}$: to satisfy this constraint and the change of variable (Eq. (3.29)) we change the atoms positions according to:

$$\mathbf{r}'_{1i,q} = (L_{Box}^{-1} - 1)\mathbf{R}_{CM_{i_q}} + \mathbf{r}_{2i,q} \qquad \mathbf{r}'_{2i,q} = (L_{Box}^{-1} - 1)\mathbf{R}_{CM_{i_q}} + \mathbf{r}_{1i,q} \tag{3.31}$$

3.7 Selecting the Interaction Potential

The pair interaction potential has been widely studied and several values for the coefficients $B_{l1,l2,l}$ have been reported [32],[33],[34],[35],[36] (see section 3.2). For the anisotropic part of the potential we select the $B_{l_1 l_2 l}$ reported by Burton *et al.* ($V^{\text{Burton}} = V^{pair}$) see Eq. (3.1), [32]. The selection of the Burton coefficients to calculate the interaction potential was made for three main reasons: i) they include the main six contribution to the gas pair potential $B_{l_1 l_2 l}$; ii) the coefficients B_{202},B_{022} and B_{224} are very similar to the ones reported in Refs. [34] and [36]; iii) they reproduce with good accuracy the energies of the different configurations calculated in Ref. [36].

To select the isotropic part of the potential we use the PIMC method to calculate the equation of state (EOS). The EOS is a key test case for validation of both the theoretical model and the intermolecular isotropic potential (see Ref. [29] and [30]). Note that the anisotropic part of V has a negligible effect in the calculation of the EOS [41]. The NpT ensemble provides a direct mean for testing the p-T-v relationship against experimental data. Here p and T are constant input parameters while v is directly measured in the equilibrated simulation cell.

In Fig. 3.7 we show the EOS for D_2 obtained in four different forms: i) experimental data reported by Hemley *et al.*, in Ref. [39] (triangles); ii) EOS proposed by Vinet *et al.*, in Ref. [44] (solid line) given by the equation,

$$\mathrm{p} = 3\mathrm{K}_0 \left(\frac{\mathrm{v}}{\mathrm{v}_0}\right)^{-\frac{2}{3}} \left(1 - \left(\frac{\mathrm{v}}{\mathrm{v}_0}\right)^{\frac{1}{3}}\right) \exp\left[\frac{3}{2}\left(\mathrm{K}_0' - 1\right)\left(1 - \left(\frac{\mathrm{v}}{\mathrm{v}_0}\right)^{\frac{1}{3}}\right)\right] \quad (3.32)$$

(Here $K_0 = 0.336$ GPa is the isothermal bulk modulus, $\mathrm{v}_0 = 19.93$ cm^3/mol is the volume at zero pressure and $K_0' = 6.78$ is the first derivative of K_0 with respect to pressure evaluated at $\mathrm{p} = 0$ [39]. This form has been shown to fit the EOS of a wide variety of materials up to high compression [44]);

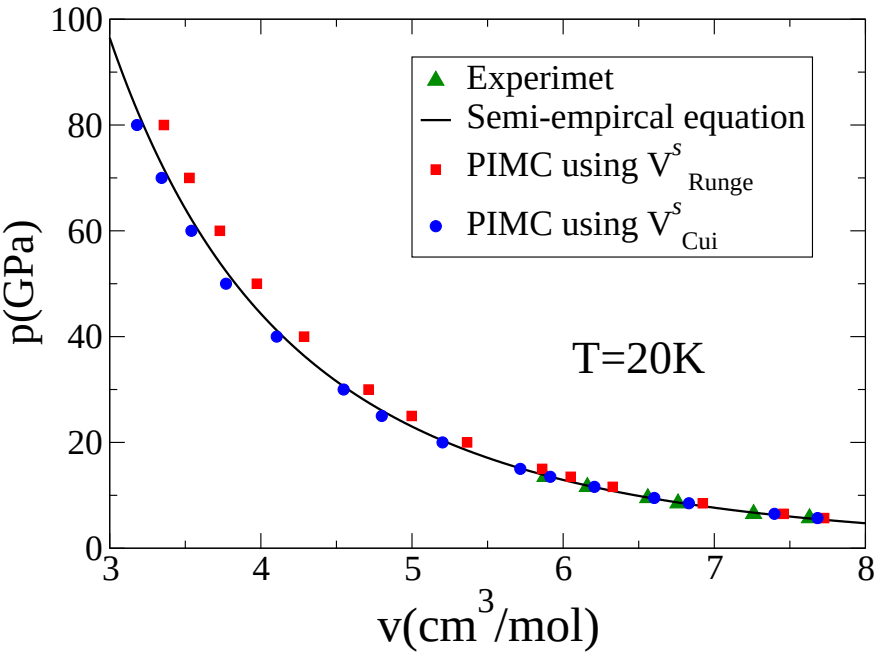

Figure 3.7: D_2 equation of state obtained in four different forms i) experimental data reported by Hemley *et al.*, in Ref. [39] (triangles); ii) EOS proposed by Vinet *et al.*, in Ref. [44] Eq. (3.32)(solid line); iii) PIMC results using V^s_{Runge} Eq. (3.10) (squares); iv) PIMC results using V^s_{Cui} (circles). The PIMC technique was applied to a system consisting of 256 molecules of *ortho*-D_2 on an FCC lattice at $T = 20K$; the cut-off of the potential was selected at the second-nearest-neighbor distance and the number of Trotter slices as $Q = 64$.

iii) PIMC results using V^s_{Runge} Eq. (3.10) (squares); iv) PIMC results using V^s_{Cui} (circles). The PIMC technique was applied to a system consisting of 256 molecules of *ortho*-D_2 on an FCC lattice at $T = 20K$, the cut-off of the potential was selected at the second-nearest-neighbor distance and the number of Trotter slices as $Q = 64$. It can be seen from the figure that even with the softest parameter η V^s_{Runge} is too repulsive while V^s_{Cui} give a better result for the EOS at high pressures. Thus in this thesis we use as interaction potential the one reported by Cui *et al.*, V^s_{Cui} [41] (see Eq. (3.11)):

3.8 The Solid Structure and the Order Parameter

It is well documented in the literature that at high temperatures the stable structure of hydrogen-like solids (H_2,D_2,HD) is the orientational disordered HCP lattice [29]. At low pressure and low temperature both even-l species (*para*-H_2, *ortho*-D_2) form an HCP lattice with molecules in spherically symmetric states (disordered). Only the $l = 1$ solids (*ortho*-H_2,*para*-D_2) have a low temperature mechanism, the orientational ordering, which can drive the crystal into the FCC structure thus, for these systems at low temperature a phase transition from orientational disorder HCP to orientational ordered FCC (Pa3 see below) takes place.

In Ref. [45], Felsteiner showed that an array of ordered electric quadrupole moments would have a lower energy on an FCC lattice than on an HCP lattice. The lowest energy, or ground state, is the Pa3 structure with four molecules per unit cell shown in Fig. 3.8. Here the molecular centers lie on the sites of an FCC lattice; the molecular axes are oriented along the four different diagonals of the four cubic sublattices. This is the structure in the ordered phases of $l = 1$ solids *ortho*-H_2 and *para*-D_2 [29].

At $T = 0$ and pressure of about 28 GPa for *ortho*-D_2 [17] and 110 GPa for *para*-H_2 [16] the ground state symmetry of the low-pressure breaks and molecules become orientationally ordered. In hydrogen and deuterium the transition temperature of the BSP line increases with increasing pressure [17],[16]. In HD this line is re-entrant and the transition temperature first decreases and then increases with increasing pressure [18]. Experimentally, the crystal structure of the BSP is unknown [46], [22].

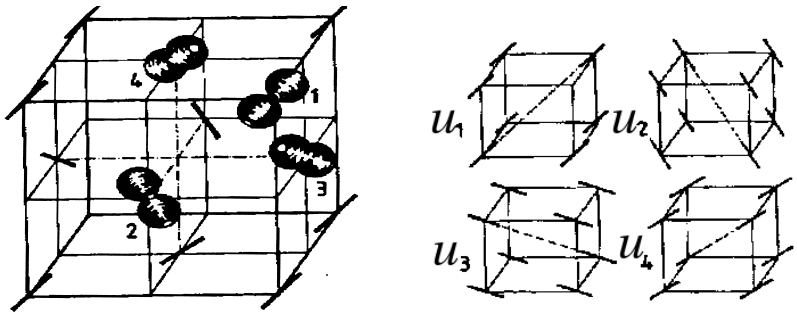

(a) Pa3 orientation of the four molecules on the FCC lattice.

(b) Quadrupoles are aligned along a different diagonal of the sublattice cubic cell

Figure 3.8: Fig.22 of Ref. [29]. The lowest energy configuration of quadrupoles on the FCC lattice.

To determine the BSP line it is necessary to monitor the lattice ordering. This is usually done by using an order parameter. Runge *et al.*, [40], have used a lattice biased order parameter that can be written as:

$$O_p = \left[\sum_{q=1}^{Q} \sum_{i=1}^{N} \frac{1}{2QN} \left(3\cos^2 \left(\mathbf{n}_{i,q} \cdot \mathbf{u}_i \right) - 1 \right) \right]^2 \tag{3.33}$$

Here $\{\mathbf{u}_i\}$ are the unit vectors pointing along a particular set of ordered directions on the FCC lattice. By definition, this order parameter can only measure the extent of ordering relative to a given orientational structure defined by the set $\{\mathbf{u}_i\}$. In Ref. [40] the set $\{\mathbf{u}_i\}$ was selected as the Pa3 ordered directions, as this is the ground state of the EQQ interaction on the FCC lattice. In the perfect ordered state of Pa3 $\langle O_p \rangle = 1$, while perfect disorder yields $\langle O_p \rangle \approx 0$.

3.9 The HD Re-entrant Phase Diagram

Solid HD in the orientational disordered phase has an HCP lattice [47]; in order to work with this structure we need an HCP ordered structure, that

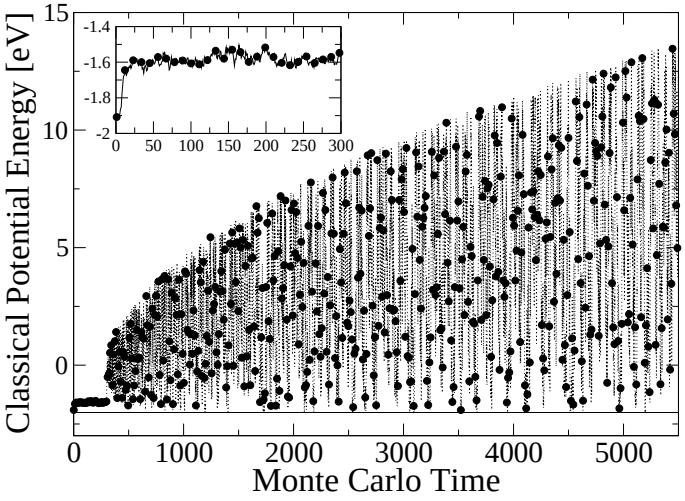

Figure 3.9: Classical potential energy for the HD system as a function of the MC time calculated using the metadynamics-based MC method proposed in section 1.8 to a system consisting of 256 classical molecules with center fixed on an HCP lattice at $T = 20K$; the cut-off of the potential was selected at the second-nearest-neighbor distance, the grid spacing is of 1×10^{-5} a.u. and a high of the Gaussians of 1×10^{-4} a.u. The inset shows a zoom in the initial transient with the MC dynamics used before the metadynamics simulation.

minimizes the rotational part of the potential energy, to be used as reference for generating the unit vectors $\{\mathbf{u}_i\}$ used in Eq. (3.33). Here we use the proposed classical metadynamics-based MC method to force the system to move in the rotational potential energy space. By doing this the dynamics will force the system to move through the potential energy space finding the minimum classical potential energy configuration for the HCP lattice.

We consider a system of 216 classical molecules fixed on an HCP lattice at $T = 20K$. The cut-off of the potential V^s_{Cui} was selected at the second-nearest-neighbor distance. As molecules can just rotate and interact, they have just rotational and potential energy. Classically the contribution of

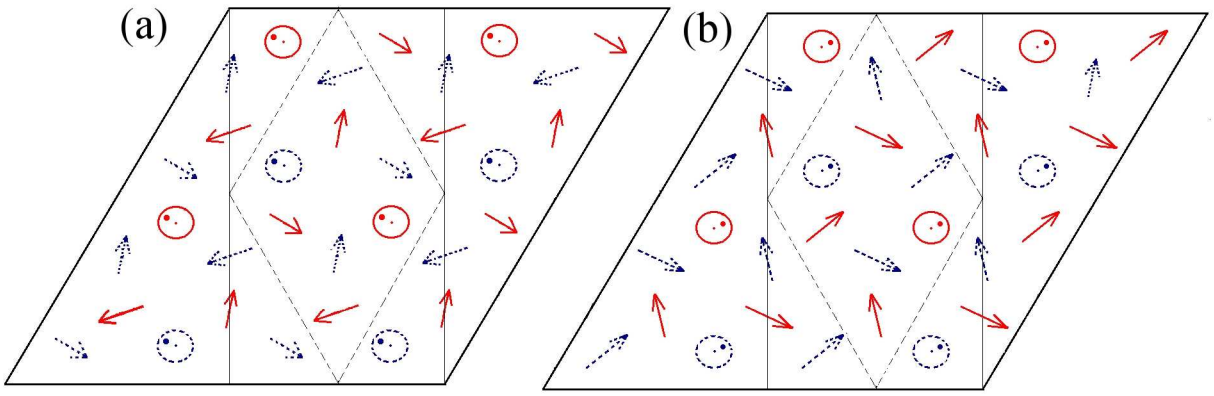

Figure 3.10: The new structure having the lowest classical energy as seen along the HCP axis. The rectangular shaped region delineated with a solid line is a unit cell containing 32 molecules. The primitive cell has a diamond shape (dashed line) and contains 16 molecules. Both cells consists of two layers AB and $A'B'$ grouped separately along the HCP axis. Molecules in the upper layers (B, B') are shown in dashed line, while the lower layer is shown with solid line. The AB layers (a) lie above the $A'B'$ layers (b).

the rotational energy to Z is constant at a fixed temperature. To find the minimum potential energy of this system we use the metadynamics-based MC method described in section 1.8; we consider as collective variable the potential energy $s = V^s_{\rm Cui}$ given by Eq. (3.11) and use a grid spacing of 1×10^{-5} a.u. and a high of the Gaussians of 1×10^{-4} a.u. As the boundaries of this collective variable were unknown (actually we want to find one of them) we use the interpolation procedure explained in section 2.7: this will generate systematic errors near the boundary, but for the moment we are just interested in getting good configuration and not in the accuracy of the free energy.

In Fig. 3.9 we show the classical potential energy for the HD system as a function of the MC time calculated using the following procedure: In a first step we start from a random configuration and do normal Metropolis MC till equi-

libration is reached (see Fig. 3.9 inset), then we turn on the metadynamics-based MC procedure and find the structure with the minimum energy (data not shown). Next, in the second step we start the simulation from the found new structure and reaped the same process again (Fig. 3.9). We see from the figure that starting from this new structure the system first equilibrates and then starts to move through energy phase space recovering also the starting structure. The configurations having higher potential energy are disordered while those with lower energy have exactly the same structure of the initial configuration with a small variation in the orientation of the molecules.

In Fig. 3.10 we show the new structure as seen along the HCP axis. The rectangular shaped region delineated with a solid line is a unit cell containing 32 molecules. The primitive cell has a diamond shape (dashed line) and contains 16 molecules. Both cells consists of two layers AB and $A'B'$ grouped separately along the HCP axis. Molecules in the upper layers (B, B') are shown as dashed, while those in the lower layer are shown as solid. The AB layers (a) lie above the $A'B'$ layers (b).

The arrows in Fig.3.10 are pointing towards the positive direction of the HCP axis. The azimuth ϕ and inclination θ angles for the molecules in the

Table 3.2: The azimuth ϕ and inclination θ angles for the molecules in the layers AB and $A'B'$ in the new structure of Fig.3.10 in a spherical coordinates system centered in one of the HD atoms.

AB			$A'B'$		
	ϕ	θ		ϕ	θ
⊙	145.5	17.0	⊙	34.0	16.8
↘	141.8	82.3	→	151.5	63.9
←	28.4	64.1	↗	38.1	82.0
↗	85.1	68.9	↑	94.7	69.2

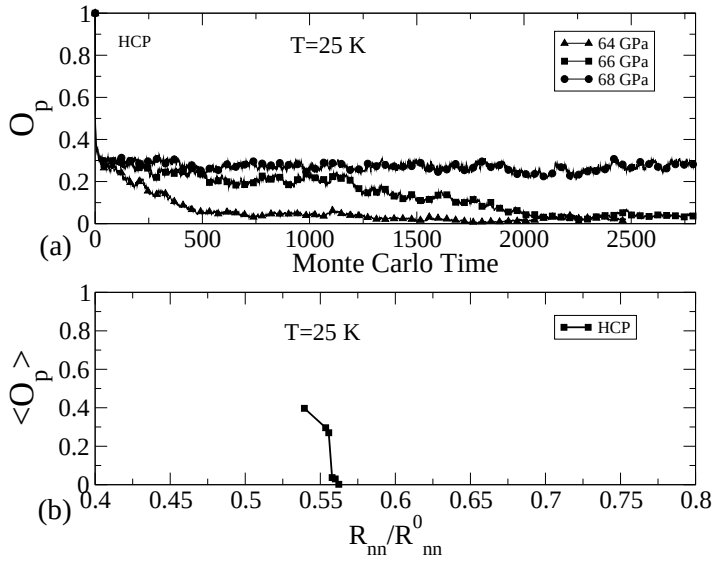

Figure 3.11: (a) Lattice biased order parameter as a function of the MC time for three pressures: 64 GPa (up solid triangles), 66 GPa (solid squares), 68 GPa (solid circles). (b) Average of the order parameter as a function of the nearest-neighbor separation in units of $R^0_{nn} = 3.6A^0$ (the zero pressure intermolecular separation of HD [47]). The PIMC technique was applied to a system consisting of 256 molecules of HD on an HCP lattice at $T = 25K$, the cut-off of the potential was selected at the second-nearest-neighbor distance and the number of Trotter slices as $Q = 64$.

layers AB and $A'B'$ for the new structure, in a spherical coordinates system centered in one of the HD atoms, are given in table 3.2. This structure is very similar to the one reported as the quantum ground state of H_2 on the HCP lattice by Surh *et al.*, [22]. That is, both structures have the same characteristics (*e.g.*, the unit and the primitive cell) but the orientation of the molecules are different.

The order parameter O_p in Eq. (3.33) is then calculated using as $\{\mathbf{u}_i\}$ the unit vectors pointing along the new structure directions. In Fig. 3.11 (a) we plot the order parameter O_p as a function of the MC time for three pressures: 64 GPa (up solid triangle), 66 GPa (solid squares), 68 GPa (solid circles).

The PIMC technique was applied to a system consisting of 256 molecules of HD on an HCP lattice at $T = 25K$, the cut-off of the potential was selected at the second-nearest-neighbor distance and the number of Trotter slices as $Q = 64$. we see from the figure that for $p < 68$ GPa, after a transient, O_p converges to a small value $O_p \approx 0$, while for $p = 68$ GPa O_p shows an upward turn and converges to a value grater than zero $O_p \approx 0.27$. This abrupt change in the order parameter indicates the presence of a phase transition. This can be best appreciated from Fig. 3.11 (b) where we show the average order parameter, Eq. (3.33), as a function of the nearest-neighbor separation (R_{nn}) in units of $R^0_{nn} = 3.6\mathring{A}$ (the zero pressure intermolecular separation of HD [47]). The error bars are smaller than the size of the point symbols in the figure. As seen from the figure, the function $\langle O(R_{nn}/R^0_{nn})\rangle$ has a step-like increase indicating a phase transition from a disordered phase, to an ordered one. Our PIMC results suggest that HD, at a temperature of $T = 25K$, orders at ≈ 44 GPa on an FCC lattice (data not shown) and at ≈ 68 GPa on the HCP lattice close to the experimental observation of 56 GPa.

The order parameter defined by Eq. (3.33) depends of the structure selected for generating the unit vectors $\{\mathbf{u}_i\}$. So, if the system converges to an ordered structure different from the reference one then $O_p \approx 0$. Thus the condition $O_p = 0$ is not sufficient to ensure that the system is in the orientationally disordered phase. To solve this problem we define a second order parameter as:

$$\langle O_Q\rangle = \frac{1}{N}\sum_{i=1}^{N}\frac{1}{6}\sum_{j,k=1}^{3}\left[\frac{1}{T_{MC}}\sum_{t=1}^{T_{MC}}\frac{1}{Q}\sum_{q=1}^{Q}\mathcal{Q}^i_{jk}(tq)\right]^2 \tag{3.34}$$

where T_{MC} is the MC time, $\mathcal{Q}^{itq}_{jk}$ is the j,k component of the quadrupolar moment tensor of the ith molecule at the qth time slice and at the tth MC time, defined as:

$$\mathcal{Q}^i_{jk}(tq) = \sum_{d=1}^{2}\left(3r^i_{j,dtq}r^i_{k,dtq} - r_0^2\delta_{jk}\right) \tag{3.35}$$

where d runs over the two atoms of the molecule, δ_{jk} is the Kronecker delta and the indices j, k run over the Cartesian components x, y, z of the quadrupole tensor. Note that Eq. (3.34) can be written as:

$$\langle O_Q \rangle = \frac{1}{N} \sum_{i=1}^{N} \frac{1}{6} \sum_{j,k=1}^{3} \left[\mathcal{Q}_{jk}^{\text{Total}} \right]^2 \tag{3.36}$$

where

$$\mathcal{Q}_{jk}^{\text{Total}} = \frac{1}{T_{MC}Q} \sum_{a=1}^{2T_{MC}Q} \left(3 r_{j,a}^{i} r_{k,a}^{i} - r_0^2 \delta_{jk} \right) \tag{3.37}$$

with $a = dtq$ a combined index, is the quadrupolar moment of a system of "$T_{MC}Q$" molecules with a charge per atom of $(T_{MC}Q)^{-1}$. If the molecules rotate in MC or Trotter time (spherical symmetry) then $\mathcal{Q}_{jk}^{\text{Total}} = 0$; if the molecules are frozen in both MC and Trotter time then $\frac{1}{6} \sum_{j,k=1}^{3} \left[\mathcal{Q}_{jk}^{\text{Total}} \right]^2 = 1$.

At low pressure, in the orientationally disordered phase, the molecules have spherical symmetry in both classical and quantum cases. At low temperature the molecules are in the spherical symmetric $l = 0$ ground state. In the classical region temperature fluctuations induce the molecule to rotate in every direction making the position time average spherical symmetric. Therefore $\langle O_Q \rangle$ will vanish in the orientationally disordered phase. On the other hand, if the molecules break the spherical symmetry, as it happens for very high pressures, $\langle O_Q(T_{MC}) \rangle > 0$. Note that $\langle O_Q \rangle > 0$ even if we have a structure with the quadrupoles moments frozen in a random configuration: thus this order parameter imposes less restrictions to the molecular configuration than O_p.

In Fig.3.12 we show the convergence of the quadrupolar moment order parameter $\langle O_Q \rangle$ as a function of the MC time for four pressures: 62 GPa (down solid triangles), 64 GPa (up solid triangles), 66 GPa (solid squares), 68 GPa (solid circles) for the same system of Fig.3.11. Even if the calculation are still preliminary (they still running), we can extract some important information

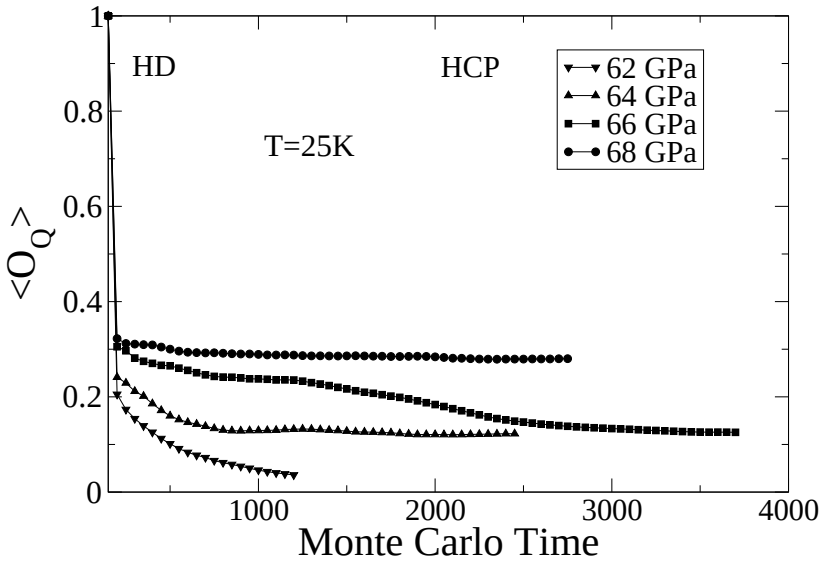

Figure 3.12: Convergence of the quadrupolar moment order parameter Eq. 3.34 as a function of the MC time for four pressures: 62 GPa (down solid triangles), 64 GPa (up solid triangles), 66 GPa (solid squares), 68 GPa (solid circles) for the same system of Fig.3.11.

from it. As in the previous case, we can say that at 68 GPa we are inside the ordered phase, while at 62 GPa the order parameter is converging to zero or at least to a very small value. This result ensures us that the system is in the rotationally symmetric phase for $p < 62$ GPa, leaving a range of pressure 62 GPa $< p <$ 68 GPa where the transition can occurs (see dashed region in Fig.3.13).

Fig.3.13 shows the temperature-pressure phase diagram of solid HD. The open circles are the experimental transition data [18]. The up open triangles are the results reported by Shin *et al.*, [21]. The open and closed squares, are respectively, the constant pressure PIMC results considering an FCC and an HCP lattice for the same system of Fig.3.11. In our HCP PIMC results (see Fig.3.13), the solid squares indicate the pressure where we find a clear or-

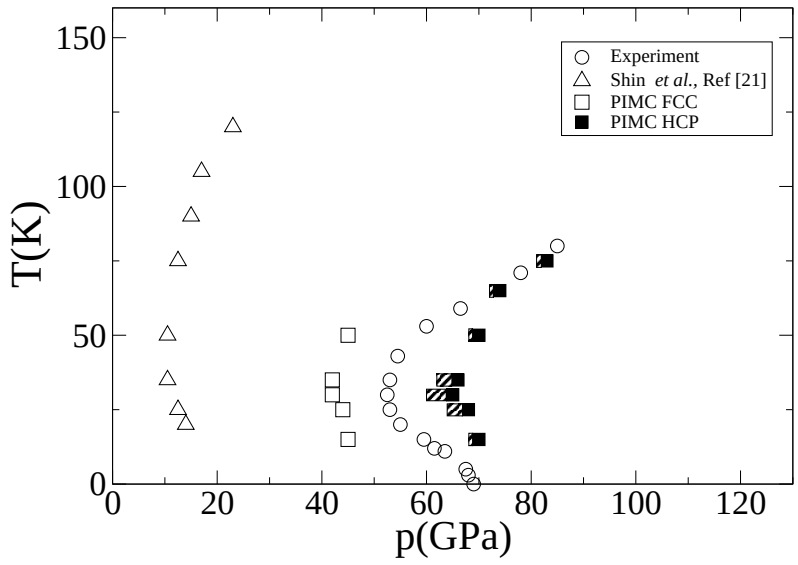

Figure 3.13: The temperature-pressure phase diagram of solid HD. The open circles are the experimental phase line [18]. The up open triangles are the PIMC results reported by Shin *et al.*, [21]. The open and closed squares are respectively the PIMC results considering an FCC and an HCP lattice for the same system of Fig.3.11. The dashed region indicates our uncertainty on the location of the transition point.

dered structure while the dashed region represents a range of pressures where the transition could take place. We obtain a re-entrant behavior for the HD phase line on both the FCC and the HCP lattice. The minimum pressure at which the transition occurs (p_m) is $p_m \approx 42$ GPa for the FCC lattice and $p_m \approx 65$ GPa for the HCP lattice, reasonably close to the experimental value of $p_m = 53$ GPa and in much better agreement than the previous PIMC calculations reported in Ref. [21], which give $p_m \approx 10$ GPa. The temperature at which p_m occurs is in very good agreement with the experimental one of $T = 30K$, and the HCP high temperature results are in very good agreement with the experiment.

In summary, we have applied PIMC within the constant pressure ensemble to the HD solid at high densities. The isotropic part of the potential was tested via the EOS, where it was shown that the pair potentials reported in the literature were too repulsive even including the density dependent correction suggested by Runge *et al.*, [40]. By using a classical metadynamics-based MC based scheme, described in section 1.8, to a classical molecular system with fixed centers, we were able to find a new structure which minimizes the anisotropic potential energy. The unit cell of this structure contains 32 molecules and the primitive cell has a diamond shape and contains 16 molecules. Both cells consists of two layers AB and $A'B'$ grouped separately along the HCP axis and the AB layers lying above the $A'B'$ layers.

Before to applying our metadynamics-based MC method to the quantum solid HD we decided to calculate the re-entrant phase line of the BSP to test both our PIMC algorithm and the interaction potential between the molecules. With the new classical HCP structure we defined an order parameter that shows a step like increase as a function of nearest-neighbor separation R_{nn} indicating a phase transition from a disordered phase to an ordered one. We also introduced an order parameter related to the total quadrupolar moment of the molecule to the better understand the rotational state of the molecule.

The HD phase line was calculated for both the FCC and the HCP lattice, obtaining the unusual re-entrant behavior in both cases. We found that the molecules were in an orientationally ordered state at a minimum pressure of $p_m \approx 42$ GPa (FCC) and $p_m \approx 65$ GPa (HCP), reasonable close to the experimental value $p_m = 53$ GPa and in better agreement than the previous PIMC calculations reported in Ref. [21], which give $p_m = 10$ GPa. The temperature at witch p_m occur is in very good agreement with the experimental one $T = 30K$ and the HCP high temperature results are in very good agreement with the experiment. The stage is now ready for the application of

the proposed metadynamics-based MC method to calculate the free energy of this quantum system: this future study will shed light on the physics of the quantum rotational melting at the physical root of the re-entrance in the phase diagram.

Chapter 4

Conclusions and Perspectives

We have presented a new metadynamics-based MC scheme that allows calculating the free energy landscape of classical and quantum systems. The efficiency of this method is similar to that of Wang-Landau method combined with stochastic series expansion scheme, the *state-of-the-art* approach in lattice models. Based on the path integral Monte Carlo (PIMC) technique, our method can be directly applied to continuous, off-lattice quantum problems, where SSE would be harder to implement.

The convergence of the method had been studied and we had shown that the history-dependent potential of metadynamics, after a transient, fluctuates around a well-defined average that, is a good approximation of the negative of the free energy. Stationary conditions were reached thanks to a novel functional form of the history-dependent potential that eliminates the systematic errors at the boundaries generated by finite-width Gaussians. The error of the algorithm in reconstructing the equilibrium free energy, after a transient, decays like umbrella sampling performed in optimal conditions, that is it decreases with a law inversely proportional to the square root of the simulation time. The proposed approach was tested on a two-dimensional quantum Ising model, where we reconstruct the free energy as a function of two and three collective variables. This allows reproducing the thermody-

namic properties in a whole neighborhood of the point in parameter space at which the calculation is performed.

We have also applied PIMC within the constant pressure ensemble to the Hydrogen-Deuterium solid near half a megabar pressure were this interesting system exhibits a re-entrant transition from orientationally disorder to ordered phase. By using the new metadynamics-based MC based scheme on a classical molecular system with centers fixed in a hexagonal closed packed lattice, we were able to find a new structure which minimizes the classical anisotropic potential energy. The re-entrant phase line was then studied by monitoring a lattice biased order parameter. We found a re-entrant phase boundary in good agreement with the experimental one.

The stage is now ready for the application of the proposed metadynamics-based MC method to calculate the free energy of this quantum system: this future study will shed light on the physics of the quantum rotational melting at the physical root of the re-entrance in the phase diagram. In particular we will applied a bias-exchange metadynamics [48] to this quantum system considering at least five collective variables, the potential energy, the translational and the rotational energy, the volume and the order parameter. This calculation will allows to do extrapolation in both the pressure and the temperature direction. Thus with just one run we will be able to obtain the thermodynamics information of a whole region in phase space. For example we will calculate the difference in entropy between the two phases, quantity that is difficult to obtain in a standard PIMC calculation.

Appendix A

Trotter formula

Theorem: *Let $\hat{A}$ and $\hat{B}$ be Hermitian operators. Then for any real t*

$$\lim_{n\to\infty}\left(e^{\mathrm{i}\hat{\mathrm{A}}\mathrm{t}/\mathrm{n}}e^{\mathrm{i}\hat{\mathrm{B}}\mathrm{t}/\mathrm{n}}\right)^n = e^{\mathrm{i}(\hat{\mathrm{A}}+\hat{\mathrm{B}})\mathrm{t}}$$

where i *is the imaginary unit. The formula holds even if $\hat{A}$ and $\hat{B}$ do not commute.*

Proof: By the Taylor series expansion:

$$e^{\mathrm{i}\hat{\mathrm{A}}\mathrm{t}/\mathrm{n}} = \hat{I} + \frac{1}{n}\mathrm{i}\hat{\mathrm{A}}\mathrm{t} + \mathrm{o}\left(\frac{1}{\mathrm{n}^2}\right) \tag{A.1}$$

then it follows

$$e^{\mathrm{i}\hat{\mathrm{A}}\mathrm{t}/\mathrm{n}}e^{\mathrm{i}\hat{\mathrm{B}}\mathrm{t}/\mathrm{n}} = \hat{I} + \frac{1}{n}\mathrm{i}(\hat{\mathrm{A}}+\hat{\mathrm{B}})\mathrm{t} + \mathrm{o}\left(\frac{1}{\mathrm{n}^2}\right) \tag{A.2}$$

thus using the formula for Newton's binomial series we get

$$\left(e^{\mathrm{i}\hat{\mathrm{A}}\mathrm{t}/\mathrm{n}}e^{\mathrm{i}\hat{\mathrm{B}}\mathrm{t}/\mathrm{n}}\right)^n = \hat{I} + \sum_{k=1}^{n}\binom{n}{k}\frac{1}{n^k}\left[\mathrm{i}(\hat{\mathrm{A}}+\hat{\mathrm{B}})\mathrm{t}\right]^k + o\left(\frac{1}{n^2}\right) \tag{A.3}$$

since

$$\binom{n}{k}\frac{1}{n^k} = \frac{n(n-1)(n-2)\cdots(n-k)}{k!n^k} = 1 + \frac{1}{k!}o(\frac{1}{n}) \tag{A.4}$$

substituting in (A.3) and taking the limit when $n \to \infty$ we have

$$\lim_{n\to\infty}\left(e^{\mathrm{i}\hat{\mathrm{A}}\mathrm{t}/\mathrm{n}}e^{\mathrm{i}\hat{\mathrm{B}}\mathrm{t}/\mathrm{n}}\right)^n = \lim_{n\to\infty}\sum_{k=1}^{n}\frac{\left[\mathrm{i}(\hat{\mathrm{A}}+\hat{\mathrm{B}})\mathrm{t}\right]^k}{k!}\left[1 + o\left(\frac{1}{n}\right)\right] + o\left(\frac{1}{n^2}\right) = e^{\mathrm{i}(\hat{\mathrm{A}}+\hat{\mathrm{B}})\mathrm{t}} \tag{A.5}$$

Appendix B

Density matrix in position basis

As the calculation of the translational and rotational density matrix is not trivial we included an appendix where they are derived in detail.

B.1 Translational density matrix

Let us assume that we have N distinguishable free particles and that they are confined in a box of side L_{Box} with periodic boundary conditions. Then the particles have only kinetic energy and the Hamiltonian can be written as:

$$\hat{H} = \hat{K}^{tra} = \sum_{i}^{N} \hat{K}_i^{tra} = \sum_{i}^{N} (-\lambda \hat{\bigtriangledown}_i^2) \tag{B.1}$$

where $\lambda = \hbar^2/2m$, $\hbar$ is the Planck's constant, $\hat{\bigtriangledown}_i^2$ is the Laplacian operator and m is the mass of the particles. The kinetic density matrix of a link (a pair of time slices $(\mathbf{R}_{q-1}, \mathbf{R}_q)$), in the position representation is:

$$\rho_q^{kin}(\mathbf{R}_{q-1}, \mathbf{R}_q, \tau) = \langle \mathbf{R}_{q-1} | \, e^{-\tau \hat{K}^{tra}} \, | \mathbf{R}_q \rangle \tag{B.2}$$

where $\mathbf{R}_q = \{\mathbf{r}_{i=1,\ldots,N,q}\}$ and $\mathbf{r}_{iq}$ the position of the particle on the ith site and the qth slice. Then the eigenfunction and eigenvalue of $\hat{K}^{tra}$ are $\Phi = L_{Box}^{-3N/2} e^{i\mathbf{k_n}\cdot\mathbf{r}}$ and $\lambda \mathbf{k}_\mathbf{n}^2$, with $\mathbf{k_n} = 2\pi\mathbf{n}/L_{Box}$ and $\mathbf{n} = \mathbf{n}_1, \mathbf{n}_2, \cdots, \mathbf{n}_N$ is a $3N$ dimensional integer vector. As the particles are distinguishable, they

can be labeled, and the eigenfunction can be taken as the product of the eigenfunction for the one particle operator, this means:

$$\hat{K}_i \left|\phi_i\right\rangle = \lambda \mathbf{k}_{n_i}^2 \left|\phi_i\right\rangle, \quad \hat{K} \left|\Phi\right\rangle = \sum_{i=1}^{N} \lambda \mathbf{k}_{n_i}^2 \left|\Phi\right\rangle = \lambda \mathbf{k}_{\mathbf{n}}^2 \left|\Phi\right\rangle \tag{B.3}$$

where

$$\left\langle\phi_i\right| \mathbf{r}_{i,q}\rangle = L_{Box}^{-3/2} e^{\mathbf{i}\mathbf{k}_{n_i}\cdot\mathbf{r}_{i,q}}, \left\langle\Phi\right| \mathbf{R}_{\mathbf{q}}\rangle = \prod_{i=1}^{N} L_{Box}^{-3/2} e^{\mathbf{i}\mathbf{k}_{n_i}\cdot\mathbf{r}_{i,q}} = L_{Box}^{-3N/2} e^{\mathbf{i}\mathbf{k}_{\mathbf{n}}\cdot\mathbf{R}_q}$$

Let us now compute the action of the operator $e^{-\tau\hat{K}}$ over the state $\left|\Phi\right\rangle$, by Taylor expansion we have:

$$\begin{aligned} e^{-\tau\hat{K}} \left|\Phi\right\rangle &= \sum_{j=0}^{\infty} \frac{(-\tau\hat{K})^j}{j!} \left|\Phi\right\rangle \\ &= \sum_{j=0}^{\infty} \frac{(-\tau\lambda\mathbf{k}_{\mathbf{n}}^2)^j}{j!} \left|\Phi\right\rangle = e^{-\tau\lambda\mathbf{k}_{\mathbf{n}}^2} \left|\Phi\right\rangle \end{aligned} \tag{B.4}$$

Let us introduce now an identity factor $\sum_{\mathbf{n}} \left|\Phi\right\rangle \left\langle\Phi\right|$ in Eq. (B.2) and use the results obtained in Eq. (B.3) and (B.4) getting

$$\begin{aligned} \rho_q^{kin}(\mathbf{R}_{q-1}, \mathbf{R}_{\mathbf{q}}, \tau) &= \sum_{\mathbf{n}} \left\langle\mathbf{R}_{q-1}\right| e^{-\tau\hat{K}^{tra}} \left|\Phi\right\rangle \left\langle\Phi\right| \mathbf{R}_{\mathbf{q}}\rangle \\ &= \sum_{\mathbf{n}} e^{-\tau\lambda\mathbf{k}_{\mathbf{n}}^2} \left\langle\mathbf{R}_{q-1}\right| \Phi\rangle \left\langle\Phi\right| \mathbf{R}_q\rangle \\ &= \sum_{\mathbf{n}} L_{Box}^{-3N} e^{-\tau\lambda\mathbf{k}^2 - \mathbf{i}\mathbf{k}_{\mathbf{n}}\cdot(\mathbf{R}_{q-1}-\mathbf{R}_q)} \end{aligned} \tag{B.5}$$

Approximating the sum as an integral $\sum_{\mathbf{n}} = (L_{Box}/2\pi)^{3N} \int d\mathbf{k}_{\mathbf{n}_1} \cdots \mathbf{k}_{\mathbf{n}_N}$, and completing the square we have

$$\rho_q^{kin}(\mathbf{R}_{q-1}, \mathbf{R}_q, \tau) = \frac{e^{-\frac{(\mathbf{R}_q-\mathbf{R}_{q-1})^2}{4\tau\lambda}}}{(2\pi)^{3N}} \left(\int d\mathbf{k} e^{-\left(\sqrt{\tau\lambda}\mathbf{k} + \frac{\mathbf{i}(\mathbf{R}_{q-1}-\mathbf{R}_q)}{2\sqrt{\tau\lambda}}\right)^2} \right)^{3N} \tag{B.6}$$

Calculating the Gaussian integral and substituting in (B.2) we get:

$$\rho_q^{kin}(\mathbf{R}_{q-1}, \mathbf{R}_q, \tau) = (4\pi\lambda\tau)^{-3N/2} e^{-\frac{(\mathbf{R}_q-\mathbf{R}_{q-1})^2}{4\lambda\tau}} \tag{B.7}$$

Finally by substituting Eq. (B.7) into the definition of the kinetic action (see Eq. (3.21)) we get;

$$A_q^{kin} = \frac{3N}{2}\ln(4\pi\lambda\tau) + \sum_{i=1}^{N}\frac{(\mathbf{r}_{i,q}-\mathbf{r}_{i,q-1})^2}{4\lambda\tau}. \tag{B.8}$$

B.2 Rotational density matrix

Let us assume that we have N distinguishable free rotors and that they are confined in a box of side L_{Box} with periodic boundary conditions. Then the particles has only rotational energy and the Hamiltonian can be written as:

$$\hat{H} = \hat{K}^{rot} = \sum_{i}^{N}\hat{K}_i^{rot} = B\sum_{i=1}^{N}\hat{L}_i^2 \tag{B.9}$$

where $B = \frac{\hbar^2}{2\mathcal{I}}$, $\mathcal{I}$ is the molecular moment of inertia and $\hat{L}$ is the angular momentum operator. The rotational density matrix of a link in the position representation is:

$$\rho^{rot}(\mathbf{\Omega}_{q-1},\mathbf{\Omega}_q,\tau) = \langle\mathbf{\Omega}_{q-1}|\, e^{-\beta\hat{K}^{rot}}\,|\mathbf{\Omega}_q\rangle \tag{B.10}$$

where $\mathbf{\Omega}_q = \{\omega_{i=1,\ldots,N,q}\}$ and $\omega_{i,q} = (\phi_{i,q},\theta_{i,q})$ are respectively the azimuth and inclination angles in a spherical coordinates system centered in one of the atoms of the ith rotor in the qth slice.

The exact eigenfunction and eigenvalue of the angular momentum operator, for one particle, are the spherical harmonic functions $Y_l^m(\omega)$ and $l(l+1)$ respectively where $l = 0, 1, \cdots$ and $m = -l, \cdots, l$ are integers. Let us take as in the case before, the following notation.

$$B\hat{L}_i^2\,|\varphi_i\rangle = Bl_i(l_i+1)\,|\varphi_i\rangle\,, B\sum_{i=1}^{N}\hat{L}_i^2\,|\Psi\rangle = \sum_{i=1}^{N}Bl_i(l_i+1)\,|\Psi\rangle = B\mathbf{l}\cdot(\mathbf{l}+1)\,|\Psi\rangle$$

$$\text{where}\quad \langle\varphi_i|\,\omega_i\rangle = Y_{l_i}^{m_i}(\omega_{i,q}),\quad \langle\Psi|\,\mathbf{\Omega_q}\rangle = \prod_{i=1}^{N}Y_{l_i}^{m_i}(\omega_{i,q}) = \mathbf{Y_l^m}(\mathbf{\Omega_q}) \tag{B.11}$$

where $\mathbf{l}$ and $\mathbf{m}$ are $3N$ dimensional integer vectors. Using the same procedure we used in Eq. (B.4) for the exponential of an operator, introducing an identity operator $\sum_{\mathbf{l}}\sum_{\mathbf{m}}|\Psi\rangle\langle\Psi|$ we get:

$$\begin{aligned}\rho^{rot}(\mathbf{\Omega}_{q-1},\mathbf{\Omega_q},\tau) &= \sum_{\mathbf{l}}\sum_{\mathbf{m}}\langle\mathbf{\Omega}_{q-1}|\, e^{-\tau\hat{K}^{rot}}\,|\Psi\rangle\langle\Psi|\,\mathbf{\Omega}_q\rangle \\ &= \sum_{\mathbf{l}}\sum_{\mathbf{m}} e^{-\tau B\mathbf{l}\cdot(\mathbf{l}+1)}\langle\mathbf{\Omega}_{q-1}|\,\Psi\rangle\langle\Psi|\,\mathbf{\Omega}_q\rangle \\ &= \sum_{\mathbf{l}}\sum_{\mathbf{m}} e^{-\tau B\mathbf{l}\cdot(\mathbf{l}+1)}\mathbf{Y}_{\mathbf{l}}^{\mathbf{m}*}(\mathbf{\Omega}_{q-1})\mathbf{Y}_{\mathbf{l}}^{\mathbf{m}}(\mathbf{\Omega}_q)\end{aligned} \tag{B.12}$$

Expanding the sums we arrive at the equation:

$$\rho^{rot}(\mathbf{\Omega}_{q-1},\mathbf{\Omega_q},\tau)=\prod_{i=1}^{N}\sum_{l}\sum_{m} e^{-\tau Bl(l+1)}Y_l^{m*}(\omega_{i,q-1})Y_l^m(\omega_{i,q}) \tag{B.13}$$

Using the addition theorem for spherical harmonics [49]

$$P_l(\cos(\Theta_{i,q}))=\frac{4\pi}{2l+1}\sum_{m=-l}^{l}Y_l^{m*}(\omega_{i,q-1})Y_l^m(\omega_{i,q}),$$

where $\cos(\Theta_{i,q})=\zeta_{i,q-1}\cdot\zeta_{i,q}$, $\zeta_{i,q}=(\cos(\phi_{i,q})\sin(\theta_{i,q}),\sin(\phi_{i,q})\sin(\theta_{i,q}),\cos(\theta_{i,q}))$, $P_l(\bullet)$ is the Legendre polynomial, we get the final form for the rotational density matrix:

$$\rho^{rot}(\mathbf{\Omega}_{q-1},\mathbf{\Omega_q},\tau)=\prod_{i=1}^{N}\rho_{i,q}^{rot}(\Theta_{i,q},\tau), \tag{B.14}$$

where $\rho_{i,q}^{rot}(\Theta_{i,q},\tau)$ is the rotational density matrix at a given site (see Eq. (3.24))

$$\rho_{i,q}^{rot}(\Theta_{i,q},\tau)=\sum_{l=0}^{\infty}\frac{2l+1}{4\pi}P_l(\cos\Theta_{i,q})e^{-\tau Bl(l+1)} \tag{B.15}$$

Finally by substituting Eq. (B.14) into the definition of the rotational action (see Eq. (3.21)) we get

$$A_q^{rot}(\mathbf{\Omega}_{q-1},\mathbf{\Omega}_q,\tau)=-\sum_{i=1}^{N}\ln\left[\sum_{l=0}^{\infty}\frac{2l+1}{4\pi}P_l\left(\cos(\Theta_{i,q})\right)e^{-\tau Bl(l+1)}\right] \tag{B.16}$$

Appendix C

Nuclear Symmetry Species for Homonuclear Molecules

The Schrödinger equation for the nuclear motion in the adiabatic approximation [30] is given by:

$$\left[-\frac{\hbar^2}{2\mu}\hat{\nabla}^2_{\mathbf{r}} + V_0(r)\right]\chi_0(\mathbf{r}) = E_0\chi_0(\mathbf{r}) \tag{C.1}$$

where $\mu = m_1 m_2/M_T$, is the reduced mass for the relative motion of the nuclei, m_1, m_2 are the masses of the nuclei, $M_T = m_1 + m_2$ the total mass, V_0 is the effective internuclear potential and E_0 is the energy of a given state. As the effective potential V_0 is spherically symmetric, the solutions of Eq. (C.1) can chosen to be simultaneous eigenfunctions of $\hat{L}^2$ and $\hat{L}_z$

$$\chi_0(\mathbf{r}) = f_{\upsilon l}(r)Y_l^m(\theta,\phi) \quad E_0 = E_{\upsilon l} \tag{C.2}$$

where $\hat{\mathbf{L}}$ is the rotational angular momentum operator of the molecule; r, θ, ϕ are the polar coordinates of $\mathbf{r}$ in a non rotating frame center at the center of mass of the molecule; υ, l are the vibrational and rotational quantum numbers and Y_l^m are the spherical harmonics.

To derive the symmetry properties of the wave functions under permutation of the identical particles contained in the molecule one must introduce the

spins of the nuclei. An interchange of the orbital variables of the two nuclei in the homonuclear molecules H_2 and D_2, amounts to a replacement of the intermolecular separation $\mathbf{r}$ by $-\mathbf{r}$. In the orbital nuclear wave function (C.2) the vibrational part ($f_{vl}(r)$) remains unchanged under this replacement since it depends only on r, and the rotational part changes by a factor $(-1)^l$, the parity of the spherical harmonics. Hence the orbital part of the nuclear wave function is *symmetric for even* l and *antisymmetric for odd* l.

For H_2 the nuclear spin is $S = 1/2$ (the nuclei are fermions), and the total nuclear wave function must be *antisymmetric*. For even l the nuclear spin function must therefore be antisymmetric *i.e.* a singlet corresponding to $I = S_1 + S_2 = 0$, and for odd l the nuclear spin function must be symmetric, *i.e.* a triplet corresponding to $I = 1$. In other words, ***H_2 molecules with antiparallel nuclear spins ($I = 0$) can exist only in the even rotational states*** $l = 0, 2, 4, \ldots$ and ***H_2 molecules with parallel spins ($I = 1$) only in the odd rotational states*** $l = 1, 3, 5, \ldots$ There is no restriction in the vibrational states.

For D_2 the nuclear spin is $S = 1$, the nuclei are bosons and the total nuclear wave function must be *symmetric*. For even l the nuclear spin function must therefore be symmetric, corresponding to $I = 0$ or $I = 2$, and for odd l the nuclear spin function must be antisymmetric $I = 1$. In other words, ***D_2 molecules with $I = 0$ or $I = 2$ can exist only in the even rotational states*** $l = 0, 2, 4, \ldots$ and ***D_2 molecules with $I = 1$ only in the odd rotational states*** $l = 1, 3, 5, \ldots$. In contrast to H_2 and D_2, the two nuclei in HD are not identical and hence distinguishable, consequently no requirement exist on the symmetry of the nuclear wave function.

The degeneracy of a rotational level due to the nuclear spin I is called "statistical weight" of the level since it determines, together with the rotational degeneracy, $2l + 1$, and the appropriate Boltzmann factor, the equilibrium

distribution of the molecules over the rotational levels. The most abundant species at high temperatures are called the *ortho* and the less abundant one the *para* species. Hence ***ortho-hydrogen refers to molecules with*** $I = 1$***,*** l ***odd, and a statistical weight*** $g_s = 3$, and ***para-hydrogen to*** $I = 0$***,*** l ***even, and*** $g_s = 1$. On the other hand, ***ortho-deuterium corresponds to molecules with*** $I = 0$ ***or*** $I = 2$***,*** l ***even, and*** $g_s = 6$, and ***para-deuterium to*** $I = 1$***,*** l ***odd, and*** $g_s = 3$.

Bibliography

[1] N. Metropolis, A. W. Rosenbluth, M. N. Rosenbluth, A. H. Teller, and E. Teller, "Equation of state calculations by fast computing machines," *J. Chem. Phys*, vol. **21**, p. 1087, 1953.

[2] F. Wang and D. P. Landau, "Efficient, multiple-range randomwalk algorithm to calculate the density of states," *Phys. Rev. Lett.*, vol. **86**, p. 2050, 2001.

[3] A. Laio and M. Parrinello, "Escaping free-energy minima," *Proc. Natl. Acad. Sci. U.S.A*, vol. **99**, p. 12562, 2002.

[4] T. Wust, D. P. Landau, C. Gervais, and Y. Xu, "Monte carlo simulations of systems with complex energy landscapes," *Comp. Phys. Comm.*, vol. **180**, p. 475, 2009.

[5] A. Laio and F. L. Gervasio, "Metadynamics: a method to simulate rare events and reconstruct the free energy in biophysics, chemistry and material science," *Rept. Prog. Phys.*, vol. **71**, p. 126601, 2008.

[6] G. Bussi, A. Laio, and M. Parinello, "Equilibrium free energies from nonequilibrium metadynamics," *Phys. Rev. Lett*, vol. **96**, p. 090601, 2006.

[7] M. Troyer, F. Alet, and S. Wessel, "Histogram methods for quantum systems: from reweighting to wang-landau sampling," *Bra. J. Phys. [online]*, vol. **34**, p. 377, 2004.

[8] A. W. Sandvik and J. Kurkijärvi, "Quantum Monte Carlo simulation method for spin systems," *Phys. Rev. B.*, vol. **43**, p. 5950, 1991.

[9] A. W. Sandvik, "Stochastic series expansion method for quantum ising models with arbitrary interactions," *Phys. Rev. E.*, vol. **68**, p. 056701, 2003.

[10] M. Troyer, S. Wessel, and F. Alet, "Flat histogram methods for quantum systems: Algorithms to overcome tunnelling problems and calculate the free energy," *Phys. Rev. Lett.*, vol. **90**, p. 120201, 2003.

[11] M. Iannuzzi, A. Laio, and M. Parrinello, "Efficient exploration of reactive potential energy surfaces using car-parrinello molecular dynamics," *Phys. Rev. Lett.*, vol. **90**, p. 238302, 2003.

[12] A. Barducci, G. Bussi, and M. Parrinello, "Well-tempered metadynamics: A smoothly converging and tunable free-energy method," *Phys. Rev. Lett.*, vol. **100**, p. 020603, 2008.

[13] Y. Crespo, A. Laio, G. E. Santoro, and E. Tosatti, "Calculating thermodynamics properties of quantum systems by a non-markovian Monte Carlo procedure," *Phys. Rev. E*, vol. **80**, p. 015702, 2009.

[14] G. M. Torrie and J. P. Valleau, "Nonphysical sampling distributions in monte carlo free-energy estimation: Umbrella sampling," *J. Comp. Phys.*, vol. **23**, p. 187, 1977.

[15] Y. Crespo, F. Marinelli, F. Pietrucci, and A. Laio, "Metadynamics convergence law in a multidimensional system," *Phys. Rev. E*, vol. **81**, p. 055701, 2010.

[16] H. E. Lorenzana, I. F. Silvera, and K. A. Goettel, "Orientational phase transitions in hydrogen at megabar pressures," *Phys. Rev. Lett.*, vol. **64**, p. 1939, 1990.

[17] L. Cui, N. H. Chen, S. J. Jeon, and I. F. Silvera, "Megabar pressure triple point in solid deuterium," *Phys. Rev. Lett.*, vol. **72**, p. 3048, 1994.

[18] F. Moshary, N. H. Chen, and I. F. Silvera, "Remarkable high pressure phase line of orientational order in solid hydrogen deuteride," *Phys. Rev. Lett.*, vol. **71**, p. 3814, 1993.

[19] Y. A. freiman, S. Tretyak, A. Jezowski, and R. J. Hemley, "Broken symetry phase transition in solid hd: Quantum behavior at very high pressures," *J. Low. Temp. Phys.*, vol. **113**, p. 723, 1998.

[20] B. Hetényi, S. Scandolo, and E. Tosatti, "Theoretical evidence for a reentrant phase diagram in ortho-para mixtures of solid h_2 at high pressure," *Phys. Rev. Lett.*, vol. **94**, p. 125503, 2005.

[21] H. Shin and Y. Kwon, "Reentrant behavior in orientational ordering of asymmetric quadrupolar quantum rotors.," *J. Kor. Phys. Soc.*, vol. **54**, p. 1582, 2008.

[22] M. P. Surh, K. J. Runge, T. W. Barbee III, E. L. Pollock, and C. Mailhiot, "Ab *initio* calculations for solid molecular hydrogen.," *Phys. Rev. B.*, vol. **55**, p. 11330, 1997.

[23] S. Sorella, G. E. Santoro, and F. Becca, *SISSA Lecture notes on Numerical methods for strongly correlated electrons*. Trieste: SISSA, 2007.

[24] D. M. Ceperley, "Path integrals in the theory of condensed helium," *Rev. Mod. Phys*, vol. **67**, p. 279, 1995.

[25] H. Kleinert, *Path integrals in quantum mechanics, statistics, polymer physics, and financial markets*. Singapore: World Scientific, 2009.

[26] H. F. Trotter, "On the product of semi-groups of operators," *Proc. Am. Math. Soc*, vol. **10**, p. 545, 1959.

[27] D. C. Handscomb, "The monte carlo method in quantum statistical mechanics," *Math. Proc. Cambridge Philos. Soc.*, vol. **58**, p. 594, 1962.

[28] J. Snider and C. C. Yu, "Absence of dipole glass transition for randomly dilute classical ising dipoles," *Phys. Rev. B.*, vol. **72**, p. 214203, 2005.

[29] I. F. Silvera, "The solid molecular hydrogen in the condensed phase: Fundamentals and static properties," *Rev. Mod. Phys*, vol. **52**, p. 393, 1980.

[30] J. V. Kranendonk, *Solid Hydrogen.* 233 Spring Street, New York, N.Y. 10013: Plenum Press, 1983.

[31] C. G. Gray, "On the theory of multipole interactions.," *Can. J. Phys*, vol. **46**, p. 135, 1968.

[32] P. G. Burton and U. E. Sneff, "The $(H_2)_2$ potential and the interaction between hydrogen molecules at low temperatures.," *J. Chem. Phys.*, vol. **76**, p. 6073, 1982.

[33] L. Monchick and J. Schaefer, "Theoretical studies of H_2-H_2 collisions. II. Scattering and transport cross sections of hydrogen at low energies: Tests of a new ab initio vibrotor potential.," *J. Chem. Phys.*, vol. **73**, p. 6153, 1980.

[34] P. Diep and J. K. Johnson, "An accurate H_2-H_2 interaction potential from first principles.," *J. Chem. Phys.*, vol. **112**, p. 4465, 2000.

[35] J. Schaefer and W. Meyer, "Theoretical studies of H_2-H_2 collisions. I. Elastic scattering of ground state para- and ortho-H_2 in the rigid rotor approximation.," *J. Chem. Phys.*, vol. **70**, p. 344, 1979.

[36] P. Wind and I. Roeggen, "A theoretical study of the $(H_2)_2$ dimer II. The potential energy surface.," *Chem. Phys.*, vol. **167**, p. 263, 1992.

[37] I. F. Silvera and V. V. Goldman, "The isotropic intermolecular potential for h2 and d2 in the solid and gas phases," *J. Chem. Phys.*, vol. **69**, p. 4209, 1978.

[38] T. S. Duffty, W. L. Vos, C. Zha, R. S. Hemley, and H. Mao, "Sound velocities in dense hydrogen and the interior of jupiter," *Science*, vol. **263**, p. 1590, 1994.

[39] J. Hemley, H. K. Mao, L. W. Finger, A. P. Jephcoat, R. M. Hazen, and C. S. Zha, "Equation of state of solid hydrogen and deuterium from single-crystal x-ray diffraction to 26.5 gpa," *Phys. Rev. B.*, vol. **42**, p. 6458, 1990.

[40] K. J. Runge, M. P. Surch, C. Mailhoit, and E. L. Pollock, "Path integral monte carlo calculations of orientational ordering in compressed H_2.," *Phys. Rev. Lett.*, vol. **69**, p. 3527, 1992.

[41] T. Cui, E. Cheng, B. J. Alder, and K. B. Whaley, "Rotational ordering in solid deuterium and hydrogen: A path integral monte carlo study," *Phys. Rev. B.*, vol. **55**, p. 12253, 1997.

[42] M. H. Müser, "The path-integral monte carlo of rigid linear molecules in three dimensions.," *Mol. Sim.*, vol. **17**, p. 131, 1996.

[43] J. V. Kranendonk, *Computer Simulation of Liquids*. Oxford University Press, Walton Street, Oxford OX2 6DP: Clarendon Press Oxford, 1987.

[44] P. Vinet, J. Ferrante, J. H. Rose, and J. Smith, "Compressibility of solids," *J. Phys. C.*, vol. **20**, p. L467, 1986.

[45] J. Felsteiner, "Structure of the ordered state of ortho-hydrogen at absolute zero," *Phys. Rev. lett.*, vol. **15**, p. 1025, 1965.

[46] L. Cui, N. H. Chen, and I. F. Silvera, "Excitations, order parameters, and phase diagram of solid deuterium at megabar pressures.," *Phys. Rev. B.*, vol. **51**, p. 14987, 1995.

[47] A. Chijioke and I. F. Silvera, "Megabar-pressure infrared study of hydrogen deuteride," *Phys. Rev. Lett.*, vol. **97**, p. 255701, 2006.

[48] S. Piana and A. Laio, "A bias-exchange approach to protein folding," *J. Phys. Chem. B.*, vol. **111**, p. 4553, 2007.

[49] J. Coster and H. B. Hart, "A simple proof of the addition theorem for spherical harmonics," *m. J. Phys*, vol. **59**, p. 371, 1991.